

REPORT DOCUMENTATION

AD-A255 483

Approved
to 0704-0188

1a. REPORT SECURITY CLASSIFICATION

2a. SECURITY CLASSIFICATION AUTHORITY

2b. DECLASSIFICATION/DOWNGRADING SCHEDULE

4. PERFORMING ORGANIZATION REPORT NUMBER(S)

92-2

6a. NAME OF PERFORMING ORGANIZATION

New York University

6b. OFFICE SYMBOL
(if applicable)

7a. NAME OF MONITORING ORGANIZATION

Air Force Office of Scientific Research

6c. ADDRESS (City, State, and ZIP Code)

Department of Physics and Psychology
4 Washington Place
New York, NY 10003

7b. ADDRESS (City, State, and ZIP Code)

Building 410
Bolling AFB, DC 20332-65588a. NAME OF FUNDING/SPONSORING
ORGANIZATION

AFOSR

8b. OFFICE SYMBOL
(if applicable)

NL

9. PROCUREMENT INSTRUMENT IDENTIFICATION NUMBER

AFOSR-90-0221

8c. ADDRESS (City, State, and ZIP Code)

Building 410
Bolling AFB, DC 20332-6558

10. SOURCE OF FUNDING NUMBERS

PROGRAM
ELEMENT NO.

61102F

PROJECT
NO.

2313

TASK
NO.

135

WORK UNIT
ACCESSION NO.

11. TITLE (Include Security Classification)

Cognition and the Brain

12. PERSONAL AUTHOR(S)

S.J. Williamson and L.Kaufman

13a. TYPE OF REPORT

Annual Technical Report

13b. TIME COVERED

FROM 910215 TO 920214

14. DATE OF REPORT (Year, Month, Day)

920525

15. PAGE COUNT

10

16. SUPPLEMENTARY NOTATION

17. COSATI CODES

FIELD GROUP SUB-GROUP

18. SUBJECT TERMS (Continue on reverse if necessary and identify by block number)

localization of cognitive processes; alpha-band suppression; memory
scanning for tones; silent speech; visual image rotation; magnetic source
imaging (MSI); magnetoencephalography (MEG); electroencephalography, (EEG)

19. ABSTRACT (Continue on reverse if necessary and identify by block number)

Magnetic fields associated with spontaneous neuronal activity of cerebral cortex are shown to be locally suppressed when an area of the brain engages in a cognitive function. Suppression occurs in visual cortex when the image of an object is compared with a memory set of objects previously seen, or with the same object rotated. Suppression occurs in auditory cortex when memory of a tone is compared with a memory set of tones. Suppression occurs first over visual cortex and subsequently over the anterior temporal area when a subject responds to a displayed word by seeking a word that rhymes with it. Significant correlations are found between the timing of cortical suppression and classic behavioral studies of reaction times. It is concluded that regional changes in cortical spontaneous activity are meaningfully related to memory scanning, image transformations, and silent speech. A computational procedure, called the minimum-norm least-square (MNLS) estimate, has been developed to provide a unique solution for the magnetic inverse problem. With this algorithm, the distribution of intracellular current across the surface of cerebral cortex can be deduced from the magnetic field pattern that it produces across the scalp. This approach has been generalized to provide a unique estimate for the distribution of time-average current power, obtained from the average field power. It can also be applied to determine the pattern of current power suppression when the subject is engaged in a cognitive task.

20. DISTRIBUTION/AVAILABILITY OF ABSTRACT

☐ UNCLASSIFIED/UNLIMITED ☒ SAME AS RPT. ☐ DTIC USERS

21. ABSTRACT SECURITY CLASSIFICATION

Unclassified

22a. NAME OF RESPONSIBLE INDIVIDUAL

Dr. John F. Tangney

22b. TELEPHONE (Include Area Code)

202/767-5021

22c. OFFICE SYMBOL

NL

DISCLAIMER NOTICE



THIS DOCUMENT IS BEST QUALITY AVAILABLE. THE COPY FURNISHED TO DTIC CONTAINED A SIGNIFICANT NUMBER OF COLOR PAGES WHICH DO NOT REPRODUCE LEGIBLY ON BLACK AND WHITE MICROFICHE.

New York University
A private university in the public service

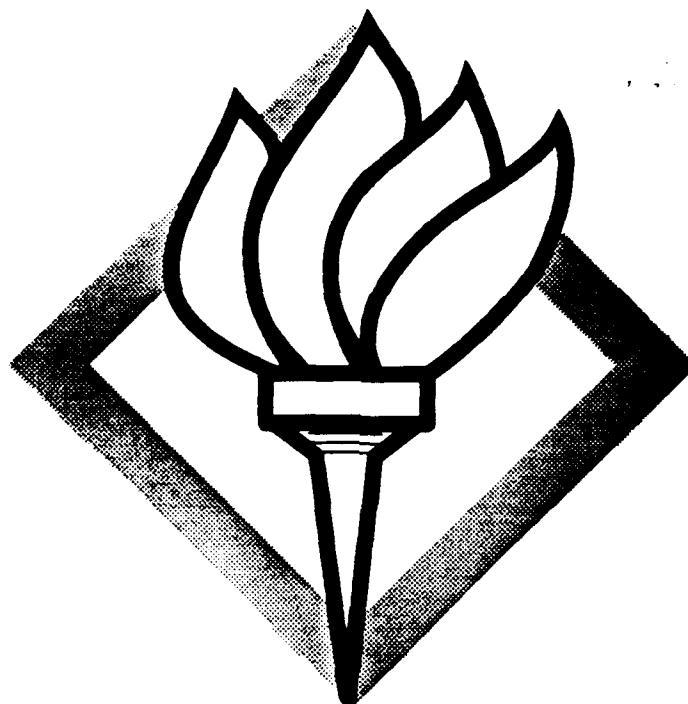
Neuromagnetism Laboratory
Departments of Physics and Psychology
and Center for Neural Science

Accession For	
NTIS Grant	<input checked="" type="checkbox"/>
DTIC TAB	<input type="checkbox"/>
Unannounced	<input type="checkbox"/>
Justification	
By	
Distribution/	
Availability Codes	
Dist	Avail and/or Special
A-1	

ANNUAL TECHNICAL REPORT

Cognition and the Brain

15 February 1991 - 14 February 1992



Samuel J. Williamson and Lloyd Kaufman
Principal Investigators

Prepared for:

Dr. John F. Tangney
Directorate of Life Sciences
Air Force Office of Scientific Research
Bolling AFB, DC 20332

Approved by:


Samuel J. Williamson


Lloyd Kaufman

92-15697



11988

20 MAY 1992

Contents

1	Introduction	3
2	Overview	3
3	Highlights of the Results	5
4	Publications	7
5	Personnel	8
5.1	Faculty	8
5.2	Collaborating Faculty	8
5.3	Research Scientists	8
5.4	Collaborating Researcher	8
5.5	Graduate Research Assistants	8
5.6	Degrees Awarded	8
6	Interactions with Other Groups	9
6.1	8th International Conference on Biomagnetism	9
6.2	Invited Talks given by Members of the Laboratory	9
6.3	Contributed Presentations	10
7	Inventions and Patent Disclosures	10

1 Introduction

This report, which is submitted in accord with the requirements of Contract AFOSR-90-0221 between Air Force Office of Scientific Research and New York University, summarizes the scientific progress made during the past year of grant support, from 15 February 1991 to 14 February 1992. As characterized in our statement on "Progress and Forecast" of research submitted in February, 1991, the emphasis in this research is to reveal the role of changing levels of spontaneous activity of neocortex that accompanies higher cognitive functions. Event-related potentials and fields have been useful in revealing sensory processes and their interactions, and effects of processes like attention, expectancy, and incongruity on the sequelae time-locked to the sensory evoked response. This newer approach deals instead with phenomena that are not time-locked to ERPs or ERFs, but are still consequences of brain processes initiated by events in the environment. As such it is complementary to the sensory approach, and the results achieved thus far prove that suppression of spontaneous activity recorded in the alpha band is not merely the result of changing levels of arousal or attention, and cannot be ascribed to differences among physical stimuli.

In parallel with these studies, we developed a novel method to determine the pattern of neuronal activity distributed across cerebral cortex that best accounts for a measured magnetic field pattern. We showed that this method provides a *unique* estimate, thereby circumventing the accepted dogma that says there is no unique solution for the magnetic inverse problem. Moreover, we were able to generalize this approach to provide a unique estimate for the cortical map of average neuronal current power from measurements of the average field power obtained over the scalp. From this we developed a method to compute the cortical map of average current power suppression. In short, it is now feasible to extend the present studies of field power suppression across the scalp to determine precisely where the corresponding spontaneous cortical activity is being suppressed. In this way it will be possible to identify the three-dimensional locations where cortical activity is suppressed during cognitive tasks. This introduces a new form of magnetic source imaging (MSI).

2 Overview

The overall theme of this research is to exploit the advantages of magnetic source imaging to elucidate the physiological basis for human cognitive functions. Specifically, four main areas of research were successfully completed during the past year:

(1) An investigation of cortical activity when subjects scan memory for tones demonstrates for the first time that auditory areas in the right and left hemisphere differ in their participation during memory scanning. Moreover, the duration of suppression of spontaneous activity in the right hemisphere correlates significantly with reaction time identifying whether or not a probe tone was a member of the memory set. These results have been published as a comprehensive paper in *Electrophysiology and clinical Neurophysiology* [1].

(2) A study of the difference in cortical participation for tasks of mental imagery and silent

rhyming reveal clear differences in timing of the onset of suppression and also the offset of suppression were observed over visual and anterior temporal areas for these different tasks. The results demonstrate that alpha suppression may be taken as a sign of enagement of these different part of the brain in specific cognitive tasks, just as blood flow serves as a similar index of activation in PET studies. A paper has been submitted for publication [2].

(3) In collaboration with Dr. Christoph Michel, supported by the Swiss National Science Foundation, we employed the alpha suppression technique and the Cooper and Shepard paradigm to determine how the duration of alpha suppression varies with rotation angle of the probe figure. A clear increase in duration with increasing angle between probe and target figures could be seen. These data are being analyzed to determine whether it is possible to distinguish differences in onset and offset times between spontaneous activity arising from visual cortex as compared with the parieto-occipital sulcus [3].

(4) Development of the 'Pointer' method providing high-accuracy alignment of a magnetic resonance image (MRI) of cortical anatomy with a magnetic source image (MSI) of cortical function. These results were published in Brain Topography [4].

(5) Conception and implementation of a computational method to characterize the distribution of intracellular cortical current from measurements of the extracranial field pattern. This minimum-norm least-squares estimation provides a unique description that best-accounts for the data. A comprehensive paper of this 'MNLS' inverse has been accepted for publication [5].

(6) Development of an extension of the MNLS inverse to image regional changes in the spontaneous activity of the brain. This provides a unique estimate for the distribution of intracellular current power across the cerebral cortex. By comparing the inverses with and without the presence of alpha-band suppression it is possible to deduce the distribution of current power suppression as well. A manuscript describing this technique and simulations employing it has been accepted for publication [6].

3 Highlights of the Results

This research program has accomplished the following objectives:

- Developed a method for accurate registration of anatomical and functional images of the brain. The method is applicable for most of the imaging modalities now being employed in sensory and cognitive studies. By recording three sets of imageable pointers when a MRI image is recorded, each directed toward a cardinal landmark on the subject's head, MRI pixels can be specified by cartesian coordinates of the same head-based system as used for neuromagnetic recordings. The accuracy in locating these landmarks is limited by how accurately the pointers are placed on the head for MR recordings. Each "point" indicated by a pointer is located by computer analysis of MR images with an accuracy of better than 0.5 mm.
- Obtained the first evidence that auditory cortex participates in the process of scanning working memory and determined when it is involved during a task based on the Sternberg paradigm. For three subjects, the duration of alpha-band suppression measured over the right hemisphere increases linearly with memory set size, as does the reaction time for task completion. The left hemisphere shows a similar but weaker tendency for right-handed subjects. The pattern of alpha suppression across the right hemisphere of the scalp is significantly correlated with the pattern of the magnetic field associated with the N100 response component, thus indicating that auditory cortex contributes to this alpha rhythm.
- Established the feasibility of monitoring the period when visual cortex is engaged in manipulating mental images. By employing the paradigm of Cooper and Shepard, it was possible to observe suppression of alpha-band activity over the occipital and parietal regions of the scalp as a subject compared an object just seen with an object previously seen to determine whether they differ or whether they are the same but rotated with respect to each other. Measurements of alpha-band activity over the posterior scalp revealed certain positions where suppression was observed and the duration of suppression was comparable to the reaction time. In these areas the duration of suppression increased monotonically with rotation angle, with identical values for clockwise and counterclockwise senses of rotation. Simultaneous measurements of the EEG with electrodes attached to the scalp showed similar features for the voltage between certain pairs of electrodes. These findings suggest it will be possible to localize the anatomical substrate of the visual area where the suppression takes place.
- Developed a mathematical approach based on lead field theory to obtain a unique estimate for the spatial pattern of cortical activity giving rise to a measured magnetic field pattern. Thus, for the first time, it is possible to represent distributed neuronal activity without having to impose restrictive models, such as a current dipole or several dipoles. The "magnetic source image" is called the minimum-norm least-squares estimate", or MNLS estimate. This image is robust with respect to the presence of noise in the recordings. It is also insensitive to errors in determining the location of the surface of cerebral cortex where it is represented.

- Extended the MNLS estimate to provide an estimate for the distribution of cortical activity that gives rise to a measured pattern of average magnetic field power. This generalized image characterizes the covariance pattern of activity across the cortical surface. In particular, it also describes the spatial distribution of mean intracellular current power. With this approach it is possible to determine for the first time the cortical locations where spontaneous neuronal activity is suppressed. This has obvious relevance to the studies of alpha suppression that are being carried out in this laboratory's research program. In this way it will be possible to identify the sequence of cortical areas where spontaneous rhythms are suppressed during cognitive tasks.

4 Publications

This section lists the papers that report the scientific and technical research carried out during the past year.

- [1] L. Kaufman, S. Curtis, J.-Z. Wang, and S.J. Williamson. Changes in cortical activity when subjects scan memory for tones. *Electroenceph. Clin. Neurophysiol.*, 82:266-284, 1991.
- [2] L. Kaufman, Y. Cykowicz, M. Glanzer, and S. J. Williamson. Selective suppression of spontaneous cortical rhythms for cognitive tasks of imaging and rhyming. *J. Exp. Psychol.: General*, submitted, 1991.
- [3] C. M. Michel, L. Kaufman, and S. J. Williamson. Effects of a mental rotation task on the suppression duration of EEG and MEG occipital alpha rhythm. in preparation, 1992.
- [4] S. J. Williamson, Z.-L. Lü, D. Karron, and L. Kaufman. Advantages and limitations of magnetic source imaging. *Brain Topography*, 4:169-180, 1991.
- [5] J.-Z. Wang, S. J. Williamson, and L. Kaufman. Magnetic source images determined by a lead-field analysis: the unique minimum-norm least-squares estimation. *IEEE Trans. Biomed. Engr.*, in press, 1992.
- [6] J.-Z. Wang, L. Kaufman, and S. J. Williamson. Imaging regional changes in the spontaneous activity of the brain: an extension of the unique minimum-norm least-squares estimate. *Electroenceph. Clin. Neurophysiol.*, in press, 1992.

5 Personnel

5.1 Faculty

Lloyd Kaufman, Ph.D., Professor of Psychology and Neural Science, Adjunct Professor of Physiology and Biophysics.

Samuel J. Williamson, Sc.D., University Professor, Professor of Physics and Neural Science, Adjunct Professor of Physiology and Biophysics.

5.2 Collaborating Faculty

Murray Glanzer, Ph.D., Department of Psychology

5.3 Research Scientists

Sarah Curtis, Ph.D., Assistant Research Scientist (Psychology)

Jia-Zhu Wang, Ph.D., Associate Research Scientist (Physics)

5.4 Collaborating Researcher

Christoph Michel, Research Assistant, Neurological Clinic, University Hospital of Zürich, Switzerland

5.5 Graduate Research Assistants

Yael Cycowicz, Ph.D. student, Department of Psychology

Daniel Karron, Ph.D. student, Department of Applied Science

Zhong-Lin Lü, Ph.D. student, Department of Physics

5.6 Degrees Awarded

Yael Cycowicz, Ph.D. in Psychology

Bruce Lubner, Ph.D. in Psychology

6 Interactions with Other Groups

6.1 8th International Conference on Biomagnetism

S.J. Williamson was Chairman of the Advisory Committee for this international conference and was a member of the Program Committee. L. Kaufman was an invited speaker at this conference.

6.2 Invited Talks given by Members of the Laboratory

- Mar 13 *Advances in Superconducting Instrumentation for Neuromagnetism* Extending our View from Physiology to Cognition." IEEE Engineering in Medicine and Biology Society, New York Metropolitan Area Division, Rockefeller University.
- Mar 19 *Functional Organization of the Human Brain Determined Magnetically.* Symposium of the Division of Biological Physics entitled "Neuromagnetism ~ From the Microscopic to Macroscopic", American Physical Society Meeting, Cincinnati, Ohio, March 18-22.
- May 21 *Magnetic Source Imaging.* Lead Speaker for Technology Applications Symposium: Technology Requirements for Biomedical Imaging, sponsored by Georgetown University Medical Center, American Medical Association, and Strategic Defense Initiative of Department of Defense, Washington, DC., May 21-22.
- May 29 *Magnetic Source Imaging of Human Cortical Activity.* Neurons, Vision, and Cognition. An International Symposium at New York University, New York City, May 28 - June 1.
- Aug 4 *Advantages and Limitations of Magnetic Source Imaging.* 3rd Congress of the International Society for Brain Electromagnetic Topography, Toronto, Canada, July 29 - August 1.
- 18 Aug *From Benchmark to Discovery: An Historical Perspective.* Plenary Address, 8th International Conference on Biomagnetism, Münster, Germany, August 18-24, 1991.
- Oct 25 *Human Auditory Primary and Association Cortex have Differing Lifetimes for Activation Traces.* Körber Foundation Symposium, Helsinki University of Technology, October 24-25.
- Nov 1 *Magnetic Source Imaging of Human Brain Functions.* Advances in Magnetic Imaging in Medicine. A Symposium Honoring Richard B. Mazess, Department of Medical Physics, University of Wisconsin, Madison, WI.
- Nov 20 *Magnetic Measures of Activity in Auditory Cortex.* Symposium on "Objective Methods for Hearing Assessment", New York Academy of Medicine, New York City, sponsored by IEEE Sections on Biomedical Engineering and Otolaryngology and the New York State Section, Engineering in Medicine and Biology Society of the Institute of Electrical and Electronic Engineers.
- Nov 21 *Magnetic Source Imaging of the Human Brain.* Colloquium, Department of Physics, University of Florida, Gainesville, FL.
- Dec 6 *Magnetic Source Imaging of the Human Brain.* Keynote address at the Inaugural Symposium celebrating the opening of the Superconducting Sensor Laboratory, sponsored by the Ministry of International Trade and Industry, Tokyo, Japan.
- Dec 11 *Magnetic Source Imaging of the Human Brain.* Margaret and Herman Sokal Faculty Award in the Sciences, NYU.

6.3 Contributed Presentations

Changes in Cortical Activity When Subjects Scan Memory for Tones

L. Kaufman, S. Curtis, J.-Z. Wang, and S.J. Williamson

7th International Conference on Biomagnetism, August, 1991, Münster, Germany.

Neuronal Sources of Human Parieto-Occipital Alpha Rhythm

Z.-L. Lü, J.Z. Wang, and S.J. Williamson

7th International Conference on Biomagnetism, August, 1991, Münster, Germany.

Latent Neuronal Activity in Human Auditory Cortex. (Slide presentation)

Z.L. Lü, S.J. Williamson, and L. Kaufman

Society for Neuroscience Annual Meeting, New Orleans, LA, Nov. 10-15, 1991.

Lifetimes of Activation Traces in Human Auditory Cortex

S.J. Williamson

Seventeenth Annual Interdisciplinary Conference

Teton Village, Jackson, Wyoming, Jan 15, 1992.

7 Inventions and Patent Disclosures

This program of research was not directed toward producing inventions. However, the minimum-norm least-squares (MNLS) estimation for obtaining a unique solution for the magnetic inverse problem was deemed of possible interest for protection, and NYU provided a small grant to help in its further development. However, after some investigation, there was insufficient commercial interest that the Office of Industrial Liaison of New York University decided not to proceed with a patent application.

EEG 91007

Changes in cortical activity when subjects scan memory for tones

L. Kaufman ^a, S. Curtis ^a, J.-Z. Wang ^b and S.J. Williamson ^b

Departments of ^a Psychology and ^b Physics, and Center for Neural Science, New York University, New York, NY 10003 (U.S.A.)

(Accepted for publication: 6 September 1991)

Summary The magnetoencephalogram (MEG) was used to detect regional changes in spontaneous cortical activity accompanying short-term memory search. This method was chosen because magnetic fields are detectable only within a few centimeters of the projections of their sources onto the scalp. The specific hypothesis that auditory cortex is involved in scanning memory for tones was tested by sensing the field of the the magnetic counterpart to N100 (N100m) which is known to originate in auditory cortex. N100m was measured at many different positions and the spontaneous cortical rhythms in the alpha bandwidth (8-12 Hz) were measured at the same places. These rhythms were found to be suppressed while subjects scanned memory for musical tones in a Sternberg paradigm. For 3 subjects, both the MEG suppression time (ST) and reaction time (RT) increased linearly with memory set size. The correlation between ST measured over the left hemisphere and set size was significant for two subjects but not significant for the third, and the slopes of the regression lines relating ST to set size were too shallow to be related to the time required to scan memory. However, the correlation between ST of the right hemisphere and set size was highly significant for all subjects, and the slopes of the regression lines were comparable to those relating RT to set size. The electroencephalogram (EEG) recorded with midline electrodes failed to reveal a significant relationship between suppression time and set size for 2 of the subjects, thus ruling out global alpha blockage and generalized arousal as the basis for the task-related suppression duration. The electric N100, measured at Cz, decreased significantly in amplitude with set size for 2 subjects, but it increased significantly in amplitude for the third subject. In contrast, RT increased with set size for all subjects. N100m measured over the right hemisphere was similar to the behavior of N100, while N100m measured over the left hemisphere showed little change in amplitude with set size, thus establishing an asymmetry in N100 between the hemispheres. Since N100 amplitude is normally larger when attention is paid to auditory stimuli, differential attention alone cannot account for the relation between ST and set size. Furthermore, the processing negativity, which may be superimposed on N100 in selective attention tasks, was not discernible for any set size. It was also found that ST prior to the button press was not correlated with RT. Hence, the covariation of set size with ST is not attributable to preparation for a motor response. In this experiment the sensors were placed where the field of N100m was approximately at its maximum value. Since many measures were made from somewhat different positions in these areas, it was possible to determine how N100m amplitude varied with sensor location over both hemispheres. These position-dependent changes in N100m amplitude were significantly correlated with corresponding position-dependent changes in percent suppression of the spontaneous MEG. Thus, auditory cortex contributes significantly to the spontaneous alpha activity suppressed during memory search. It is concluded that regional changes in cortical spontaneous activity are meaningfully related to ongoing memory scanning.

Earlier work on the relation between short-term memory and the N100 and P300 ERP components is reviewed in an Appendix. It is concluded that published conjectures on the relation between N100 and short-term memory are inconclusive, and neither P300 latency nor amplitude have been convincingly related to short-term memory scanning *per se*. These ERP components are complementary to the regional changes in spontaneous activity studied here, and reflect different facets of the processes involved in memory scanning.

Key words: Alpha; Magnetoencephalogram; Local suppression; Short-term memory; N100

In the classic Sternberg (1966) experiment a subject views or listens to a sequence of items ranging from 1 to as many as 7 in length. Then, 2 sec later, is exposed to a "probe" item and asked to press one button if the probe had been a member of the memory set, and another if it had not. As Sternberg demonstrated, reaction time (RT) increases linearly with the size of the memory set being searched by subjects. Also, RT increases with set size at approximately the same rate

for "new" probes (those that had not been members of the set) as for "old" probes (those that had been members of the set). Sternberg accounted for these results by postulating a serial and exhaustive search of short-term memory. This is predicated on the assumption that RTs of well-trained subjects who perform in a nearly error-free manner are not dissociated from the process of searching memory. Given this same assumption, we test the hypothesis that regional fluctuations in the brain's spontaneous activity accompany the scanning of short-term memory and reflect ongoing cognitive processes. The main advantage in adopting this approach to short-term memory is that many hundreds of papers have been devoted to the Sternberg paradigm,

Correspondence to: Lloyd Kaufman, Professor of Psychology and Neural Science, New York University, 6 Washington Place, New York, NY 10003 (U.S.A.)

and the conditions under which its main effects occur are well understood. Despite criticisms of Sternberg's theory that memory search is both serial and exhaustive, his basic results are well established and documented. The basic assumption that RT is not dissociated from processing time is shared even by investigators who question the theory. Therefore, Sternberg's paradigm is extremely useful in psychophysiological investigations.

Spontaneous activity and memory scanning

The work of Mishkin (1982), Ungerleider and Mishkin (1982), and Ungerleider and Desimone (1986) indicate that many areas of neocortex, including the sensory projection areas, are involved in memory. This is reflected in a rough "schematic" or "circuit" representing the "anatomy of memory," in which the sensory area transmits information to hippocampus/amygdala, thence to the diencephalon, to the prefrontal cortex, to the basal forebrain, and then back to the sensory area. Although based on monkey, this map parallels that generated by the less complete data offered by human clinical cases. Behavioral evidence that short-term memory may be modality-specific (Murdoch and Walker 1969) is consistent with this view, since it implies that working (short-term) memory involves sensory areas of neocortex. Similarly, some theorists suggest that the machinery of the visual system is actively involved in mental rotation — a form of imagery in which mental operations are performed on objects that may be present only in working memory (cf., Kosslyn 1983; Finke and Shepard 1986).

Direct evidence that different areas of neocortex are involved in short-term memory *per se* is difficult to find. Regional blood flow studies employing positron emission tomography (PET) reveal local differences in levels of cortical activity, depending upon the nature of mental tasks (cf., Petersen et al. 1989). However, the coarse temporal resolution afforded by PET (~40 sec) proscribes identifying regions specifically involved in searching short-term memory. The experiment described in this paper was specifically designed to make use of the MEG in determining if neocortex is indeed active while subjects scan short-term memory.

A major assumption underlying the work described here is that regional differences in levels of brain activity occur during the performance of various mental tasks. This assumption is shared by PET blood flow studies, where different levels of blood flow are assumed to reflect different levels of brain activity (Petersen et al. 1989). It is also consistent with the work of Pfurtscheller (1988), Pfurtscheller and Aranibar (1978, 1979), and Klimesch et al. (1988) who found

that power in the alpha band between 8 and 13 Hz showed a sharp reduction (*event-related desynchronization*) subsequent to visual stimulation as well as voluntary motor acts. Their method is similar to one devised by Kaufman and Price (1967) to study modulation of high-frequency EEG by visual stimuli, and by Kaufman and Locker (1970) to study effects of attention on visual modulation of alpha activity. The only difference between these methods is that Kaufman et al. measured the variance around the average response remaining within the EEG after it was filtered, while Pfurtscheller et al. included the residual average response in their measures. The work of Pfurtscheller and his colleagues strongly suggests that regional changes in the level of the brain's spontaneous activity reflect ongoing cognitive processes. The main reason for using the MEG rather than the EEG is that the latter is often difficult to interpret. The intracranial sources of potential differences at the scalp may be a large distance away. By contrast, because the magnetic fields of neural sources fall off very sharply with distance, their maximum extracranial fields are detectable only over a relatively confined area at the scalp. In the case of cortical sources, sensors placed near field extrema are only a few centimeters away from the scalp projections of their sources. Ambiguity is reduced by the fact that the MEG is a truly monopolar measure, i.e., it does not need the equivalent of a "reference electrode," which contributes to the uncertainty about locations of sources of EEG phenomena.

To exploit this advantage of the MEG, Kaufman et al. (1990) measured the variance (power) about the event-related field (ERF) within the alpha band of the MEG while subjects engaged in a mental imagery task. The subjects were presented with a memory set composed of 3 abstract polygons. Three seconds later, a fourth abstract polygon (the *probe*) was shown. Subjects then responded as instructed for either a *simple RT* condition or a *choice RT* condition. In the simple RT condition they pressed a button as soon as they saw the probe (without regard for whether it had been a member of the memory set). In the choice RT condition they pressed one button if it had been a member of the set or another button if it had not been a member of the set. Naturally, in the choice RT condition the reaction time (RT) was much longer than in the simple RT condition. The power in the alpha band (8–12 Hz) of the spontaneous MEG was markedly reduced after presentation of the probe, and this activity continued to be *suppressed* until the memory search task was completed. The duration of suppression of spontaneous alpha band activity was highly correlated with the RTs in both the simple and choice conditions. It was concluded that searching memory for visual forms is associated with a temporally commensurate reduction in spontaneous brain activity. The suppres-

sion across the parietal and occipital areas of the scalp was markedly enhanced over the midline. Again, because the extracranial field is close to the surface projection of its source, this indicates that the suppressed activity originates in the visual areas of the brain. A control condition involving the searching of memory for visually presented words (as opposed to nonsense forms) revealed no difference in the duration of suppression between simple and choice RT conditions when the MEG was recorded over the visual areas, although the simple task results in a dramatically shorter RT than the choice, with the RTs being about the same for the corresponding simple and choice tasks involving the visual forms.

These results imply that visual cortex is actively engaged in searching visual memory. By extension, other regions of neocortex may be involved when scanning working memory for non-visual "items." Thus, the distribution of cortical activity following visual presentation of verbal stimuli could depend upon the nature of the task the subject is asked to perform in response to stimuli. For example, subjects could be asked to respond to words by forming mental images. In this case the visual areas could become active. However, if asked to respond to the same words by searching memory to find rhyming words, then speech areas could become more active.

Kaufman et al. (1989) actually performed this experiment and found that when subjects form mental images of objects represented by words flashed on a screen, the pattern of the brain's extracranial magnetic field differed from the pattern associated with performing a verbal task using the same words. The two tasks (one involving mental imagery and the other involving rhyming) were equated for difficulty. More specifically, the occipital MEG in the 8–12 Hz band exhibited a period of suppression that began when the word was presented and had a duration that was significantly correlated with the time it took for subjects to report that they had completed forming the mental image. Although finding a rhyming word in memory took the same average amount of time, the duration of the suppression of the occipital MEG was much shorter, and was the same as that associated with flashed and passively viewed nonsense words. This suggested that forming a mental image involves the visual areas, but completing a verbal task involves still other portions of cortex. In subsequent work (Kaufman et al. 1991a) it was found that activity measured over the fronto-temporal area — particularly of the left hemisphere — exhibits a similar RT-related increase in suppression duration when the verbal task is performed, but not when the nonsense word was viewed passively. Therefore, as is the case for PET blood flow indicators, changes in patterns of spontaneous cortical activity do occur when subjects perform functionally different

mental tasks, even when the tasks are initiated by similar sensory stimuli.

The foregoing considerations motivated this first full use of the Sternberg paradigm to study the relation between short-term memory scanning and the spontaneous activity of the brain. In this paper we describe an experiment designed to test the hypothesis that increases in RT with memory set size are reflected in the duration of local changes in level of spontaneous activity of neocortex. More specifically, we tested the hypothesis that spontaneous activity arising in auditory cortex is suppressed when subjects scan memory for previously heard musical tones, and this suppression is correlated with processing time as indicated by reaction time.

Method

Two young adult female subjects (GK and FK) and one male (AM) subject listened to memory sets composed of one, 3 or five 200 msec long musical tones presented sequentially 300 msec apart and then, 2 sec later, to a probe tone. The probe had a 50% chance of being a member of the previously heard memory set. The task was to press one button if the probe had been a member of the memory set, and another button if it had not been a member of the set. Subjects were given 20 trials for each memory set, and this was repeated at least ten times over each hemisphere for each subject.

The musical tones were generated by an Amiga 1000 computer and presented via a loudspeaker placed at a porthole in the wall of a magnetically shielded room. The particular tones heard by the subjects were drawn from a pool of 16 musical notes ranging in pitch from 311.13 Hz to 739.99 Hz. All subjects were given as many practice sessions as they needed to insure that their performance accuracy was at least at the 95% level before embarking on the main experiment.

The subjects were placed on a kneeling stool inside the shielded room. With their foreheads and arms resting on padded supports, they listened to the stimuli and then, after presentation of the probe, depressed one of two buttons to indicate if the probe had been "old" or "new." The buttons were pressed with the right hand when neuromagnetic fields were recorded over the right hemisphere, and with the left hand when the fields were recorded over the left hemisphere. This was to prevent contamination of the recordings by activity of motor cortex in the hemisphere contralateral to the hand being used.

RT, which is the time between probe presentation and the button press, was measured while the subject's EEG and MEG were being recorded. For all subjects active electrodes were placed at Cz and Oz, and for the third subject (FK) at Pz and Fz as well. A reference electrode was placed on the right mastoid. The EEG

was recorded with a Grass Model 12 Neurodata Acquisition System located inside the shielded room. The recording bandwidth was between 0.01 and 100 Hz with rolloffs at 6 dB/octave. The outputs of the Grass were applied to the data acquisition unit of a Hewlett Packard 9000-350 computer located outside the shielded room.

The MEG was recorded using a 5-channel neuromagnetometer, which is fully described elsewhere (Williamson et al. 1984). The 5 sensors are located within a fiber glass cryogenic vessel (dewar) where they are immersed in liquid helium. The detection coils of the sensors are second-order gradiometers 1.5 cm in diameter and 4 cm baseline. One coil is in the center of the tail section of the dewar and the other four arranged around it in a circular pattern, with 2 cm radius. The bottom of the tail section has a 9 cm radius of curvature, so that all five of the coils can be placed with axes nearly radial to the scalp. The lowest coil of each gradiometer is then 1.3 cm from the scalp, owing to the thickness of the dewar. With this geometry it is possible to measure the field normal to the scalp at 5 different places 2 cm apart.

In the main experiment no attempt was made to map the entire field distribution around the head. Earlier experiments (Pelizzone et al. 1984; Curtis et al. 1988) and extensive pilot work had already revealed the approximate locations of the field extrema associated with the *N100m* component of the auditory evoked field. In the coordinates of the 10–20 system, one extremum over the left hemisphere is about 2 cm below the line connecting F7 and T3, and the other about 2 cm above T5, toward the vertex. Similarly, over the right hemisphere the extrema are below the line connecting F8 and T4, and above T6. In the experiment the neuromagnetometer was placed with its center pick-up coil about 2 cm above either T5 or T6 to insure that one of the coils would be at or near the field extremum. Thus, on alternate blocks of trials, the dewar was placed over the left and right hemispheres where it was certain that strong *N100m* responses would be recorded despite small changes in the positions of the pick-up coils from one block of trials to another.

The voltage outputs of the superconducting electronics of the neuromagnetometer are proportional to the field (in femtotesla (fT)) linking the pick-up coils. These outputs were first applied to analog filters set to pass activity between 0.1 and 50 Hz, and then to the same data acquisition unit of the 9000-350 computer as was used in recording the EEG data. Other inputs to the unit included the outputs of the two buttons used to record RT, and signals from the Amiga computer indicating time of presentation of memory set and probe tones, as well as whether the probe tone was new or old.

Subjects were presented with 3 sets of trials, corresponding to memory set sizes 1, 3 and 5, with the dewar over one hemisphere. After completion of the 3 sets, the dewar was moved to the opposite hemisphere. This was repeated until at least 10 complete blocks of trials were measured over each hemisphere. Throughout all of the blocks of trials, the EEG was recorded with midline electrodes insuring the accumulation of a large number of epochs for each set size.

After the EEG and MEG data were acquired, they were digitally filtered within 4 different passbands, to create 4 different records. The passbands were 1.0–40 Hz, 0.2–40 Hz, 8–12 Hz, and 16–24 Hz. These data were then averaged using the onset of the probe tone as the temporal reference signal. The epoch began between 6.5 and 4.5 sec prior to presentation of the probe, depending upon the size of the memory set, and terminated 4.5 sec after probe onset. A new memory set began 1 sec after the end of the epoch.

The 1–40 Hz record was used to compute the average response to the probe and to verify the presence of the *N100* and *N100m* in the EEG and the MEG. The high-pass of 1 Hz was used to reduce the contribution of any low-frequency baseline shift commensurate in duration to the time needed to scan memory. Also, the amplitudes of the electric and magnetic *N100* component were recorded as a function of set size for both the new and the old probes. To maximize the effect of any processing negativity on the amplitude of *N100* and *N100m*, the same computation was performed using the 0.2–40 Hz bandpass.

The average response was also computed using the 8–12 Hz (alpha band) record, and the variance about that response was used as a measure of the power within the spontaneous alpha band activity of the MEG and the EEG. Plotting the smoothed alpha power shows how the level of this background activity varies with time and as a function of set size (Kaufman et al. 1990). An identical procedure was applied to the same data after it was bandpassed between 16 and 24 Hz, to capture any differential effects in the beta band of the EEG and MEG.

In determining how alpha power varies as a function of time, the averaging was performed with the onset of the probe as a reference trigger. To test the hypothesis that systematic changes in these plots may be due to a change in level of alpha accompanying readiness to make a motor response, the same activity was averaged backward using the button press rather than the probe as the reference trigger.

Results

Basic behavioral data

To insure that the electric and magnetic measures reflect the processes actually involved in performing

TABLE I

Reaction time (RT) versus memory set size (MSZ). The slopes (in sec/item) of regression function relating RT to MSZ are given in column 1 for RTs obtained with "old" probes and with "new" probes. Column 3 contains the Pearson product-moment coefficients of correlation between RT and MSZ for all subjects. All correlations are highly significant (column 3). Column 4 contains the values of t resulting from comparing the slopes of the regression functions. The slopes of new and old probe regression functions all differ significantly, with $P < 0.0001$.

Reaction time vs. memory set size	Slope	Corr. coef.	Sig. level	t test	df
AM old	0.15	0.56	0.0001	25	376
AM new	0.11	0.59	0.0001		
GK old	0.13	0.54	0.0001	65	486
GK new	0.06	0.28	0.0001		
FK old	0.13	0.48	0.0001	115	1326
FK new	0.07	0.28	0.0001		

the Sternberg task, we first examine the behavioral (RT) data and will then compare it with the physiological data. Fig. 1 summarizes the way in which RT varied as a function of memory set size (MSZ). The regression lines relating RT to MSZ for old and new probes are shown for the 3 subjects. As in Sternberg's original experiments, the correlations are high and significant, implying a linear relationship between set size and RT. However, a t test on two independent samples for the differences between slopes for old and new items for each subject shows the differences between them to be highly significant (Hayes 1981). The values of these slopes (in sec/item) are shown in Table I. For all subjects the scan rate is faster for new probes than for

old. Since the acoustic stimuli differed in some cases by more than an octave in pitch, on some "new" trials the probe was very different in apparent pitch from any member of the memory set. Hence, on those trials subjects could react solely to the relatively unique pitch of the new probe and assume that it had not been a member of the set. This seems to be a likely cause of the difference in slopes. Therefore, the slopes associated with the old probe are assumed to be more accurate indicators of memory scan rate than those associated with new probes. Averaging the slopes for old probes across subjects indicates that subjects scanned memory for tones at an average rate of about 138 msec/tone. Overall, the average scan rate for both old and new probes was 109 msec/item. We may now compare these data with those obtained using the MEG and the EEG.

Effects of memory scanning on the electric N100 and the magnetic N100m

For reasons considered in the Appendix to this paper, Picton et al. (1978) and Näätänen (1982, 1986) suggested that N100 and related ERP components may reflect short-term memory processes. Therefore, before turning to the effects of memory scanning on the spontaneous MEG, let us consider the N100 component of the ERP. As described earlier, the EEG was bandpassed between 1 and 40 Hz and between 0.2 and 40 Hz prior to averaging. This permitted the recovery of N100 at Cz with a bandwidth wide enough to insure detection of the processing negativity (0.2–40 Hz), and also with the processing negativity, if any, attenuated

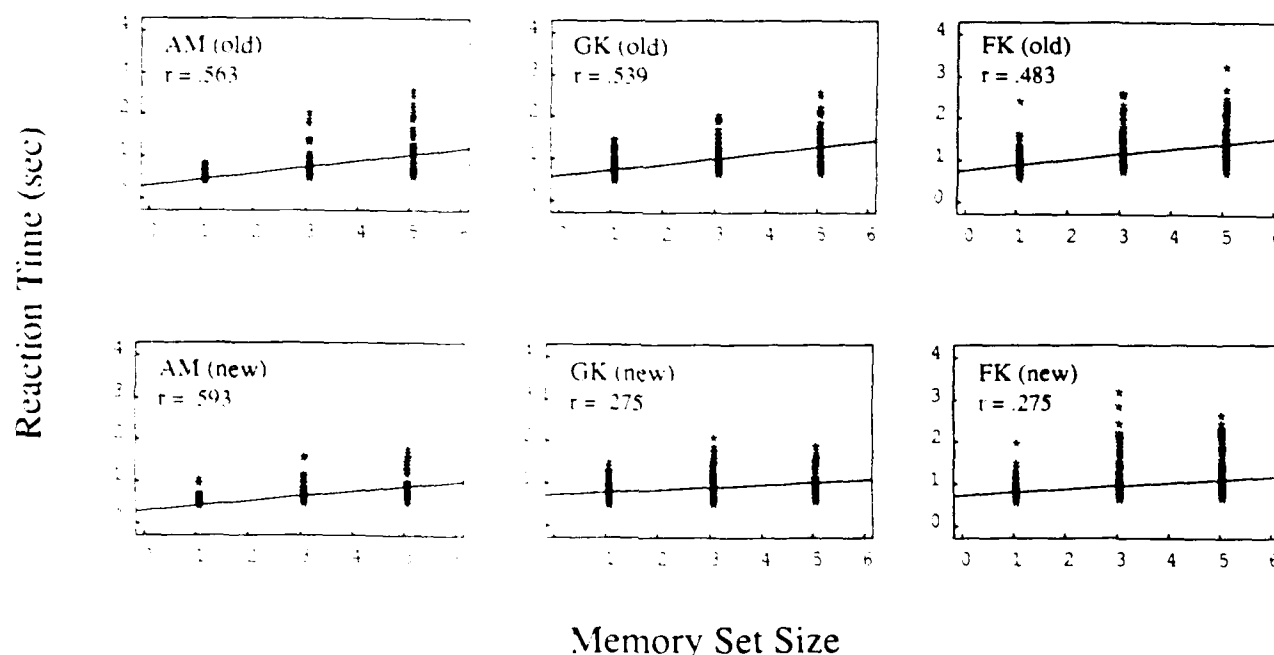


Fig. 1. Reaction time (RT) versus memory set size (MSZ) for subjects AM, GK and FK. RT vs. MSZ for old and new probe are plotted separately. Pearson product moment coefficients of correlation (r) are presented in each graph.

by the filter (1–40 Hz). Visual inspection of the resulting wave forms in the EEG failed to reveal any greater early negativity in the responses derived from the 0.2–40 Hz data. A sample N100 response filtered using the two bandwidths is shown at the bottom of Fig. 2. N100 was essentially the same in the 1–40 Hz record as in the 0.2–40 Hz record and there was no obvious increase in baseline negativity superimposed on N100 in either case. This was true of responses obtained with all set sizes.

While 20 trials per set size were recorded in each block of trials, the electrodes were kept at the same positions from one block of trials to another. Conse-

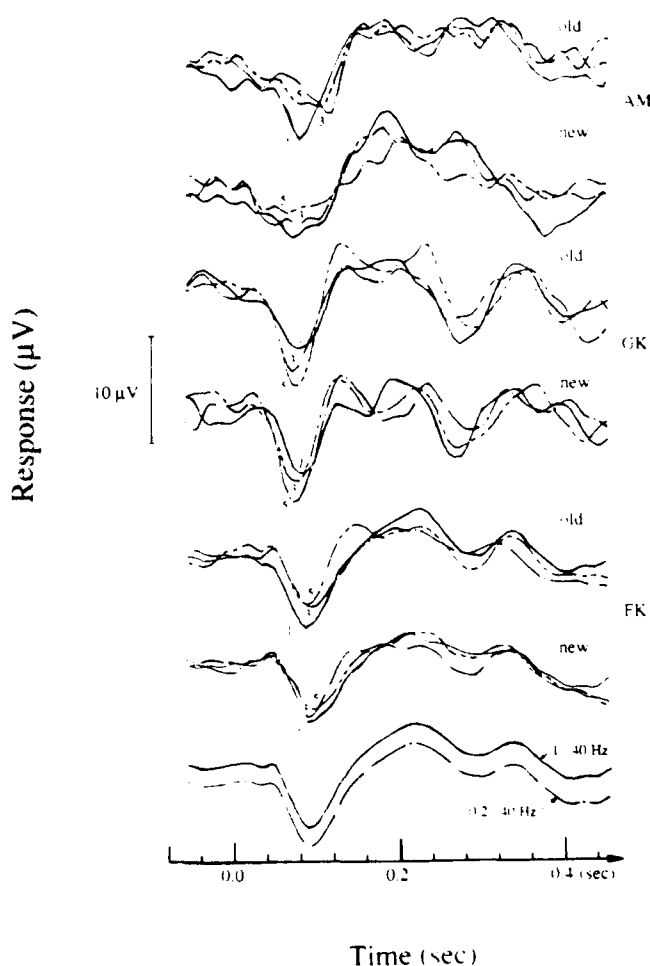


Fig. 2. Average N100 recorded at vertex for each of 3 subjects (AM, GK and FK). The numerals associated with each trace represent the set size prior to the probe stimulus to each of the N100s. Responses to old and new probes are shown separately. Negativity is downward, and N100 peaks approximately 100 msec after 0.0 on the x-axis, which is the onset time of the probe. N100 amplitudes associated with old and new probes decrease as set size increases for AM and FK. However, for GK the N100 amplitudes increase with set size for both old and new probes. The bottom two traces are sample responses (subject FK) after digital filtering within two different passbands (0.2–40 Hz and 1–40 Hz). There is no discernible low-frequency component, e.g., baseline shift, within either passband. The same is true for all subjects and all set sizes.

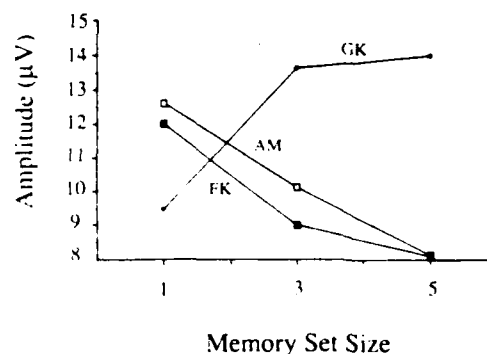


Fig. 3. Amplitude of N100 (averaged over old and new probes) as a function of MSZ for subjects AM, GK and FK. While the amplitude of N100 changes monotonically with set size, it increases in amplitude for subject GK and decreases for subjects AM and FK.

quently, it was possible to pool data for each set size across all blocks of trials, insuring a large enough N to compute reliable average ERPs. Fig. 2 contains the actual average N100 wave forms from each set size for all 3 subjects, computed separately for old and new probes. Since there is no significant difference between N100 amplitudes for old and new trials, they were averaged, and the resulting overall N100 amplitudes are included in the graph shown in Fig. 3. Clearly, as is also evident for both old and new trials in Fig. 2, the amplitude of N100 diminished with set size for 2 subjects, while it increased significantly with set size for the third subject.

As we have seen, RT increased linearly and significantly with set size for all 3 subjects (Fig. 1). However, the variation in N100 amplitude with set size is quite different from that of RT. First, the direction of its change in amplitude with set size differs significantly among the subjects while RT increases with set size for all subjects. It is notable that ANOVAs for each subject show that the differences in N100 amplitude over set size are highly significant and the agreement between the data for new and old probes (Fig. 2) is evidence of the repeatability of the results. Also, unlike the RTs, the change in N100 amplitude with set size is non-linear for two of the subjects.

Similar results were obtained for N100m. Since 5 coils were placed at slightly different positions over each hemisphere and, on alternate blocks, switched from one hemisphere to the other, the outputs of the 5 channels over all blocks of trials were averaged for each hemisphere and each set size. While the pick-up coils were at different locations, and these locations varied from one block to another, the locations of the coils were the same for all set sizes within each block. Hence, the variations in N100m with location were the same for all set sizes. The average amplitudes vary differently with set size over the two hemispheres.

The amplitude of N100 measured at the vertex is determined by sources in both hemispheres. However,

any measure of N100m is due to the activity within the hemisphere over which the measurement is made. Therefore, the marked differences between N100m of the left and right hemispheres of all subjects demonstrate a previously unknown asymmetry in the responses of the two hemispheres to acoustic stimuli. The functional significance of this asymmetry, if any, is not known.

As shown in Fig. 4, N100m measured over the right hemisphere of subjects AM and FK exhibits the same qualitative changes in amplitude as does N100, i.e., there is a monotonic reduction in N100m amplitude with set size for AM and FK and increases in amplitude for GK. GK's right hemisphere shows an increase in N100m amplitude with set size, which is also what was found for N100.

Regardless of the hemisphere over which it is measured, N100m is not consistently related to RT, which is the putative indicator of memory scanning. Neither is N100. Nor do their latencies vary with set size. However, since both N100 and N100m are sensitive to levels of auditory attention, they may well reflect attentional components of the Sternberg task. Therefore, the reliable individual differences noted here could be

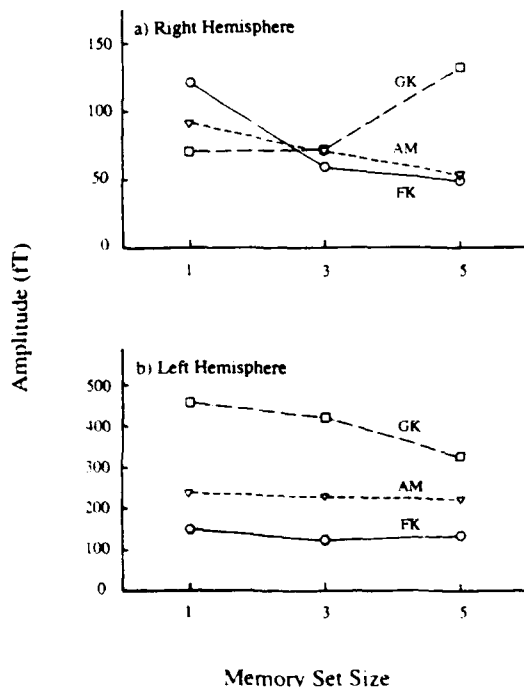


Fig. 4. N100m amplitude (averaged over old and new probes) over: (a) the right hemisphere, and (b) the left hemisphere of each subject. When recorded over the right hemisphere N100m diminishes in amplitude with MSZ for AM and FK and increases in amplitude for GK. N100m recorded over the left hemisphere has approximately the same amplitudes over set sizes for AM and FK, but diminishes in amplitude with set size for GK. However, the percent change in amplitude for GK is small as compared with the percent change in amplitude of the right hemisphere's N100m. There is no systematic relation to the RT vs. MSZ functions of Fig. 1.

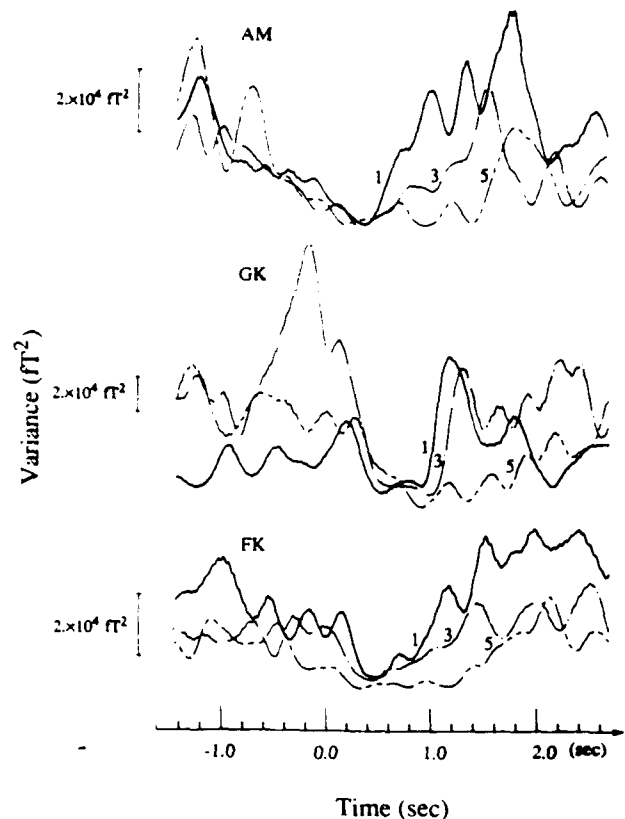


Fig. 5. Sample graphs of changes in MEG power (variance) in the 8-12 Hz band as a function of time for 3 set sizes. The 0.0 point on the abscissa represents the time of presentation of the probe tone. The subsequent dip in power is shortest for MSZ = 1, of intermediate duration for MSZ = 3 and of longest duration for MSZ = 5. Note the examples of early and late onset of suppression relative to time of probe presentation. Early onset or "anticipatory" suppression occurs prior to memory scanning.

due to differences in attentional strategies. This requires further study.

The failure of N100 and of N100m to show any clear relationship to the process of auditory memory scanning as reflected in the Sternberg procedure does not rule out the participation of neurons of auditory cortex in this process. We now turn to the question of whether variations in levels of spontaneous activity of auditory cortex and adjacent regions reflect this process.

Effects of memory scanning on spontaneous activity

The spontaneous MEG between 8 and 12 Hz was retrieved from the same recordings as those used to obtain N100m. The variance about the average response in this bandwidth was plotted at each point in time within the averaging epoch, and then the resulting records of fluctuation of variance (power) with respect to time were smoothed. Sample plots of data from the 3 subjects are shown in Fig. 5. Unlike N100m, these were not obtained by averaging the outputs of the 5 sensors. Rather, they are average power plots ($N = 20$) obtained from a single sensor for responses at each set

size. The zero point along the x-axis indicates the time at which the probe stimulus was presented. Note the drop in field power which occurs near this point in time and persists for some time afterwards. In fact, as is evident in the sample traces shown in Fig. 5, the time between presentation of the probe and recovery from suppression (*suppression time* (ST)) tends to increase with memory set size (MSZ). Therefore, to determine if this apparent increase in ST is reliably related to MSZ, the duration of ST in each power plot was divided into two parts. The first part (ST-) is the time between the onset of the probe and the onset of suppression. A positive value refers to the case where the suppression began prior to actual probe presentation. A negative value refers to the time between probe onset and later occurring suppression onset. We tested the hypothesis that ST- is correlated with RT for each subject. We also tested the hypothesis that time between the presentation of the probe and the termination of suppression (ST+) is positively correlated with RT. Since it is known that RT is correlated with MSZ, then a positive correlation would show that suppression is correlated with the time to scan memory and make a response. This was done separately for new and old probes so that only 10 epochs were used to compute the "old" and "new" power for each set size over all blocks of trials.

When the old and new items are compared with RT separately, the correlations are weak and largely not significant. However, when the old and new data are

combined, the correlations become highly significant. The regression lines for the combined data are shown in Fig. 6. The resulting coefficients of correlation relating ST+ to RT are: $r = 0.64$ ($P = 0.0015$), 0.43 ($P = 0.03$), and 0.63 ($P = 0.0006$) for subjects AM, GK and FK, respectively. For subjects AM and GK the correlations relating ST- to RT are not statistically significant and the regression lines are essentially flat. However, for subject FK ST- is significantly correlated with RT ($r = -0.59$, $P = 0.0014$). Generally, FK's suppression starts well after presentation of the probe, but the interval between probe and suppression onset diminishes as RT increases. Therefore, FK's longer RTs could have been due to a delay in onset of processing. (RT is given by the Y-intercept of the RT versus MSZ regression functions of Fig. 1, which shows that, overall, FK's RT was longer than that of the other two subjects.)

The strong positive correlations of ST+ with RT were obtained only by combining old and new data. While it suggests that ST+ is also highly correlated with MSZ, it is possible to directly examine the relation between ST+ and MSZ for both old and new trials.

Correlations between ST+ and MSZ were computed for old and new probes separately, and the slopes of these regression lines are presented in Table II. Also, unlike the correlations with RT, the correlations of the ST+ data from old and new trials with MSZ are all highly significant. As shown in Table II, a 1-tailed t test (predicated on the hypothesis that the

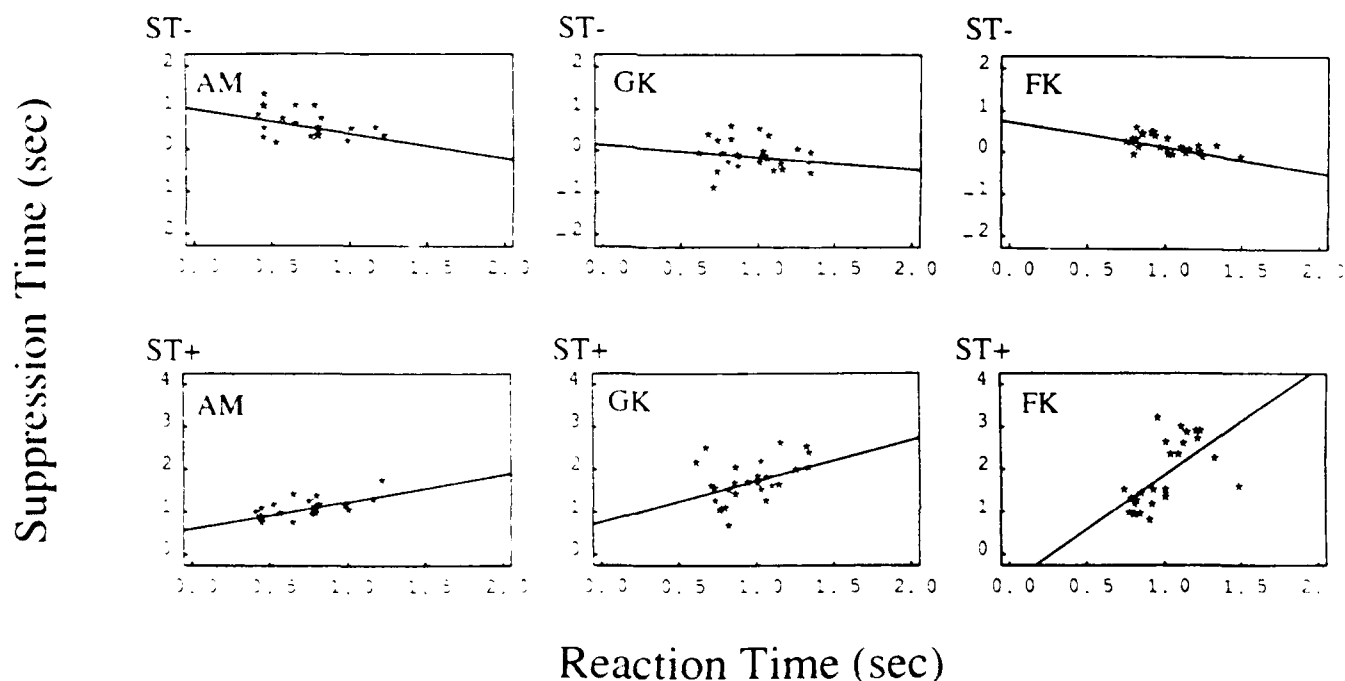


Fig. 6. Regression lines showing how suppression time (averaged over old and new trials) varies with RT for all 3 subjects. ST- graphs indicate the time between onset of suppression and probe presentation, with positive values indicating "anticipatory" suppression and negative values suppression that begins after the probe presentation. ST+ is the time between onset of probe (0.0) and termination of suppression (see text).

TABLE II

Suppression time (ST) versus memory set size (MSZ). (A) The slopes (in sec/item) of the regression functions relating suppression time between probe onset and offset of suppression (ST+) for old and new probes are given in the first column. The correlation coefficients are given in the second column, and their levels of significance are given in the third. All are statistically significant. The *t* tests (fourth column) are for the significance of the differences between the slopes of the "old" and "new" regression functions. The difference between the "old" and "new" slopes reaches statistically significant levels of $P < 0.05$ for subject AM and of $P < 0.01$ for subject FK. For all 3 subjects, the slope is lower for new than for old trials, as in the RT data. (B) The same data as in (A), but sorted by hemisphere over which recorded rather than new and old probes. The correlation between ST+ and MSZ, where ST+ is based on data recorded over the left hemisphere, fails to reach significance beyond chance for subject GK. While coefficients of correlation (column 3) are significant with $P < 0.003$ for subjects AM and FK, the slopes of the regression functions (column 1) are low. Over the right hemisphere ST+ is significantly correlated with MSZ for all subjects. The *t* tests of the significance of the differences between the slopes of the left and right hemisphere's regression functions are all very significant ($P < 0.00001$) for all subjects.

Suppression time vs. memory set size	Slope	Corr. coef.	Sig. level	<i>t</i> test	<i>df</i>	
(A)						
AM (ST +)	old	0.11	0.47	0.0001	1.92	193
	new	0.06	0.33	0.001		
GK (ST +)	old	0.12	0.28	0.006	1.1	190
	new	0.07	0.32	0.001		
FK (ST +)	old	0.34	0.66	0.0001	3.35	279
	new	0.19	0.44	0.0001		
(B)						
AM (ST +)	left	0.052	0.37	0.0035	23.2	100
	right	0.131	0.77	0.0001		
GK (ST +)	left	0.069	0.28	0.112	14.6	112
	right	0.174	0.52	0.0001		
FK (ST +)	left	0.256	0.58	0.0001	15.4	143
	right	0.362	0.72	0.0001		

slope is lower for new than old probes) comparing the slopes of old and new regression lines show that they differ significantly for subject AM ($P < 0.05$) and for FK ($P < 0.01$). The slopes for new items are lower than

for old for all subjects, as was found in the original RT data. Comparing the differences in slopes for old and new items for ST+ vs. MSZ and for RT vs. MSZ, they are 112 msec/item vs. 149 msec/item for AM, and 121

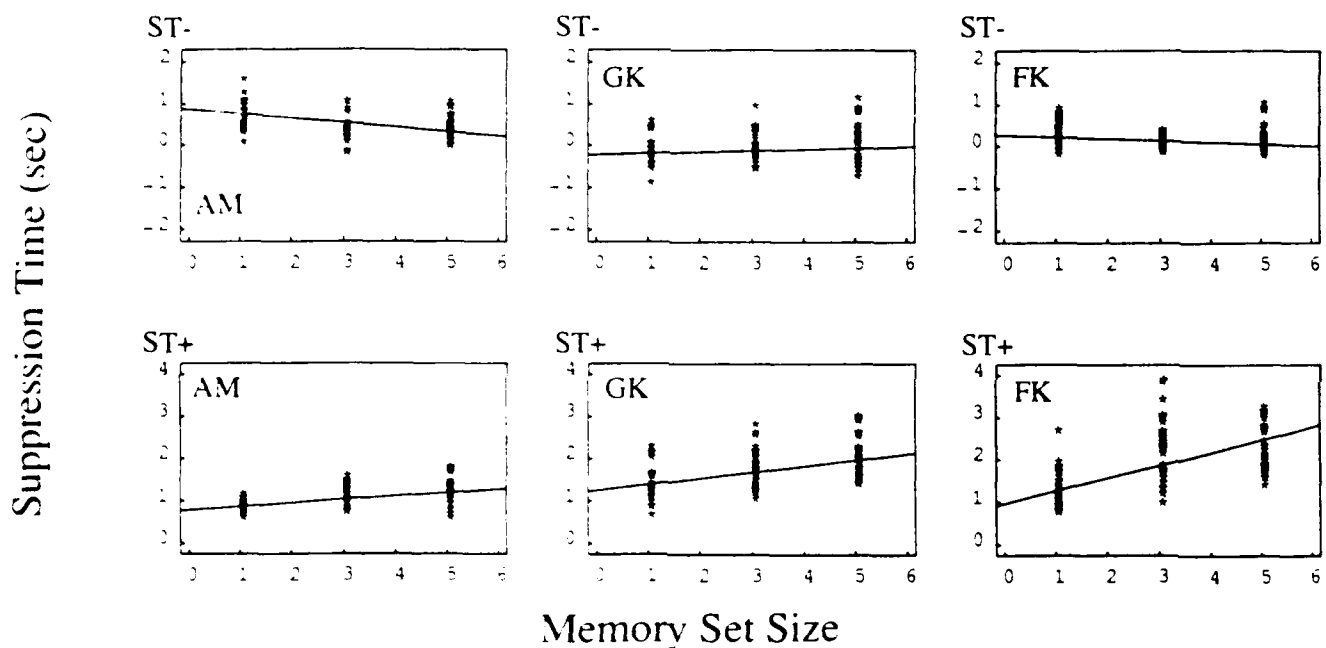


Fig. 7. Suppression time versus MSZ. Similar to Fig. 6, but plotting MSZ instead of RT. ST+ is significantly correlated with MSZ for all 3 subjects.

msec/item vs. 133 msec/item for GK. Most of the difference of about 25 msec/item could be accounted for by the criterion we adopted to determine the point in time at which the suppression "ended." However, subject FK's suppression time slope was almost a factor of 3 greater than the slope relating her RT to MSZ. Note, however, that for new probes the slope of her ST+ vs. MSZ regression line was only 189 msec. The ratio of old/new slopes for ST+ vs. MSZ is 1.82 and that for RT vs MSZ is 1.84 indicating that the faster scan rate for new items relative to old is about the same for both measures.

Fig. 7 contains regression lines based on the combined new and old data. They indicate that the rela-

tionship between ST- and MSZ is inconsistent across subjects. It is to be noted that FK is the only subject in whom ST- is significantly correlated with MSZ, but the correlation coefficient ($r = 0.04$) is so weak that it can be neglected.

At the present time we can only speculate as to why the slopes of the regression lines for FK relating ST+ to MSZ and to RT differ so dramatically from other subjects. While there is a strong positive correlation between ST+ and MSZ for FK as well as the other subjects, the greater slope for FK suggests that a serial search of short-term memory alone cannot explain her data, which are characterized by a constant percent increase in ST across set size. We also note that FK

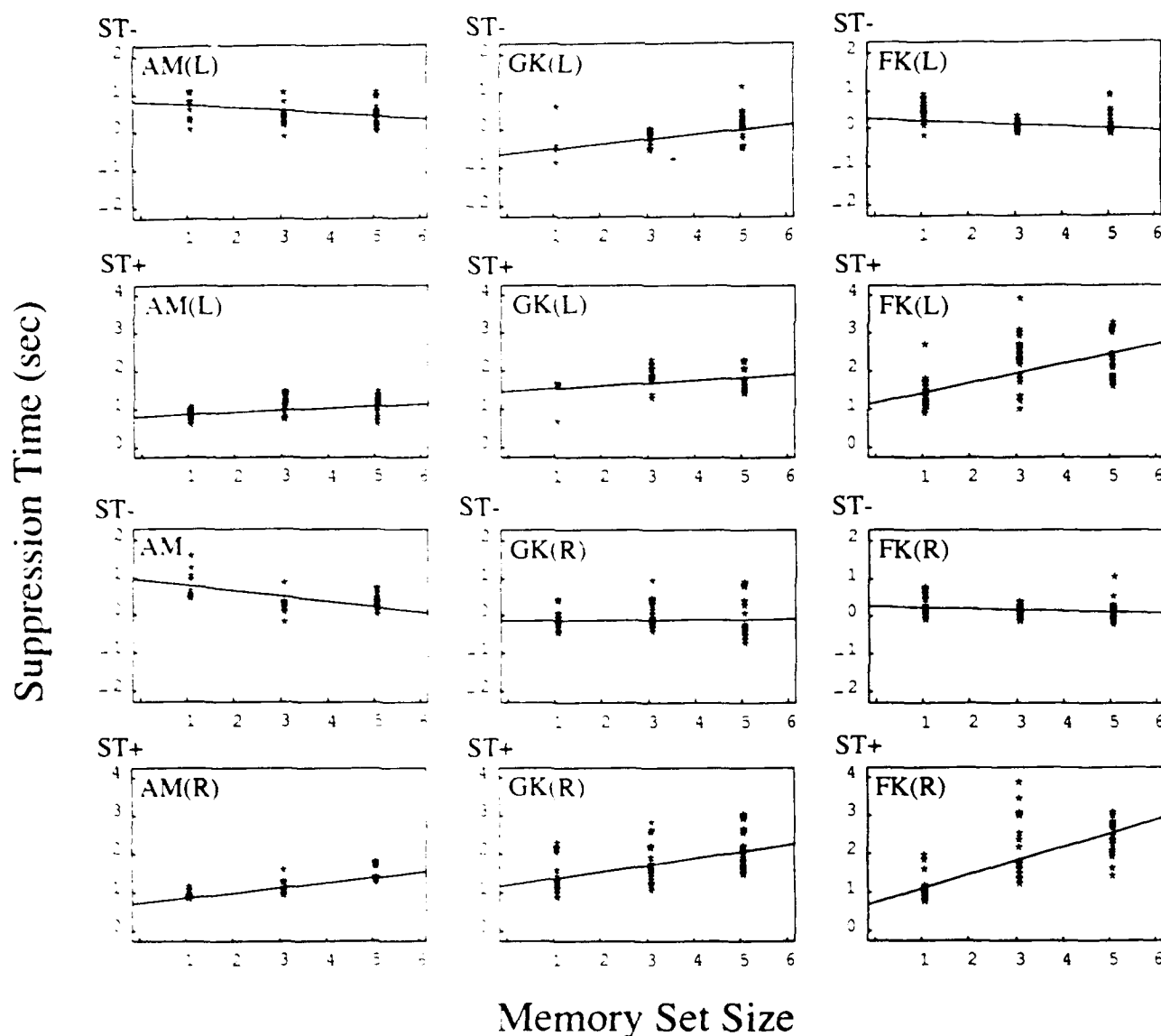


Fig. 8. Suppression time versus MSZ for (L) the left hemisphere and (R) the right hemisphere. ST+ is significantly correlated with MSZ for all 3 subject's right hemisphere data, but, for only one subject (FK) in case of left hemisphere.

almost failed to meet our accuracy criterion and had to undergo many additional practice sessions before her performance was finally acceptable.

Since the MEG was recorded separately over the left and right hemispheres, it is possible to determine if the spontaneous activity of both hemispheres is affected in the same way during memory search. If suppression during memory search were a global effect of attention or arousal, one would expect the two hemispheres to respond in the same way to memory sets of different size. Alternatively, if regional changes in cortical activity reflect processes such as scanning memory for acoustic stimuli, then hemispheric differences are not unlikely. Unfortunately, if "old" and "new" trials are analyzed separately for each hemisphere, the sharply reduced sample size makes any conclusions too uncertain. However, the differences between old and new trials were shown to be of little consequence in analyzing the effects of set size on RT. Therefore, the data from old and new trials were combined and a sufficient number of trials were obtained to compute statistically reliable coefficients of correlation between suppression duration ($ST+$) and set size for each hemisphere (Fig. 8). When measured over the left hemisphere the correlation coefficients for subjects AM, GK and FK respectively were 0.372 ($P = 0.0035$), 0.301 ($P = 0.48$), and 0.579 ($P < 0.0001$). The slopes of these regression lines were 52, 28, and 256 msec/item, respectively. Over the right hemisphere the corresponding correlations were 0.769 ($P < 0.0001$), 0.519 ($P < 0.0001$), and 0.717 ($P < 0.0001$) for AM, GK, and FK respectively. Again, the slopes of these regression lines were 131, 174, and 364 msec/item for AM, GK, and FK, in that order. Based on these results, the right hemisphere appears to provide an index of memory scanning that is consistent with the classic RT data, while the left hemisphere does not. This result is consistent with the general belief that the right hemisphere predominates in processing musical stimuli (Springer and Deutsch 1985). The scan rates for AM and GK are comparable to those predicated on their RT data. However, as pointed out previously, FK's data reflect a much longer scan rate than that reflected by her RT data. This suggests that suppression time in her case reflects processes in addition to memory scanning. As intimated previously, this asymmetry in suppression across hemispheres is strong evidence against the view that suppression of the MEG during memory search is simply global alpha blockage caused by generalized arousal or change in level of attention.

Let us now consider the EEG data. First, it was not possible to analyze the EEG data obtained from FK. In her case the suppression, when detectable, began at about the same time as in the MEG, but it rarely recovered prior to the end of the epoch for the two

larger set sizes. In many cases it apparently extended from one epoch to the next. This was true for electrode positions Cz, Oz, and Pz and the data were even less useful from Fz. By contrast, the data recorded at Cz and Oz from subject AM were quite similar to those obtained from the same subject with the MEG. However, the Cz and Oz records obtained from subject GK failed to produce a significant correlation between $ST+$ and MSZ. These results also imply that the significant correlations between the MEG's $ST+$ and MSZ are not merely instances of global alpha blockage, perhaps due to covariation in generalized arousal and MSZ. For if global alpha blockage were the cause, then the EEG data from all of the subjects should have revealed the effect of MSZ on $ST+$, and it should have been detectable wherever alpha activity is observed. However, the results demonstrate that specific regions of cortex are selectively affected by memory search and that simple midline recordings are not suitable for studying effects of memory scanning on the brain's spontaneous activity. This difference between EEG and MEG is probably due to activity of distant cortical regions affecting the EEG. This is avoided in MEG recordings, where even subtle differences between the hemispheres become apparent. Of course, other electrode montages might reveal effects similar to those obtained with the MEG.

It might be argued that ST really reflects the time to prepare a motor response and has nothing to do with mentally comparing the probe with memory set items. To investigate this idea we used the button press itself as the trigger for backward averaging and recomputed all of the variance plots to determine new values of $ST-$ and $ST+$, where $ST-$ refers to the suppression before the button press and $ST+$ the suppression after the button press. The hypothesis is that if $ST-$ signifies preparation to make a motor act, then its duration should covary with RT. These correlations were not significant.

When the pre-button press $ST-$ as computed above was compared with MSZ rather than RT, significance was achieved for two subjects. Subject GK's $ST-$ was weakly but significantly correlated with MSZ ($r = 0.23$; $P = 0.0053$). A somewhat stronger correlation was found for subject FK ($r = 0.39$; $P < 0.0001$). For subject AM the suppression time prior to the button press ($ST-$) was not correlated significantly with MSZ ($r = 0.013$).

The 16–24 Hz (beta band) was processed in precisely the same way as was the alpha band activity. While suppression was observed in some sets of trials, it was not consistently present, and when present it was seemingly unrelated to set size or RT. As Kaufman et al. (1990) found, the distribution of beta power about the scalp is largely independent of that of alpha power, suggesting different neuronal generators. It may be

necessary to measure beta at many other places to determine if it is related to memory scanning in other cortical regions.

As indicated earlier, we found no systematic relationship across subjects between N100 or N100m and set size, thus ruling out a differential effect of auditory attention as the cause for findings. The fact that N100m was measured wherever the sensors measured the alpha band activity and its suppression also makes it possible to test the hypothesis that the auditory cortex contributes to the spontaneous activity suppressed by memory search. It is known that the source of N100m lies in auditory cortex (Elberling et al. 1980; Hari et al. 1980; Pantev et al. 1988; Yamamoto et al. 1988). Since the magnetic field sensors were all separated from each other by 2 cm, the amplitudes of the N100m component they sensed differed from each other. Furthermore, the coils were moved to slightly different positions from one block of trials to the next, which also caused a variation in N100m amplitude. Based on the theory that the neurons in auditory cortex that give rise to N100 are also spontaneously active and contribute to the fields we observed, it was hypothesized that position-dependent fluctuations in N100m amplitude would be reflected in the percent suppression detected on the same trials and at the same positions. Percent suppression is defined as the ratio of the mean power over a 1 sec interval 400 msec prior to presentation of the probe and the mean power within a 200 msec interval after the presentation of the probe stimulus. The hypothesis was confirmed as the position-dependent changes in N100m amplitude were found to be positively correlated with corresponding position-dependent changes in percent suppression of the spontaneous MEG. The coefficients of correlation between percent change in alpha and N100m amplitude are 0.31 ($P = 0.0002$) for GK, 0.30 ($P = 0.0003$) for FK, and 0.20 ($P = 0.04$) for AM. The consistency of this relationship and the magnitudes of the correlations indicate that auditory cortex contributes substantially to the spontaneous activity suppressed during memory search. Nevertheless, this only accounts for a portion of the spatial variance in the suppression phenomenon, so areas of parietal and temporal cortex (other than auditory cortex) may also be involved in memory scanning. This too is a topic for further study.

Discussion

The main conclusions are quite clear. The level of MEG activity in the alpha band detected over the temporal and adjacent parietal areas of both hemispheres is sharply reduced when subjects scan short-term memory for previously heard tones. Fields associated with the magnetic counterpart to N100 (denoted

N100m) are at their strongest in these same regions. While the suppression occurs bilaterally, the duration of suppression over the right hemisphere covaries significantly with the size of the memory set for all subjects. The covariation is not so good for the left hemisphere. This hemispheric asymmetry is evidence against a global alpha blockage explanation of the data. Since the equivalent current dipole source of N100m lies in auditory cortex, it is reasonable to assume that auditory cortex also contributes to the spontaneous activity that is suppressed during memory search. In view of the significant spatial covariation between the amplitudes of N100m and the percent suppression of the MEG exhibited by all subjects in this experiment, it is concluded that auditory cortex contributes to the affected spontaneous activity. The failure to find the same suppression patterns in the EEG recorded at vertex and occipital electrodes is further proof that the suppression is of local cortical areas and not entirely a global effect, such as might occur because of generalized arousal. Otherwise the MEG and EEG would have yielded similar results. Also, while N100 detected at the vertex showed a statistically significant change in amplitude with set size, the direction of the change for one subject was in exact opposition to the direction of change for the other two. Yet the reaction times of all subjects increased reliably and linearly with size of the memory set, as did the duration of alpha suppression. Therefore, changes in N100 are not indicative of memory search *per se*, but may reflect effects of stimulation and early processing, including attention. Moreover, N100m recorded over the two hemispheres showed asymmetrical changes in amplitude with set size, i.e., the right hemisphere exhibited the changes similar to those detected in N100 with a midline electrode. However, there was no relatively marked change in N100m measured over the left hemisphere, which is consistent with the predominance of the right hemisphere in attending to and processing musical tones. The fact that the right hemisphere's auditory cortex is also differentially affected by different memory set sizes, even though the effect is different across subjects, is further evidence that the neural source of N100m contributes to the spontaneous activity whose suppression tracks the RT data. Furthermore, it is consistent with the conjecture that N100 reflects early stages of cognitive processing preliminary to memory search, which is then revealed by changes in ongoing activity originating at least in part in the same cortical areas.

In the Appendix to this paper we review much of the pertinent literature on the ostensive roles of N100 and P300 in short-term memory. It is concluded that N100 is not a direct indicator of memory scanning, although it might well reflect neural processes related to echoic memory. We also review existing empirical data that are widely interpreted as showing that P300

latency reflects short-term memory scanning (Gopher and Donchin 1986; Bashore 1987; Buchwald 1987). A closer analysis reveals that, in the context of the Sternberg paradigm, P300 latency and amplitude are often dissociated from reaction time. In view of the basic assumption that in this task RT reflects processing time, it is difficult to establish that P300 latency or amplitude are direct indicators of memory scanning. A more suitable interpretation appears to be that P300, like N100, reflects other cognitive processes that happen to accompany or precede memory scanning. A contrary conclusion would require an alternative to Sternberg's theory — a theory in which reaction time is not closely tied to memory scanning even though subject accuracy is high. To our knowledge, no such alternative theory exists. Rather, existing alternatives deal with the issues of whether parallel processing (as well as or in lieu of serial processing) and self-terminating search (as opposed to exhaustive search) can underlie the observed RT or related behavioral data, which nonetheless reflects processing time.

It is possible that some ERP components represent specific aspects of an overall memory scanning process. The timing and amplitudes of these components could be pertinent to memory scanning, but still be inconsistent with a more global measure, such as that provided by reaction time. However, no specific hypotheses have been offered as to the processes ostensibly signified by these components. The finding that a change in the brain's activity covaries with the more global measure of reaction time makes it possible to infer that specific regions of neocortex are involved in the overall process. This does not cast any light on the deeper theoretical issues, but it makes it likely that the involved cortical regions can be identified and studied.

Finally, in this paper we emphasized an indirect approach to the problem of identifying the cortical regions affected by memory scanning. We relied on spatially correlated changes in spontaneous activity and the amplitude of an ERP component with its source in a known location. While this helped to establish that auditory cortex made a significant contribution, a more precise description of the cortical source is still possible, provided that the extracranial field is mapped completely from many positions at one time.

In a recent theoretical study, Kaufman et al. (1991b) simulated a convoluted region of cortex populated by many dipoles having random moments. The net field pattern they produced at the surface of the spherical head model was computed using different sets of random dipole moments. This resulted in an ever-changing pattern, and invariant features could not be discerned in it. However, by averaging field power (as was done in this paper) rather than field, invariant features that depended upon the underlying cortical geometry (which constrains the possible field configurations) as

well as levels of activity in different regions of the cortex did emerge. It was demonstrated in this simulation that it is possible to identify the location and depth of a region whose activity is locally incremented or decremented relative to a baseline of activity. Therefore, in principle it is possible to make use of cortical maps reflecting differences in levels of spontaneous activity as functional images similar to those generated by PET. In that case the spontaneous activity of incoherent sources may well serve as a valuable quantitative complement to ERPs in understanding how the brain's activity is related to cognition.

Appendix

As stated in the body of this paper, the N100 component of the ERP may well represent early stages of the cognitive processing involved in short-term memory search, and changes in levels of spontaneous activity that extend much farther in time appear to accompany the search process itself. Moreover, both phenomena arise in at least partly overlapping sets of neurons. Despite the likelihood of these complementary roles, we emphasized the role of spontaneous activity in short-term memory scanning and did not dwell extensively on the classic ERP components. In this Appendix we review some of the previous work relating the N100 and P300 components to short-term memory. This review was not included in the body of the paper because it would have distracted from the development of the main ideas and results. Since we would be remiss to ignore this work, this Appendix is provided. It will enable the reader to see the present paper in a broader context, and provide further justification for not dealing more explicitly with these components as indices of short-term memory scanning in the body of the paper.

N100 and short-term memory

Picton et al. (1978) and Näätänen (1982, 1986) suggested that N100 and related components may reflect short-term memory processes. N100 is thought to be composed of several superimposed components having origins in different portions of the brain, and possibly differing in functional significance (Näätänen and Picton 1987). The variations in N100 associated with selective attention are described as being due to the *processing negativity* (Näätänen 1982) or *negativity difference wave (Nd)* (Hansen and Hillyard 1980) which is superimposed on N100. Nd is characterized as a negative shift in the baseline which may occur prior to N100 with a latency as short as 50 msec and extend for as long as about 500 msec. As compared with N100, Nd is a low-frequency phenomenon. The scalp distribution of Nd does not coincide precisely with that of N100, e.g.,

its later part is apparently more frontal. Typically, when subjects selectively attend to one "channel" (usually an auditory stimulus of particular pitch or one arriving from a particular spatial direction) the resulting N100 is of greater amplitude than that obtained when the channel is ignored. The difference between these two wave forms reveals the presence of Nd, which is widely interpreted as a separable ERP component which is temporally superimposed on N100, to create an apparent change in its amplitude. However, N100m, measured at the output of a high-pass filter (so that there is no residual Nd), also exhibits an effect of selective attention similar to that found for Nd (Curtis et al. 1988). In fact, the amplitude of N100m may vary by as much as a factor of 2, depending upon whether or not the subject is paying attention to the acoustic stimulus. This is significant because it is known that the equivalent current dipole source of N100m is located in auditory cortex (Elberling et al. 1980; Hari et al. 1980; Pantev et al. 1988; Yamamoto et al. 1988). Furthermore, there is strong evidence to support the view that neurons in auditory cortex are also major contributors to the electrical N100 (Vaughan and Ritter 1970), although other sources may contribute as well (Näätänen and Picton 1987).

Noting that the increase in amplitude of N100 with interstimulus interval (ISI) may reflect a psychological refractory period, Picton et al. (1978) suggested that the refractory period may be a characteristic of the short-term storage system whenever it is activated by a sensory event. As evidence they show that when the ISI between similar stimuli is small, the amplitude of N100 is also small. However, when the same stimuli are sufficiently dissimilar (in pitch) the amplitude of N100 is as large as when the ISI is made twice as long. Hence, measures of this ISI effect could well allow the characterization of this early modality-specific store.

While this is indeed a plausible hypothesis, alternative possibilities have not yet been ruled out. For example, the state of the subject's expectancy or arousal level may also change with ISI, and this could affect N100. Also, even if correct, the refractory period may be characteristic of sensory (echoic) store rather than of working short-term memory — a distinction that is sometimes made in the literature of cognitive psychology. In any event, there are as yet no conceptual links to connect the refractoriness identified by Picton and his colleagues to the process of searching short-term memory.

Näätänen (1982) suggested that the later occurring portion of Nd is related to the rehearsing of features of the stimulus to which attention is being paid. He suggests that this rehearsal goes on in short-term memory. Again, beyond this conjecture no hypotheses are offered that connect this ostensible rehearsal to the operation of scanning short-term memory.

The mismatch negativity (MMN) of Näätänen et al. (1982) is another low-frequency component that partly overlaps N100 in time. It occurs in response to deviant stimuli, whether subjects are attending to them or not. Näätänen (1985, 1986) proposed that the MMN is a sign of a mismatch between an internal neural model of anticipated events and ongoing sensory inputs. Its earlier phases may be coincident with echoic store, and the later phases a sign of the comparison process itself. Since subjects performing the Sternberg task try to match recent sensory events with stored representations of prior events, Näätänen's conjecture may be taken to imply that the time required to complete the search task could be reflected in the MMN.

The results described in this paper fail to demonstrate any covariation of the MMN or Nd with set size or with RT. Therefore, whatever the roles of these phenomena in short-term memory, they are not revealed in the context of the Sternberg task. However, the amplitudes of N100 and of the right hemisphere's N100m do change with set size, albeit, inconsistently with RT since they change in different directions for different subjects. As we have seen, there is no clear way in which to relate this finding to short-term memory *per se*, although it may well reflect aspects of the task not dealt with in any existing theory.

P300 and memory scanning

The full complexity of memory processes suggested by the distinctions between short-term and long-term memory, episodic, semantic and declarative memory, and declarative versus procedural memory, is barely if at all reflected in the ERP literature. Even so, it remains an open question as to how the various components of the ERP are related to the many facets of such processes. Yet P300 has sometimes been assumed to be a universal indicator of virtually all cognitive processes. Here we discuss the role of P300 in short-term memory scanning as revealed in the existing literature.

P300 is empirically related to stimulus evaluation time, which is considered distinct from the process of response selection and motor response time (Magliero et al. 1984). Thus, P300 latency (evaluation time) may be dissociated from RT in cognitive experiments where response selection varies independently of stimulus evaluation or perceptual processes (Isreal et al. 1981). More generally, P300 is presumably related to the maintenance of the subject's internal model of the context of the environment (Donchin and Coles 1988) and may even occur in the absence of an expected stimulus.

The rationale for experiments in which P300 is measured in the context of the Sternberg paradigm stems from the fact that P300 has been related to stimulus evaluation time (Kutas et al. 1977), and the

updating of memory (Donchin 1975, 1981). In oddball experiments P300 is elicited when the event is classified by the subject as belonging to the category of rare events (McCarthy and Donchin 1981; Magliero et al. 1984). This classification cannot be made before the stimulus is fully evaluated. If (and only if) RT signifies the completion of an evaluation of a stimulus, then P300 latency should covary with RT.

The foregoing makes P300 an ideal candidate for investigation as an indicator of memory search time. Assuming that high levels of accuracy are maintained, the latency of P300 should vary with the time required to determine if a probe had or had not been a member of the memory set. This hypothesis would be confirmed if P300 is a truly general indicator of all cognitive processes. However, if it should turn out that P300 represents the time to complete only some kinds of cognitive processes, then it might or might not reflect those involved in searching short-term memory.

There are some *a priori* reasons why P300 may not be an indicator of short-term memory scanning. For example, if its dominant neural generators should lie in the hippocampal formation (cf., Okada et al. 1983; Harrison and Buchwald 1987), then it is possible that it could be related to the transfer of information from short-term to long-term memory, but not to the scanning of short-term memory. This follows from the fact that bilateral damage to medial temporal cortex results in anterograde amnesia, which prevents patients from storing information in long-term memory, but it need not lead to deficits in short-term memory (cf., Squire 1987). So it is not automatically given that P300 must unambiguously reflect short-term memory scanning. Even so, several reviewers have concluded that such a relationship has been demonstrated (Gopher and Donchin 1986; Bashore 1987; Buchwald 1987).

Using acoustical stimuli, Gaillard and Lawson (1984) found no relationship between P300 latency and set size, but its amplitude did decrease with set size. Also, RT increased significantly with set size. By contrast, Gomer et al. (1976), using visually displayed alphanumerics, did find an increase in P300 latency with set size. However, P300 latency increased with set size at the extraordinarily fast rate of 6 msec/item, while for RT the scan rate was only 14 msec/item, which alone is far short of the highest rate of 38 msec/item found in this type of task (Sternberg 1966). The atypical RTs make it very difficult to evaluate this experiment. However, Marsh (1975) did find a substantial increase in P300 latency with set size in an experiment comparing older and younger subjects. These results are quite similar to those obtained in many of the subsequent studies reviewed below. Marsh used 3 set sizes composed of 1, 3, or 5 items and the RTs were quite typical of those reported in the psychological literature. That is, the scan rates reflected in the RT data were about

35 msec/item for the young subjects, and 31 msec/item for the older subjects, although the RTs of the older subjects were considerably longer than those of the young subjects. The slopes of the functions relating P300 latency to set size were 18 msec/item for the young subjects and 22 msec/item for the older subjects. Although the average P300 latency was longer for the old subjects than for the young (the difference being about 60 msec), it did not reflect the large difference between the average RTs, which was about 358 msec.

Adams and Collins (1978) used visually presented digits in a Sternberg task where the set sizes ranged from 1 through 11 items. We disregard set sizes greater than 7 in this review, because the larger numbers of items lie outside the usual range of short-term memory, and the results are atypical. Over the range of from 1 to 7 items, P300 latency increased with set size. However, as in the Marsh experiment, the rate of increase was only 22 msec/item, a much faster rate than is indicated by Adams and Collins's RT data, which indicated an average scan rate of 38 msec/item. Adams and Collins sought to account for this discrepancy by adding the slopes of the regression functions relating both a 250 msec positivity (which we labeled "P300") and a 350 msec positivity (which gave results similar to "P300") to set size, but this does not appear to be a legitimate way in which to derive a net "latency." Adams and Collins found no correlated change in P300 amplitude with set size. In a similar visual digit experiment Ford et al. (1979) found that while set size 1 was associated with the shortest latency, set sizes 2 and 3 had about the same latency, while set size 4 had the longest latency. Similar results were obtained in younger and older subjects, with the latter showing an overall increase in latency. Interestingly, Pfefferbaum (1980) obtained qualitatively similar results over the same set sizes for young subjects, but, for older subjects the latency of P300 increased for set sizes 1 and 2, and then decreased for set sizes 3 and 4. Despite an overall increase in P300 latency, Ford et al.'s older subject's data reflected a scan rate of about 29 msec/item. However, the scan rate reflected in their RT data was 55 msec/item. For younger subjects the scan rate given by RT was 35 msec/item, and the rate given by P300 about 27 msec/item. None of these P300 results appear to be well correlated with RT. In one interpretation the scan rate given by P300 reflects true cognitive processing, and the difference in the young and old RT data reflects differences in response selection. However, response complexity did not increase with set size, so the effect of aging should have been the addition of a constant to RT, which would only affect the Y-intercept of the regression function and not its slope. Ford et al. (1981) conducted an experiment in which the quality of the stimulus was

varied along with set size. Degrading the stimulus affected the intercept for both the RT and P300 functions, and the slope of the former was about double that of the latter. The data are inconsistent with any straightforward relation between P300 and memory search time as they suggest that degrading the stimulus affects processes both prior to and after P300.

Pratt et al. (1989a,b,c) had younger and older subjects scan short-term memory for items composed of visually presented digits, and also acoustically presented digits, and musical tones. After averaging over subjects, Pratt et al. (1989a) identified an early occurring P300 (referred to as P3a) which was strongest frontally (at Fz and Cz), and a later occurring P300 (P3b) which was strongest at Pz. P3a (with a latency of about 350–400 msec) diminished in amplitude with set size, but did not change in latency. P3b (400–700 msec) increased in latency with set size. However, in the case of the visual and auditory digits, the latency increase with set size was at about half the rate of the increase in RT. More importantly, while RT increased with set size for musical tones, there was almost no change in latency for P3b. Moreover, as in the work of Pfefferbaum and of Ford et al., in all conditions, there was a non-linear relation between latency and set size. Thus, the latency of P3b for set sizes 3 and 5 did not differ significantly from each other, although both differed significantly from the latency associated with a set size of 1 digit. The failure to show a change in latency for musical tones despite an increase in RT with set size on the same trials is clearly at odds with the classic RT results. So far that matter is the non-linearity in the variation in latency with set size. However, in some cases Pratt et al. accepted data with error rates as high as 20%, which is far greater than that accepted by Sternberg (1969), and this raises questions about whether cognitive processing time was truly represented by RT.

Pratt et al. (1989b) report that the RTs of their older subjects were generally longer than for the younger, but for both groups, RT was shorter for a set of 1 item than when the set size was 3 or 5 items. However, except for the visually presented digits, the latency of P3b was not delayed in the older subjects relative to the younger. Again, although RT results suggest a slowing of the search process in older subjects, this is not borne out in the latency results. P300 latency related to acoustically presented digits increased with set size at the same rates for both older and younger subjects. However, the set size effect for P300 did not occur at all for older subjects for either visually presented digits or musical tones, even though their RTs indicated an increase in time to scan memory as a function of set size. Therefore, RT and P300 are largely dissociated from each other in the work of Pratt et al.

Kramer et al. (1986) observed considerable variability in their P300 data which they assumed was due to "response jitter." This jitter, which presumably caused P300 to shift in latency from trial-to-trial, made it difficult to evaluate the relation between set size and amplitude. In consequence, Kramer et al. employed a latency adjustment procedure to obtain less variability among the single trial P300s. Averaging amplitudes of latency-corrected single-trial measures of P300 both within and across subjects revealed a lower amplitude of P300 for set size 4 than for set size 1, where P300 was detected at Pz (not Cz or Fz as in Pratt et al.) and with an average peak latency of about 500 msec. This late P300 exhibited behavior similar to the P3a of Pratt et al., despite the difference in scalp location.

On average, the P300 latency, determined after jitter correction, was longer for set size 4 than for set size 1. This latency difference diminished when the task was deliberately altered so that the subject's reactions would be more nearly automatic. This mirrored the reduction in difference between the RTs associated with the two set sizes.

With only two set sizes it is not possible to determine if the relation between P300 latency and set size is similar to the linear relation between RT and set size found by Sternberg. Therefore, it is particularly interesting that when they used 3 set sizes in a related experiment, Kramer and Strayer (1988) also found a non-linear relationship between P300 latency and set size, the latency of P300 for set size 1 was shorter than for set sizes 3 and 4, which had the same latencies. Despite this, the RTs increased monotonically with the 3 set sizes of this experiment.

Strayer and Kramer (1990) examined the relationship between P300 amplitude and RT, but ignored the latency dimension. They found that P300 amplitude recorded at Pz, Cz and Fz varied with the degree of attention subjects devoted to the task relative to a different but concurrent task. This suggests that P300 amplitude may reflect the level of attention related to scanning different memory sets rather than the scanning of memory *per se*. Clearly, controls for attentional demands due, perhaps, to rehearsal of memory sets of different sizes are needed.

Several other investigations of P300 and memory scanning are described in the literature. Some of these reported only on the results of using two set sizes, which is not sufficient to determine whether or not the resulting regression functions are linear. These are not discussed here as they would not be relevant to the matter at hand. Other studies, particularly those by Brookhuis and colleagues, are more elaborate than those based strictly on the Sternberg paradigm.

Brookhuis et al. (1981, 1983) combined a visual search task and a memory scanning task to investigate several interesting hypotheses. Memory sets consisted

of 1–4 consonants displayed on a screen. Subsequently 1, 2, 3, or 4 consonants were displayed on the screen with non-consonant positions filled by a dot mask. Subjects had to search the visual display of consonants to find stimuli and then had to decide if the stimuli had been members of the set. As many as 16 possible stimuli could be presented, 4 in the memory set and 4 in the display. Brookhuis et al. (1981) found that the slopes of the RT regression functions differed for old and new items, with the former being scanned at about 30 msec/item, and the latter at the rate of about 60 msec/item. This is consistent with self-terminating rather than exhaustive search (Schneider and Schiffrin 1977). However, this difference failed to appear in the corresponding P300 data, where the scan rate was about 16 msec/item for both old and new items. This implies that RT reflects one kind of search, and P300 another (exhaustive). Furthermore, the absolute number of comparisons, whether they be made in memory or in visual search, was more important than was the nature of the comparisons being made. The authors offer several different and interesting hypotheses as to why these differences occur, but none of them are consistent with a simple division of processing into stimulus evaluation and response selection categories. Using a somewhat different paradigm Brookhuis et al. (1983) came to similar conclusions. By altering response probabilities they were able to demonstrate RT data reflecting a self-terminating memory search process. However, the P300 data were consistent with an exhaustive serial search process. While the RT results are consistent with the work of Schneider and Schiffrin, for some subjects there was a low correlation between the RT and P300 data, even after removal of outlier data. Brookhuis et al. suggest that this may be due to those subjects basing their responses only partly on a full evaluation of the stimuli.

As in many other studies reviewed above, Brookhuis et al. found P300 amplitude to diminish with load. They suggest that the confidence of the subjects in their decisions may vary with set size, and this results in the reduction in P300 amplitude. They also discuss alternative hypotheses, e.g., that of Isreal et al. (1980) that the higher the amplitude of P300, the higher the available amount of processing capacity. This points to a major problem of interpretation, since the phenomenon of the change in P300 amplitude with set size could be due to any number of factors, and there are no hypotheses that link a change in amplitude to the process of memory scanning *per se*.

Because of the ambiguity in the relationship between P300 and RT in the context of the Sternberg paradigm, we decided not to study this relationship in our experiment as we could not contribute more than has already been reported. We have no theory that could account for the dissociation of these measures in

different age groups, nor can we explain the widely observed non-linearity of the relation between set size and P300. The work of Brookhuis et al. might ultimately shed some light on this issue, since they discuss alternative theories, but there is as yet no agreement as to the underlying processes that may be suitable for ERP studies. We leave the possibility open that P300 is not a ubiquitous measure, since it may not reflect all cognitive processes.

We thank Murray Glanzer, Larry Maloney, and Misha Pavel for their help and Arthur Kramer and Emanuel Donchin for valuable comments on an earlier version of the discussion of P300.

This work was supported in part by AFOSR Grant Nos. AFOSR-90-0221 and F49620-88-K-0004 (L. Kaufman, Principal Investigator).

References

- Adams, N. and Collins, G.I. (1978) Late-components of the visual evoked potential to search in short-term memory. *Electroenceph. clin. Neurophysiol.*, 44, 147–156.
- Bashore, Jr., T.R. (1987) Age-related changes in mental processing revealed by analysis of event-related brain potentials. In: J.W. Rohrbaugh, R. Parasuraman and R. Johnson, Jr. (Eds.), *Event-Related Brain Potentials: Basic Issues and Applications*. Oxford University Press, New York, pp. 242–278.
- Buchwald, J.S. (1987) Animal models of cognitive event-related potentials. In: J.W. Rohrbaugh, R. Parasuraman and R. Johnson, Jr. (Eds.), *Event-Related Brain Potentials: Basic Issues and Applications*. Oxford University Press, New York, pp. 57–75.
- Curtis, S., Kaufman, L. and Williamson, S.J. (1988) Divided attention revisited: selection based on location or pitch. In: K. Atsumi, M. Kotani, S. Ueno, T. Katila and S.J. Williamson (Eds.), *Biomagnetism '87*. Tokyo Denki University Press, Tokyo, pp. 138–241.
- Donchin, E. (1975) On evoked potentials, cognition and memory. *Science*, 190, 1004–1005.
- Donchin, E. (1981) Surprise!... surprise? *Psychophysiology*, 18, 493–513.
- Donchin, E. and Coles, M. (1988) Is P300 a manifestation of context updating? *Behav. Brain Sci.*, 11, 355–425.
- Elberling, C., Bak, C., Kofoed, B., Lebech, J. and Saermark, K. (1980) Magnetic auditory response of the human brain. A preliminary report. *Scand. Audiol.*, 9, 185–190.
- Ford, J.M., Roth, W.T., Mohs, R.C., Hopkins, W.F. and Kopell, B.S. (1979) Event related potentials recorded from young and old adults during a memory retrieval task. *Electroenceph. clin. Neurophysiol.*, 47, 450–459.
- Ford, J.M., Mohs, R.C., Pfefferbaum, A. and Koppell, B.S. (1980) On the utility of P3 latency and RT for studying cognitive processes. In: H.H. Kornhuber and L. Deecke (Eds.), *Motivation, Motor and Sensory Processes of the Brain: Electrical Potentials, Behavior and Clinical Use. Progress in Brain Research*, Vol. 54. Elsevier/North Holland Biomedical Press, Amsterdam, pp. 661–668.
- Gaillard, A.W.K. and Lawson, E.A. (1984) Evoked potentials to consonant-vowel syllables in a memory scanning task. *Ann. NY Acad. Sci.*, 425, 204–209.
- Gomer, F.E., Spicuzza, R.J. and O'Donnell, R. (1976) Evoked potential correlates of visual item recognition during memory-scanning tasks. *Physiol. Psychol.*, 4, 61–65.
- Gopher, D. and Donchin, E. (1986) Workload – an examination of the concept. In: K.R. Boff, L. Kaufman and J.P. Thomas (Eds.),

- Handbook of Perception and Human Performance. Vol. II. Cognitive Processes and Performance. Wiley, New York, pp. 41-1-41-49.
- Hansen, J.C. and Hillyard, S.A. (1980) Endogenous brain potentials associated with selective auditory attention. *Electroenceph. clin. Neurophysiol.*, 49, 277-290.
- Hari, R., Aittoniemi, M.-L., Jarvinen, T., Katila, T. and Varpula, T. (1980) Auditory evoked transient and sustained magnetic fields of the human brain: localization of neural generators. *Exp. Brain Res.*, 40, 237-240.
- Harrison, J.B. and Buchwald, J.S. (1987) A cat model of the P300: searching for generator substrates in the auditory cortex and medial septal areas. In: R. Johnson, Jr., R. Parasuraman and J.W. Rorbaugh (Eds.), *Current Trends in Event-Related Potential Research (EEG Suppl. 40)*. Elsevier Science Publishers, Amsterdam.
- Hillyard, S.A., Hink, R.F., Schwent, V.L. and Picton, T.W. (1973) Electrical signs of selective attention in the human brain. *Science*, 182, 177-180.
- Isreal, J.B., Chesney, G.L., Wickens, C.D. and Donchin, E. (1980) P300 and tracking difficulty: evidence for multiple resources in dual-task performance. *Psychophysiology*, 17, 259-273.
- Kaufman, L. and Locker, Y. (1970) Sensory modulation of the EEG. *Proc. Am. Psychol. Ass.*, 75th Meeting, 179-180.
- Kaufman, L. and Price, R. (1967) The detection of cortical spike activity at the human scalp. *IEEE Trans. Biomed. Eng.*, BME-14, 84-90.
- Kaufman, L., Glanzer, M., Cywowiez, Y. and Williamson, S.J. (1989) Visualizing and rhyming cause differences in alpha suppression. In: S.J. Williamson, M. Hoke, M. Kotani and G. Stroink (Eds.), *Advances in Biomagnetism*. Plenum Press, New York, pp. 241-244.
- Kaufman, L., Schwartz, B.J., Salustri, C. and Williamson, S.J. (1990) *J. Cogn. Neurosci.*, 2, 124-132.
- Kaufman, L., Cywowiez, Y., Glanzer, M. and Williamson, S.J. (1991a) Verbal and imaging tasks have different effects on cortical activity. In preparation.
- Kaufman, L., Kaufman, J.H. and Wang, J.-Z. (1991b) On cortical folds and neuromagnetic fields. *Electroenceph. clin. Neurophysiol.*, 79, 211-226.
- Klimesch, W., Pfurtscheller, G. and Mohl, W. (1988) Mapping and long-term memory: the temporal and topographical pattern of cortical activation. In: G. Pfurtscheller and F.H. Lopes da Silva (Eds.), *Functional Brain Imaging*. Hans Huber Publishers, Toronto, pp. 131-142.
- Kosslyn, S.N. (1983) *Ghosts in the Mind's Machine*. Norton, New York.
- Kramer, A., Schneider, W., Fisk, A. and Donchin, E. (1986) The effects of practice and task structure on components of the event-related brain potential. *Psychophysiology*, 23, 33-47.
- Kutas, M. and Donchin, E. (1978) Variations in the latency of P300 as a function of variations in semantic categorizations. In: D. Otto (Ed.), *Multidisciplinary Perspectives in Event-Related Brain Potential Research*. EPA-600/9-77-043. U.S. Government Printing Office, Washington, DC, pp. 198-201.
- Kutas, M., McCarthy, G. and Donchin, E. (1977) Augmenting mental chronometry: the P300 as an index of stimulus evaluation time. *Science*, 197, 792-795.
- Magliero, A., Bashore, T., Coles, M.G.H. and Donchin, E. (1984) On the dependence of P300 latency on stimulus evaluation processes. *Psychophysiology*, 21, 171-186.
- Marsh, G.R. (1975) Age differences in evoked potential correlates of a memory scanning process. *Exp. Aging Res.*, 1, 3-16.
- McCarthy, G. and Donchin, E. (1981) A metric for thought: a comparison of P300 latency and reaction time. *Science*, 214, 77-80.
- McCarthy, G. and Donchin, E. (1983) Chronometric analyses of human information processing. In: A.W.K. Gaillard and W. Ritter (Eds.), *Tutorials in Event-Related Potential Research: Endogenous Components*. Advances in Psychology, Vol. 10. North Holland Publishing Co., Amsterdam, pp. 251-268.
- Mishkin, M. (1982) A memory system in the monkey. *Phil. Trans. Roy. Soc. Lond. B (Biol. Sci.)*, 298, 85-95.
- Murdoch, Jr., B.B. and Walker, K.D. (1969) Modality effects in free recall. *Verb. Learn. Verb. Behav.*, 86, 665-676.
- Näätänen, R. (1982) Processing negativity: an evoked potential reflection of selective attention. *Psychol. Bull.*, 92, 605-640.
- Näätänen, R. (1985) Selective attention and stimulus processing: reflections in event-related potentials, magnetoencephalogram, and regional cerebral blood flow. In: M.I. Posner and O.S.M. Marin (Eds.), *Attention and Performance*, Vol. XI. Erlbaum, Hillsdale, NJ, pp. 355-373.
- Näätänen, R. (1986) Neurophysiological basis of the echoic memory as suggested by event-related potentials, and magnetoencephalogram. In: F. Klix and H. Hagendorf (Eds.), *Human Memory and Cognitive Capabilities*. Elsevier, Amsterdam, pp. 615-628.
- Näätänen, R. and Picton, T. (1987) The N1 wave of the human electric and magnetic response to sound: A review and an analysis of the component structure. *Psychophysiology*, 84, 375-425.
- Okada, Y.C., Kaufman, L. and Williamson, S.J. (1983) The hippocampal formation as a source of the slow endogenous potentials. *Electroenceph. clin. Neurophysiol.*, 55, 417-426.
- Pantev, C., Hoke, M., Lehnertz, K., Lutkenhoner, B., Anogianakis, G. and Witowski, W. (1988) Tonotopic organization of the human auditory cortex revealed by transient auditory evoked magnetic fields. *Electroenceph. clin. Neurophysiol.*, 69, 160-170.
- Pelizzone, M., Williamson, S.J., Kaufman, L. and Schafer, K.L. (1984) Different sources of transient and steady state responses in human auditory cortex revealed by neuromagnetic fields. *Ann. NY Acad. Sci.*, 435, 570-571.
- Petersen, S.E., Fox, P.T., Posner, M.I., Mintun, M. and Raichle, M.E. (1989) Positron emission tomographic studies of the processing of single words. *J. Cogn. Neurosci.*, 2, 153-170.
- Pfurtscheller, G. (1988) Mapping of event-related desynchronization and type of derivation. *Electroenceph. clin. Neurophysiol.*, 70, 190-193.
- Pfurtscheller, G. and Aranibar, A. (1977) Event-related cortical desynchronization detected by power measurements of scalp EEG. *Electroenceph. clin. Neurophysiol.*, 42, 817-826.
- Pfurtscheller, G., Steffan, J. and Maresch, H. (1988) ERD-mapping and functional topography - temporal and spatial aspects. In: G. Pfurtscheller and F.H. Lopes da Silva (Eds.), *Functional Brain Imaging*. Hans Huber, Toronto, pp. 117-130.
- Picton, T.W., Campbell, K.R., Baribeau-Brown, J. and Proulx, J.B. (1978) The neurophysiology of human attention: a tutorial review. In: J. Requin (Ed.), *Attention and Performance VII*. Erlbaum, Hillsdale, NJ, pp. 429-467.
- Pratt, H., Michalewski, H.J., Patterson, J.V. and Starr, A. (1989a) Brain potentials in a memory scanning task. I. Modality and task effects on potentials to the probes. *Electroenceph. clin. Neurophysiol.*, 72, 407-421.
- Pratt, H., Michalewski, H.J., Patterson, J.V. and Starr, A. (1989b) Brain potentials in a memory-scanning task. II. Effects of aging on potentials to the probes. *Electroenceph. clin. Neurophysiol.*, 72, 507-517.
- Pratt, H., Michalewski, H.J., Patterson, J.V. and Starr, A. (1989c) Brain potentials in a memory scanning task. III. Potentials to the items being memorized. *Electroenceph. clin. Neurophysiol.*, 73, 41-51.
- Schneider, W. and Schiffrin, R.M. (1977) Controlled and automated human information processing. I. Detection, search, and attention. *Psychol. Rev.*, 84, 1-50.
- Squire, L.R. (1987) *Memory and Brain*. Oxford Univ. Press, New York.

- Starr, A. and Barrett, G. (1987) Disordered short-term memory in man and event-related potentials. *Brain*, 110, 935-959.
- Sternberg, S. (1966) High speed scanning in human memory. *Science*, 153, 652-654.
- Sternberg, S. (1969) **Memory scanning**: mental processes revealed by reaction time experiments. *Am. Scient.*, 57, 421-457.
- Strayer, D.L. and Kramer, A.F. (1990) Attentional requirements of automatic and controlled processing. *J. Exp. Psychol.: Learn. Mem. Cogn.*, 16, 67-82.
- Ungerleider, L.G. and Desimone, R. (1986) Cortical connections of visual area MT in the macaque. *J. Comp. Neurol.*, 248, 190-222.
- Ungerleider, L.G. and Mishkin, M. (1982) Two cortical visual systems. In: D.J. Ingel, R.J.W. Mansfield and M.A. Goodale (Eds.), *The Analysis of Visual Behavior*. MIT Press, Cambridge, MA, pp. 549-586.
- Vaughan, Jr., H.G. and Ritter, W. (1970) Electroenceph. clin. Neurophysiol., 28, 360-367.
- Williamson, S.J., Pelizzone, M., Okada, Y., Kaufman, L., Crum, D.B. and Marsden, J.R. (1984). In: H. Collan, P. Berglund and M. Krusius (Eds.), *Proc. 10th Int. Cryogenic Eng. Conf., ICEC10*. Butterworth, Guilford, Surrey, pp. 339-348.
- Yamamoto, T., Williamson, S.J., Kaufman, L., Nicholson, C. and Llinás, R. (1988) Magnetic localization of neuronal activity in the human brain. *Proc. Nat. Acad. Sci. (U.S.A.)*, 85, 8732-8736.

Verbal and Imaging Tasks have Different
Effects on Spontaneous Activity of
Cerebral Cortex

L. Kaufman, Y.M. Cycowicz, M. Glanzer, and S.J. Williamson

New York University

Abstract

This research presumed that changes in levels of the brain's spontaneous activity would occur in different areas, depending on the nature of the task performed by the subject. Thus, one specific hypothesis was that spontaneous activity (in the alpha band of 8-12 Hz) would exhibit a period of suppression over visual cortex commensurate with the time required to form mental images of objects represented by words. Alternatively, performing a verbal task in response to the same words (finding rhymes) would not result in the same pattern of suppression. The latter would produced suppression over the fronto-temporal (speech) areas. Since the sources of the brain's magnetic field close to their sensor are the predominant phenomena detected in magnetoencephalography (MEG), the use of this method avoided contamination of results by changes in activity of sources distant from electrodes used in electroencephalography. When subjects formed mental images the activity exhibited a prolonged suppression over the occipital area, and a shorter *suppression with delayed* onset over the fronto-temporal areas. However, while performing the rhyming task, suppression was longer over the fronto-temporal region than over the occipital area. Here too the onset of the suppression measured over the fronto-temporal areas was about 100 msec later than it was over the occipital area. This implies that alpha is not a global phenomenon, but differs in different parts of the brain. Thus, it may be taken as a sign of engagement of these different parts of the brain in specific cognitive tasks, just as blood flow serves as a similar index of activation in PET studies.

Recent positron emission tomography (PET) experiments provide evidence for different distributions in blood flow within the cortex of the human brain when passively viewing words, as opposed to performing a semantic task with those words [Petersen et al., 1989]. It is plausible to assume that the changes in distribution of blood flow are accompanied by changes in levels of neural activity of these same regions. We have carried out magnetic source imagery studies of a similar problem by directly monitoring changes in the electrical activity of cortex when words are employed in different mental tasks. More specifically, we tested whether there are differential regional changes in electrical activity, as reflected in the magnetoencephalogram (MEG), that accompany performance of different mental tasks. Our procedure requires that subjects process single words in two different tasks, one a mental imagery task and the other a verbal (rhyming) task. The tasks are quite different from each other so that the differences in the accompanying distributions of cortical activity would be relatively easy to detect. The tasks have, moreover, an additional value in that they shed light on an important issue concerning the brain processes underlying mental imagery.

This issue concerns the role of the visual system in mental imagery and has been the subject of considerable controversy ever since Shepard and Metzler [1971] published their paper on mental rotation. The controversy is amply discussed by Finke and Shepard, [1986] Pylyshyn [1973] and Kosslyn [1983]. The question is whether mental imagery is based on neural representations of visual objects, or on a more abstract process, involving propositions about visual objects. This issue may be resolved by a demonstration that forming or rotating mental images involves the area of the brain engaged in vision. This question motivated experiments by Farah et al. [1988] who found that event related potentials (ERPs) subsequent to presentations of letter stimuli differ, depending on whether or not the subjects had formed mental

images of letters prior to their presentation. The effects were stronger when detected at occipital and parietal electrodes but the actual locations of the neuronal activity were not established. Nevertheless, this seems to implicate visual areas of the brain in forming mental images, even when there are no concurrently present visual stimuli.

The preceding work indicates the possible involvement of the visual cortex in mental imagery. A number of questions, however, remain to be answered. The answers could change our interpretation of the preceding work. It is possible, for example, that visual cortex and other visual areas may be active in propositional thinking. Therefore, visual cortex could be active when subjects engage in non-visual problem solving tasks initiated by the presentation of visual stimuli. It is also possible that mental imagery may be accompanied by changes in activity of non-visual as well as visual portions of the brain. Neither of these two possibilities have been fully examined. Therefore, a complete understanding of the neural substrate of mental imagery first requires an understanding of how activity is allocated among several different cortical regions during mental imagery and during performance of non-visual tasks that are equal in difficulty and in attentional demands. Clearly, failure to demonstrate any involvement of the visual areas would rule out its part in the cognitive process. Alternatively, demonstration of involvement of areas normally not involved in perceiving objects would illustrate the probable complexity of the underlying process.

Using the MEG, Kaufman, Schwartz, Salustri, and Williamson [1990] found that the spontaneous activity of occipital cortex within the 8-12 Hz band is modulated when subjects search short-term memory for previously seen visual forms. Moreover, the depth of modulation (suppression) was greater along the midline indicating that mental imagery involves the visual cortex. In comparison, when subjects scan memory for musical tones Kaufman, Curtis, Wang, and Williamson [1992] observed an

analogous suppression that probably originated in temporal areas, particularly of the right hemisphere. Their data suggest that the auditory cortex contributes significantly to the spontaneous activity modulated by auditory memory scanning. The duration of the suppression of spontaneous brain activity is strongly correlated with the time subjects needed to decide if a tone was one of a set of previously heard tones. Similarly consistent results were not obtained with the simultaneously measured EEG using midline vertex and occipital electrodes. This rules out global alpha blockage, conventionally attributed to a change in generalized arousal, as the cause of the suppression. Furthermore, simultaneous measures of N100 failed to reveal differential effects of attention. The amplitude of N100 did not vary systematically with size of the memory set or with reaction time.

In summary, it now seems clear that the changes in level of spontaneous brain activity originating in visual areas occur during search of visual memory. It also seems clear that search of auditory memory affects other areas.

In this paper we report an experiment in which imaging and verbal tasks initiated by the same visual stimuli are performed by the same subjects. We will demonstrate the differential distribution of brain activity during performance of these tasks. That is, different cortical regions are affected by each different type of task. The differential distribution of activation will be shown to be related to a logically consistent picture of brain function during the tasks.

The effects of memory scanning on brain activity seems to be most pronounced within a spectral band of about 8-12 Hz [Kaufman et al., 1990]. This is the characteristic frequency band of the *alpha rhythm*. Presumably, this is also the case for changes in brain activity accompanying mental imagery and similar cognitive tasks. Earlier researchers have reported evidence that changes in level of alpha activity accompany many different cognitive processes [Golla et al., 1943, Slatter, 1960]. In

the EEG, the occipital alpha rhythm is strongest when recorded from alert healthy adults at rest, with eyes closed. If subjects open their eyes and attend to visual objects the alpha spindles are inhibited (blocked). Generalized arousal is also presumed to be a cause of alpha blockage. The alpha activity is especially prominent in the occipital region, and the visual cortex is apparently a major contributor [Chapman et al., 1984, Vvedensky et al., 1985, Williamson et al., 1989]. Other brain areas are characterized by still other rhythms. For example, the *mu rhythm* (7-10 Hz) appears to be characteristic of the motor cortex. It too is attenuated when subjects engage in performing motor tasks [Pfurtscheller and Aranibar, 1977], just as alpha is attenuated by visual tasks. It is also widely reported that when alpha activity is blocked it is replaced by *beta* activity which occupies the 16-24 Hz band of the EEG. This is taken to be a sign of *activation*. However, Kaufman et al. [1990] did not detect any increase within the beta bandwidth during suppression of alpha. Moreover, they found that beta band exhibits a suppression that coincides in time with the reduction observed in the alpha band.

In the present study we investigate the spatio-temporal pattern of ongoing activity in alpha (8-12Hz) and, as a subsidiary matter, the beta (16-24Hz) bandwidths when subjects engaged in cognitive tasks. The tasks, mental imagery and rhyming, were equated for difficulty to minimize the differential effect of attentiveness. The physical stimuli, to which the subject responded, were essentially equivalent.

Method

Subjects

Five paid subjects, participated in the experiment, two young female and three young male adults, all right handed and with normal vision.

Tasks

Three different tasks were used. In all three, items were presented sequentially, one at a time, on a screen. Items were drawn from three different lists. These were the *imagery*, *rhyming*, and *nonsense* (control) lists. Each list was composed of 24 words. Those in the imagery list referred to objects that were easily imaged, e.g., "pen". When presented with these words the subjects had been asked to form mental images of the objects they represented (imaging condition). The rhyming list was composed of 12 easily imaged words and 12 abstract words, i.e., words that did not refer to objects that were easily imaged objects, e.g., "law". These two types were included to check whether they induced different response pattern in the rhyming condition. (Since no differences were found between the two types this characteristic of the list will not be considered further.) Subjects viewed these words with the instruction to find a word that rhymed with the one they had just seen (rhyming condition). The nonsense (control) list consisted of meaningless sequences of letters equal in number to the letters in the words on the other lists. This condition was designed to examine the effect of the visual stimuli themselves, since other than detection, no mental task was required while subjects viewed the nonsense list.

The subjects were instructed to press a button as soon as they had formed a mental image (in the imaging condition), found the rhyme (in the rhyming condition), or detected the nonsense word (in the control condition). Subjects were instructed,

however, to continue to hold the images in the imagery task, or to search for other rhymes in the rhyming task until the next word was shown on the screen. This was done to keep the subject from engaging in other tasks e.g., forming an image after finding a rhyme, or finding a rhyme after forming an image.

When the neuromagnetic field over the lateral areas of the scalp was measured, the subject was instructed to respond with the ipsilateral hand in order for the sensors not to detect signals associated with motor activity.

Procedure

The subjects were tested in a magnetically shielded room. A neuromagnetometer probe containing five sensors was placed above the appropriate areas of the head. The subject knelt on a stool with cushioned head and arm rests and looked down into a mirror at the reflected images of the presented words. The word stimuli were generated by an Amiga 1000 computer and projected onto a screen inside the magnetically shielded room. The virtual image of the screen, viewed by the subjects in the mirror, was at an optical distance of 2.0 meter from the eyes. Looking downwards made it possible to measure the magnetic fields over the posterior portion of the scalp. To compensate for head position changes, e.g., when the probe was placed over the sides of the scalp, the mirror was tilted to keep the locations of the stimuli approximately constant in the visual field. A fixation point was maintained in the middle of the of the screen and the subject was instructed to maintain fixation at all times. Each word was presented for 200 msec at a position centered on a point just beneath the fixation point. The interstimulus interval (ISI) was 7 sec.

Magnetic Recording

MEG recordings were made with a SQUID-based Neuromagnetometer (Bio-magnetic Technologies, Inc.) containing five sensors, which simultaneously registered the component of the field perpendicular to the scalp. The probe was placed over the occipital, right temporal or left temporal areas in different sessions while the subject carried out imagery, rhyming and control tasks. The superconducting detection coil of each sensor is 1.5 cm in diameter and wound in the configuration of a second order gradiometer with a 4 cm baseline. The detection coils, superconducting quantum interference devices (SQUIDs), and other superconducting electronics were immersed in liquid helium, contained in a cryogenic vessel (dewar). The bottom of the tail section of the dewar had a 9 cm radius of curvature which made it possible to keep all of the detection coils approximately normal to the surface of the head. The five detection coils were arranged with one in the center and the other four around it in a circular pattern of 2 cm radius. Thus, they simultaneously detected the field at five different places spaced 2 cm apart. A Probe Position Indicator system (PPI) determined the position and orientation of each of these detecting coils with respect to the subject's head with a precision of 2 mm [Yamamoto et al., 1988].

The MEG was measured for 6 seconds for each stimulus, beginning 2 seconds before the stimulus appeared and continuing 4 seconds afterwards. This was followed by one more second with no recording to provide a total interstimulus interval of 7 seconds. The outputs of each of the five SQUID channels were bandpass filtered (0.1-50 Hz) and stored for subsequent analysis. The computer also stored reaction times, based on by the time of button press. Each 6 sec epoch was digitally bandpass filtered from 8-12 Hz and also from 16-24 Hz before computing the average response and the variance about the average within each of these bands. Each average response

was based on 24 epochs, where each epoch was belonged to specific word list. The variance represents brain activity that is not coherently related to the presentation of the stimuli and is equal to the mean power (mean square field) of spontaneous activity within the bandwidth of the filtered MEG. Thus we use the term *alpha power* to describe the power within the 8-12 Hz band of the MEG recorded in each of the five channels. Similarly, the term *beta power* is used to designate the power in the 16-24 Hz MEG band.

For each subject, the five channel neuromagnetometer was placed at several positions over the occipital, parietal, frontal and temporal areas. For purposes of description, it is convenient to divide the scalp into three regions. Looking at the head from above, consider a circle in the transverse plane with the nasion arbitrarily located at 0 deg. Then, in the counterclockwise direction, the left fronto-temporal region (LFT) is designated as the area included the angular range between 40-130 deg, the occipital-parietal area (OCP) within the 130 - 220 deg range, and the right fronto-temporal region (RFT) within the 220 - 300 deg range. These regions and the sites used to make recordings within them are shown schematically in Figure 1. All three experimental conditions were run at each location of the neuromagnetometer, so that five simultaneous measures of brain activity were made at five different positions of the probe within an area. Several replicated measurements were made within each area, with the five sensors at somewhat different positions. The averaging and variance computations were done separately for each sensor at each location.

Two subjects withdrew from the experiment before all measures were completed. Therefore, full sets of data are available for only three subjects. For one subject, JB, measurements were made only from the OCP area. The other incomplete subject, LS, gave measures from the OCP and LFT areas.

Figure 1 about here

Data Analysis

The duration and onset of alpha suppression were measured for each sensor location in each test condition. The criterion for onset and offset of suppression was based on the average level of power within the entire recording epoch. The point in time at which alpha power prior to the presentation of the stimulus descended to the level of this average is designated as the "onset" time of suppression. The point in time at which the alpha power (and beta) rose to the level of the average is designated as the "offset" time. The duration of the suppression (suppression period=SP) is the offset time minus onset time. (An example of the definition of suppression period in this fashion is given in Figure 3.)

The RTs for each set of 24 epochs were averaged for each condition and averaged again over all locations. These average RTs over each condition enable us to determine whether the tasks themselves require different amounts of time for their performance.

Results

Response Times

The mean RTs of the 5 subjects for each condition are shown in Figure 2. It is obvious that the mean RTs for the control condition are the shortest for all subjects. This is expected since subjects were simply asked to press the button as soon as they saw the nonsense word appear on the screen. However, when a mental task was required the mean RTs showed a marked increase. This is shown for both imaging

and rhyming. For 3 out of 5 subjects, the mean RTs are essentially the same for the two experimental conditions. This suggests that the two tasks are equivalent in terms of the amount of time needed to complete them and, therefore, the amount of effort they required. The other two subjects display a different pattern. Subject LS takes a considerably longer time to form an image than to find rhymes, while subject STF shows the opposite effect. Nevertheless, a repeated measure ANOVA shows that the RT of the two tasks does not differ significantly (at $p=0.05$ level). Moreover, the RT for the control task is significantly different from each of the other two tasks for all subjects.

Figure 2 about here

Alpha Suppression

Figure 3 shows examples of alpha suppression as picked up by all five recording channels simultaneously located over the OCP area during each of the tasks for subject MP. The records in all three panels were made during a single session. Alpha suppression begins within the first 100 msec of the word's presentation. Its duration depends on the task that the subject is performing. Imaging produces longer suppression than rhyming (2.1 vs 1.4 seconds), and the latter appears to be no longer than the suppression duration accompanying the control task (1.3 seconds). Task difficulty was equal in the two experimental conditions as revealed by RT, therefore task difficulty could not be responsible for this difference in suppression duration. Furthermore, since the RTs for the control task were much shorter than for the rhyming task, indicating a difference in difficulty, the similarity in the SP occurring during these two tasks is also inconsistent with the idea that SP is related to generalized

effort or arousal.

Figure 3 about here

Figure 4 illustrates how the SP varies over the LFT area during each of the tasks, again for subject MP. Here the onset of suppression starts about 200 msec after the word's presentation. The SPs for each task differ from those measured over the OCP area. For imaging, SP is shorter than it was in the OCP area (only 1.2 seconds). However, SP is much greater for the rhyming condition (1.7 seconds), while that of the control condition is still short (1.1 seconds). These sample responses are typical, and were found for the other subjects as well.

Figure 4 about here

Figure 5 shows the mean onset time of the suppression. It is clear that the onset of the suppression is later when recorded on either side of the head than it is over the posterior portion. This difference is statistically significant for all subjects except STF. The averaged difference between the mean onset time over the occipital area and the sides of the head is about 100 msec. This reflects the amount of time needed for signals to be transferred from one area of the brain to another.

Figure 5 about here

Histograms describing how SP varies for each subject at a specific location for each condition are shown in Figure 6a, 6b and 6c. In Figure 6a we see that for the imaging condition SP measured over the OCP region is longer for three out of four subjects than in the temporal regions (LFT and RFT).

Figure 6b shows that SP for rhyming is shorter over the OCP region than over the temporal regions for all four subjects. For the three subjects measured over both LFT and RFT, all show a longer SP during rhyming for the left hemisphere than for the right hemisphere.

We started with the hypothesis that SP would be very short for the control condition over all regions of the scalp where it was detectable. The results, shown in Figure 6c, indicate that overall SP is shorter at every location compared with the other two tasks. It should be noted, however, that SP for the control condition over the OCP region is shorter than over both fronto-temporal areas. It is noteworthy that SP for the control condition is as long over the right temporal region as it is over the left, while SP for rhyming is asymmetrical for 2 out of 3 subjects (as noted above).

Figure 6 about here

Figures 7a and 7b show the same data as Figures 6a, b and c but compare the tasks at a given location. From Figure 7a it is clear that, over the OCP, SP for the imaging task is longer than for either rhyming and control tasks. While three subjects show an equal SP for both rhyming and control task, subjects BOR and JB show a larger SP for the rhyming task than for the control task.

The pattern of SP is different over the LFT as is shown at Figure 7b. Here three out of four subjects show a longer SP for the rhyming task. Both the imaging and the control tasks show a shorter and a similar SP for those subjects. Subject BOR is somewhat different. That subject shows a longer SP for the imaging task than for the rhyming task, and shortest for the control condition. Although this pattern appears for this subject over the OCP area as well, the difference in the SP between the three conditions is much smaller over the LFT region.

Figure 7 about here

The t-test was used to determine the significance of the differences in SP. We carried out two types of tests. We compared SP for one task at various locations (Table 1), and we compared tasks at the same location (Table 2). Measurements for the right hemisphere were not included in the analysis since the sample of data points was too small, and we had them for only three subjects.

Although the analysis of variance is generally used for making multiple comparisons, the lack of an equal number of measurements for the various conditions, required the use of multiple t-tests instead. This introduced the risk of an increased probability of α type errors. To offset the risk we required a higher level of significance, using the Bonferroni correction in which the conventional α type error is divided by the number of the comparisons. Thus, in this case 0.05 was divided by 17 given us a 0.003 level of significance. That level served as our criterion for a statistically significant difference between mean SPs. Comparing the SP of the imaging task over the OCP and LFT areas reveals a significant statistical difference for two out of four subjects. The SP of the rhyming tasks over the LFT was significantly

longer than over the OCP region for three out of four subjects. All subjects show a significant statistical difference when the imaging task is compared to the rhyming task over the OCP area, while no subject shows such a significant difference over the LFT area. The conservative approach we adopted (by the Bonferroni correction) required a large difference between the SPs of the two tasks. Therefore, although the rhyming task appears to show a longer suppression over the LFT area, for most subjects, it is not that much larger than the suppression measured for the imaging task at that location.

Table 1 and 2 are about here

Beta Suppression

As noted earlier there is a question raised in the literature as to whether beta (16-24 Hz) replaces alpha when alpha is blocked. We checked this hypothesis by examining the pattern of beta power during the performance of the tasks. As indicated in the method section, power in the 16-24 Hz band was examined in the same way as was that of the 8-12 Hz band. However, many of the measurements showed no suppression. In general, the power level of beta is much smaller than that of alpha, and where suppression seemed present it was of shorter duration. Figures 8a, 8b, and 8c show the histograms of the SP of beta power measured at every location for each subject for each condition. The SP of beta power does not show the systematic pattern found in the SP of the alpha power. For example, the SP for alpha in the imaging condition over OCP (Figure 7a) is longer than SP at the other locations, for all subjects. However, the SP for beta power in the same locations for the same task is inconsistent. This is true for the other conditions as well. Furthermore, the

variations within subjects (indicated by the error bar) are high.

Figure 8 about here

We were unable to detect facilitation in the beta bandwidth during suppression of alpha. Sometimes beta exhibited a suppression where its onset coincided with that of alpha. Figure 9 shows the onset time of the beta suppression. On average, beta suppression starts about 100 msec after stimulus presentation over the OCP area, and at about 200 msec over the LFT and RFT areas.

Figure 9 about here

Discussion

In this study, we asked the subjects to perform two cognitive tasks. The tasks were designed so that they took approximately the same time, assuming that the same level of attention would be used in each one. Thus any difference of alpha power or spontaneous activity must be explained by task-related differences in brain activity. The main findings of this study are: 1) SP of alpha varies depending upon the task performed and the area of the brain recorded. The imaging task shows a long SP over OCP, while the rhyming task shows a long SP over the LFT area. 2) Onset of the suppression shows delay over fronto-temporal regions compared with parieto-occipital area.

Our findings are not conclusive evidence for either of the two main theories of mental imagery. Both visual cortex and clearly non-visual fronto-temporal areas reveal activity that is correlated with the imaging process. In fact, the results are consistent with the view that the two approaches complement each other. Both have elements that must be considered in any theory designed to account for the data of mental imagery experiments.

Alpha power is suppressed over the OCP region for all tasks. It is however significantly longer for the imaging task than for rhyming and control tasks. The shorter duration of suppression for the latter tasks, rhyming and control, may be due to the fact that the suppression here is due primarily to processing of the sensory-perceptual properties of the words and has little or nothing to do with processing of their semantic properties. This conclusion is supported by the fact that the mean RT for imaging and rhyming tasks are about the same for most subjects. Thus, although subjects continue to seek rhymes, the occipital alpha activity returns to its base level. Furthermore the suppression of occipital alpha power for the control condition, which only requires the subject to detect a visual stimulus, is about the same as for the rhyming condition. In contrast, the duration of the alpha suppression over the LFT and RFT areas shows different temporal patterns than the one over the OCP area. Over the LFT area the duration of suppression for the imaging task is significantly shorter for 3 out of 4 subjects than it is over the occipital region, while for the rhyming task SP for all four subjects is significantly longer. This evidence is consistent with the hypothesis that alpha frequencies are generated by cortical sources in different regions and these sources are affected in different ways, depending on the mental activity subjects perform.

There are strong individual differences in the durations of alpha suppression for all conditions. However, for the imaging condition this variability is most pronounced

when the probe is located in the OCP area. Under the same conditions, the same subjects show less variability with the probe in the LFT area. Just the reverse is true for the rhyming condition, where individual differences are strongest in the LFT area, and less strong in the OCP area.

It is clear from these results that the visual areas of the brain are engaged in mental imagery. However, it is equally true that non-visual areas also become involved in such tasks. Therefore, performing the imaging task involves regions of the cortex that are not normally engaged in visual sensory-perception. More specifically, the task appears to involve language-related centers as well.

The duration of suppression accompanying the control stimuli is longer over the fronto-temporal regions than over the occipital region. The longer suppression duration for these same nonsense words recorded over the left fronto-temporal area may be related to the fact that the language centers were involved in some degree in the processing of the nonsense words. After the experiments the subjects reported that, contrary to instructions, they tended to sound out the nonsense words or to identify them with orthographically similar meaningful words.

It is obvious that mental imagery tasks are not devoid of verbal content. In fact, subjects also reported that they manipulated verbal materials while performing the imaging task. They reported mentally imaging the word stimulus itself. However, no subjects reported having mental images when they performed the rhyming task.

For all subjects the suppression in the left hemisphere during performance of the rhyming task was significantly longer in duration than in the occipital area. This is consistent with the fact that all subjects were right handed and, presumably, their speech centers were located in the left hemisphere. Similarly, for three of four subjects the duration of suppression was longer for the rhyming task than for the control task over the left hemisphere. The picture is less clear for the right hemisphere, where

only one subject showed a similar difference between rhyming and the control task. However, we have insufficient data to draw any conclusions on the role of the right hemisphere.

The onset time for suppression is similar for all tasks but it differs between the occipital and fronto-temporal areas of the brain, with marked variability across subjects for the fronto-temporal area. Over the occipital area the suppression starts at about 130 msec while at the sides of the head it starts at about 200 msec after stimulus presentation. This supports the idea that it takes about 70 msec for information to be transferred from one region of cortex to another [Klemic et al., 1989]. Here, as expected, the visually presented stimulus first produces activity in the occipital cortex, and then information is transferred to other areas for further processing. Since this processing entails language, the left fronto-temporal is likely to become involved.

Goncharova and Barlow [1990] observed that when subjects moved from a state of relaxation to one of arousal, the EEG power in the alpha and beta bands was reduced. Similar findings were reported by Kaufman et al. [1990] in the MEG in a memory search task. The present results are consistent with both sets of findings. When alpha band activity is suppressed, activity in the beta band may either be suppressed as well or show no change at all in average level. Since the MEG is a true unipolar mode of recording and unaffected by volume currents flowing in the scalp, it must be insensitive to sources far from the pickup coils of the neuromagnetometer. Therefore, there is no compensation of local changes in level of alpha detected by the neuromagnetometer by changes in levels of beta. Also, Kaufman et al. [1990] found that the distribution of MEG alpha band activity over the scalp is largely uncorrelated with the spatial distribution of level of beta band activity. This implies an at least partly independent set of alpha and beta generators in the cortex. Although the alpha and beta suppression encountered over the occipital area had a

common onset time (no doubt due to the concurrent effect of the visual stimulus on the two generator systems), their subsequent time courses were largely uncorrelated with each other. This too is consistent with the hypothesis that different generator systems are involved. The precise functional significance of these systems is a subject for future study. Whether further narrow-band divisions of the MEG or EEG activity in low-band and high-band alpha, as suggested by Pfurtscheller ([1988], will reveal further significant functional differences is, in our view, to be doubted. This doubt is reinforced by the well-know fact of wide individual differences in central alpha frequencies and in alpha bandwidth. Therefore, the last word on whether functionally different and independent frequency generators exist in the nervous system has yet to be uttered. In any event, the possibility of such generators is a suitable subject for further research.

References

- Chapman, R. M., Ilmoniemi, R. J., Barbanera, S., and Romani, G. L. (1984). Selective localization of alpha brain activity with neuromagnetic measurements. *Electroencephalography and Clinical Neurophysiology*, 58,569-572.
- Farah, M., Peronnet, F., Weisberg, L. L., and Perrin, F. (1988). Electrophysiological evidence for shared representational medium for visual images and visual percepts. *Journal of Experimental Psychology*, 117,248-257.
- Finke, R. and Shepard, R. (1986). Visual functions of mental imagery. In Boff, K., Kaufman, L., and Thomas, J., editors, *Handbook of Perception and Human Performance: Vol. II, Cognitive Processes and Performance*, chapter 37, pages 1-55. John Wiley and Sons, New York.
- Golla, F., Hutton, E. L., and Walter, W. G. (1943). The objective study of mental imagery. I. Physiological concomitants. *Journal of Mental Science*, 75,216-223.
- Goncharova, I. I. and Barlow, J. S. (1990). Changes in EEG mean frequency and spectral purity during spontaneous alpha blocking. *Electroencephalography and clinical Neurophysiology*, 76,197-203.
- Kaufman, L., Curtis, S., Wang, J., and Williamson, S. (1992). Changes in cortical activity when subjects scan memory for tones. *Electroencephalography and Clinical Neurophysiology* page in press.
- Kaufman, L., Schwartz, B., Salustri, C., and Williamson, S. (1990). Modulation of spontaneous brain activity during mental imagery. *Journal of Cognitive Neuroscience*, 2,124-132.

Kaufman, L. and Williamson, S. J. (1990). Responses to steady-state auditory stimulation. In Grandori, F., Hoke, H., and Romani, G. L., editors, *Auditory Evoked Magnetic Fields and Electric Potentials*, volume 6 of *Advances in Audiology*, pages 283-312. Karger, Basel.

Klemic, G. A., Buchanan, D. S., Cycowicz, Y. M., and Williamson, S. J. (1989). Sequential spatially distributed activity of the human brain detected magnetically by CryoSQUIDS. In Williamson, S. J., Hoke, M., Stroink, G., and Kotani, M., editors, *Advances in Biomagnetism*, pages 685-688, New York. Plenum.

Kosslyn, S. N. (1983). *Ghosts in the Mind's Machine*. Norton, New York.

Petersen, S. E., Fox, P. T., Posner, M. I., Mintun, M., and Raichle, M. E. (1989). Positron emission tomographic studies of the processing of single words. *Journal of Cognitive Neuroscience*, 2, 153 - 170.

Pfurtscheller, G. (1988). Mapping of event related desynchronization and type of derivation. *Electroencephalography and Clinical Neurophysiology*, 70:190-193.

Pfurtscheller, G. and Aranibar, A. (1977). Event-related cortical desynchronization detected by power measurements of scalp EEG. *Electroencephalography and clinical Neurophysiology*, 42, 817-826.

Pylyshyn, Z. (1973). What the mind's eye tells the mind's brain. *Psychological Review*, 80, 1-24.

Shepard, R. N. and Meltzer, J. (1971). Mental rotation of three-dimensional objects. *Science*, 171, 632-634.

Slatter, K. H. (1960). Alpha rhythm and mental imagery. *Electroencephalography and clinical Neurophysiology*, 12, 851-895.

Vvedensky, V. L., Ilmoniemi, R. J., and Kajola, M. J. (1985). Study of the alpha rhythm with a 4-channel SQUID magnetometer. *Medical and Biological Engineering and Computation*, 23 Supp., Part 2, 11-12.

Williamson, S. J., Wang, J., and Ilmoniemi, R. J. (1989). Method for locating sources of human alpha activity. In Williamson, S. J., Hoke, M., Stroink, G., and Kotani, M., editors, *Advances in Biomagnetism*, pages 257-260, New York. Plenum.

Yamamoto, T., Williamson, S. J., Kaufman, L., Nicholson, C., and Llinás, R. (1988). Magnetic localization of neuronal activity in the human brain. *Proceedings National Academic of Science, USA*, 85, 8732-8736.

Figure 1: A schematic picture of the areas of the scalp within which the magnetic field was measured.

Figure 2: Mean RT for the imaging, rhyming and control tasks for each subject. The mean RT is averaged for each task over all sessions.

Figure 3: Alpha power recordings over the OCP region while subject MP engaged in the imaging task (top panel), the rhyming task (middle pannel), and in the control condition (bottom pannel). SP line represents the suppression period which is about the same for the rhyming and control conditions, but it is longer for the imaging condition. The vertical line below it, extending across the entire figure is the mean of power for the entire epoch. Its intersection with the power curve defines onset and offset.

Figure 4: Alpha power recordings over the LFT region while subject MP engaged in the imaging task (top panel), the rhyming task (middle pannel), and in the control condition (bottom pannel). The SP line represents the suppression period which is short for the imaging and control conditions but long for the rhyming task.

Figure 5: The onset time of alpha suppression for each subject at OCP, LFT (left side) and RFT (right side) locations. There is a delay in the onset time of the suppression at both LFT and RFT.

Figure 6: The SP of alpha power for each subjects for the three probe location. Panel (a) shows the data for the imaging condition, panel (b) for the rhyming task and (c) for the control.

Figure 7: The SP of alpha power for each subject for all conditions. Panel (a) show the data for OCP area and panel (b) shows it for the LFT region.

Figure 8: The SP of beta power for each subjects at different probe location. Panel (a) shows the data for the imaging condition, panel (b) for the rhyming task and (c) for the control.

Figure 9: The onset time of beta suppression for each subject at OCP, LFT and RFT locations. There is a delay in the onset time of the suppression at both LFT and RFT.

Table 1: The p-values for a significant difference obtained by comparing the mean SP obtained at the two probe locations OCP and LFT for the imaging and for the rhyming tasks.

Conditions Subject	Imaging	Rhyming
LS	$p < 0.0005$	$p < 0.0005$
STF	$p < 0.01$	$p < 0.0005$
MP	$p < 0.05$	$p < 0.0005$
BOR	$p < 0.0005$	$p > 0.1$
JB	—	—

Table 2: The p-values of for a significant difference obtained by comparing the mean SP of the imaging and rhyming tasks in the OCP and LFT areas.

Conditions Subject	OCP	LFT
LS	$p < 0.0005$	$p > 0.1$
STF	$p < 0.0005$	$p < 0.025$
MP	$p < 0.0005$	$p < 0.005$
BOR	$p < 0.0005$	$p < 0.05$
JB	$p < 0.0005$	—

Figure 1:

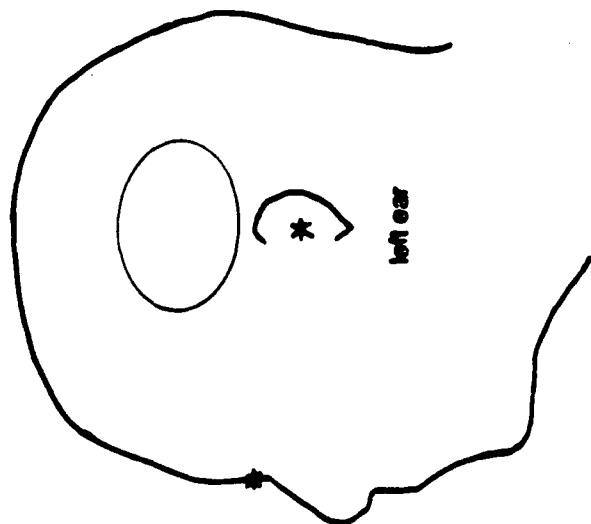
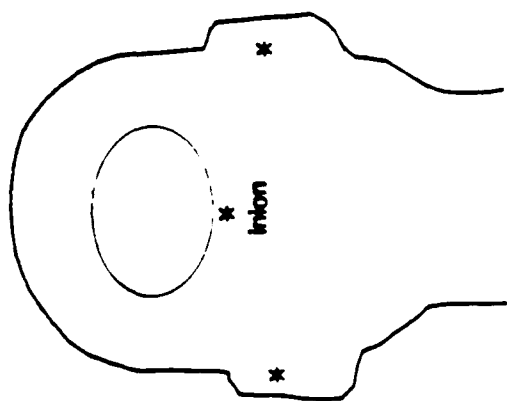
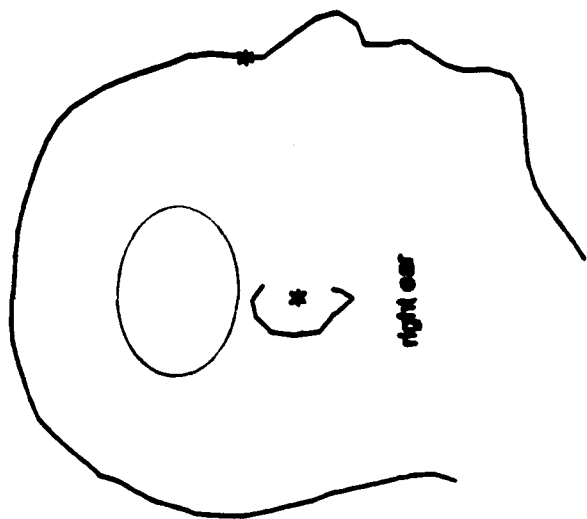


Figure 2.

MEAN REACTION TIME

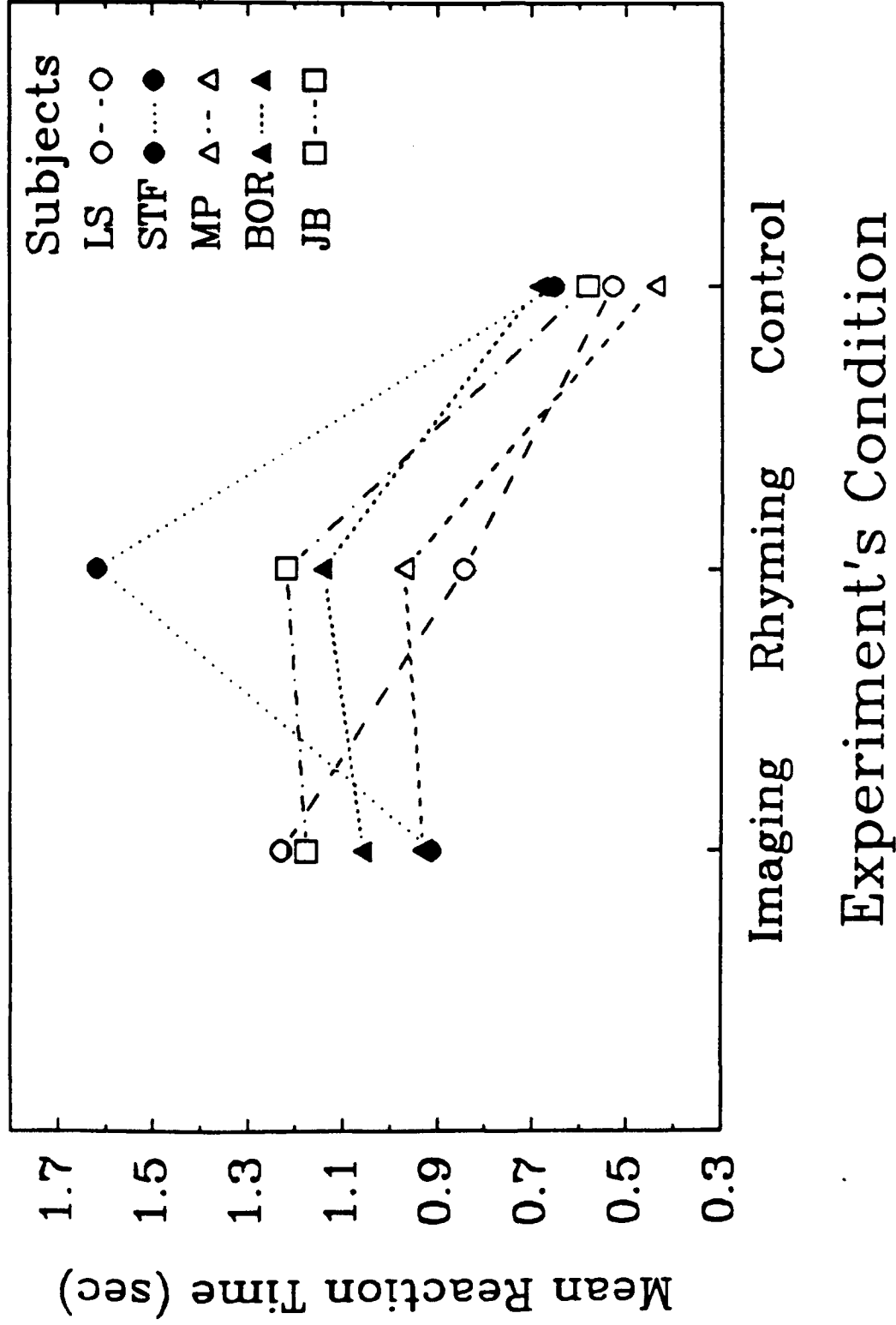


Figure 3:

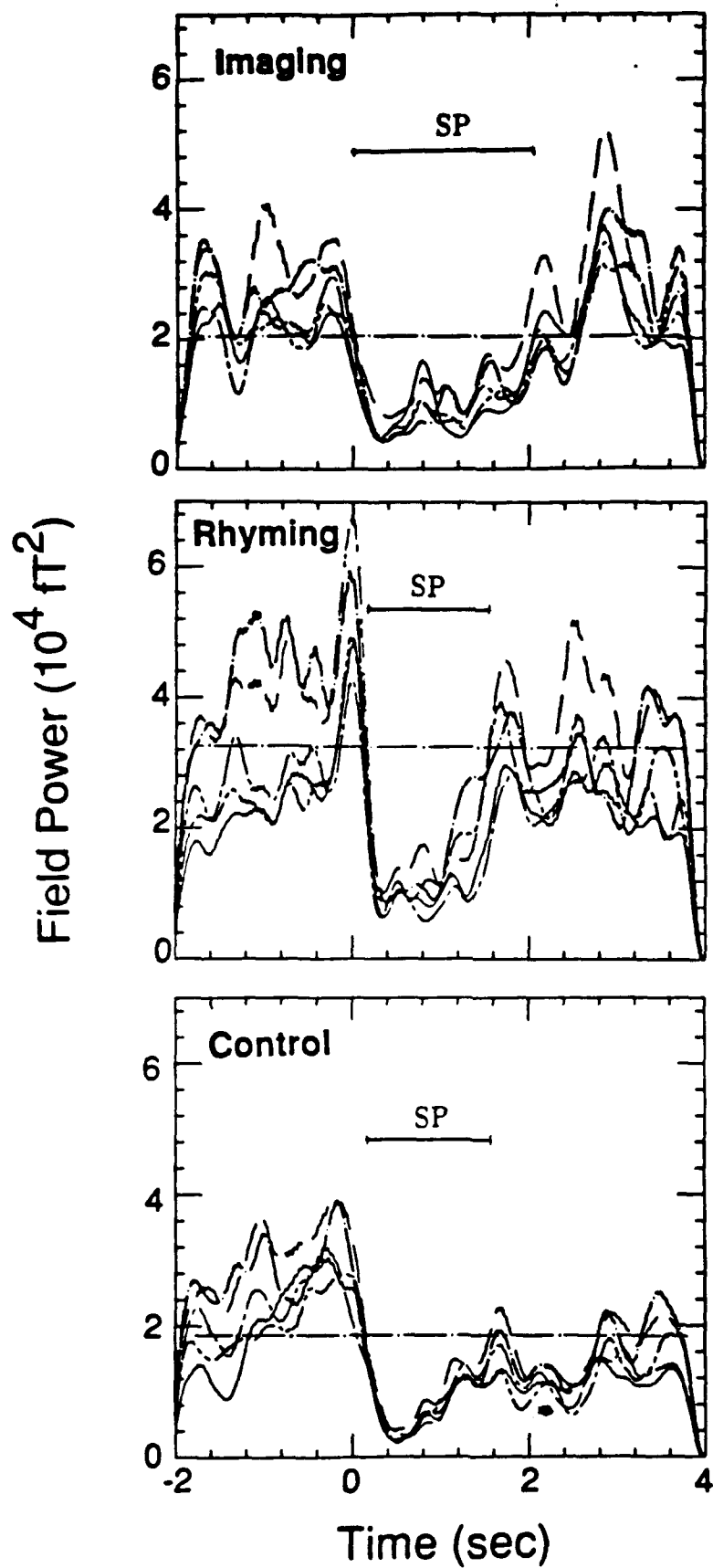


Figure 4:

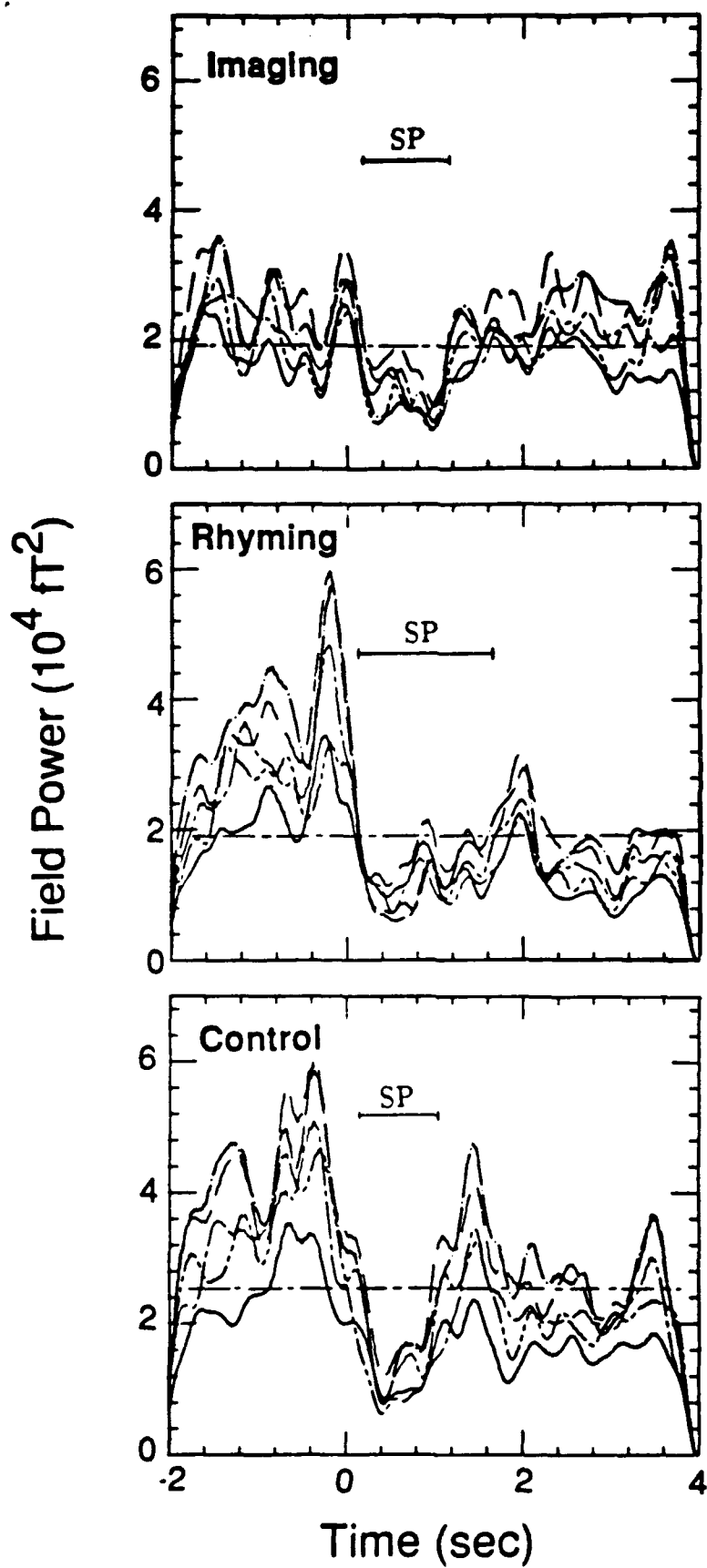


Figure 5:

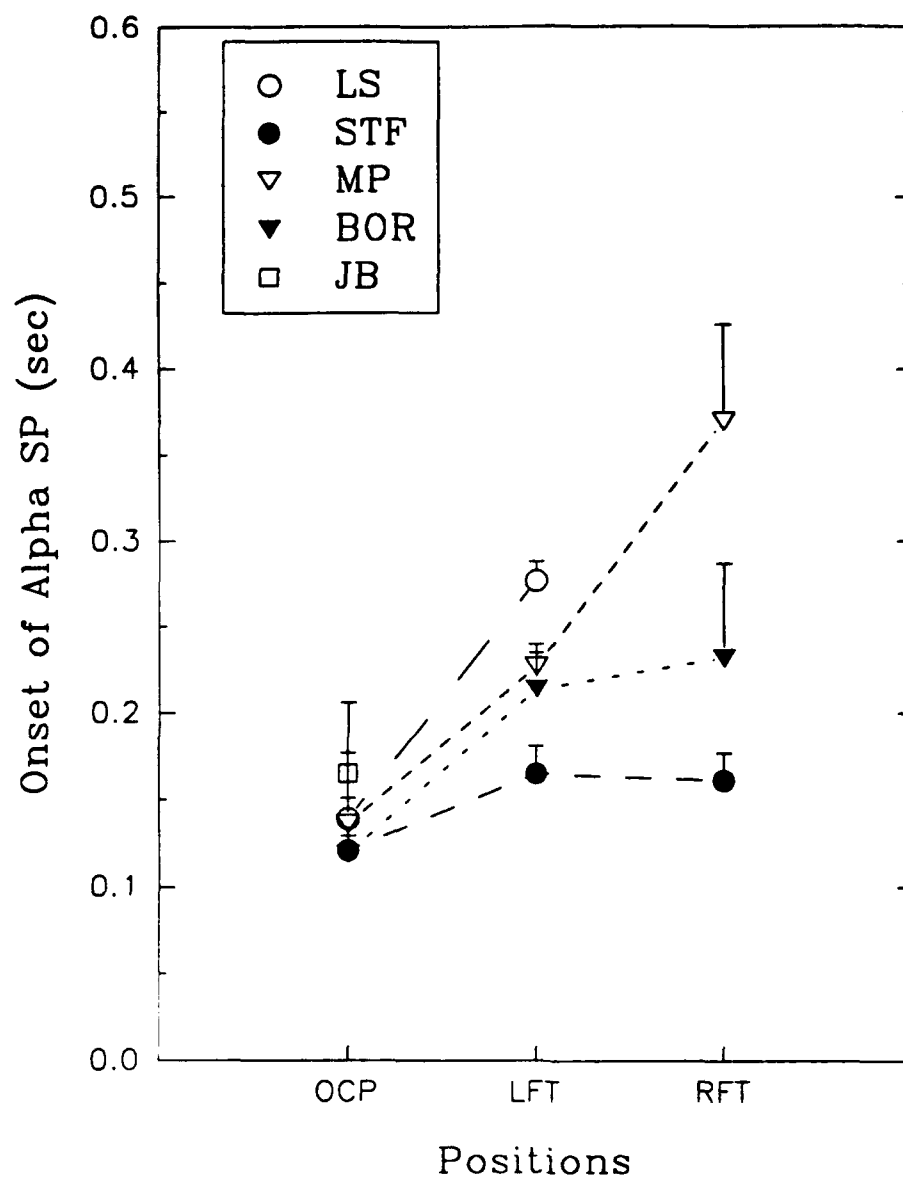


Figure 6

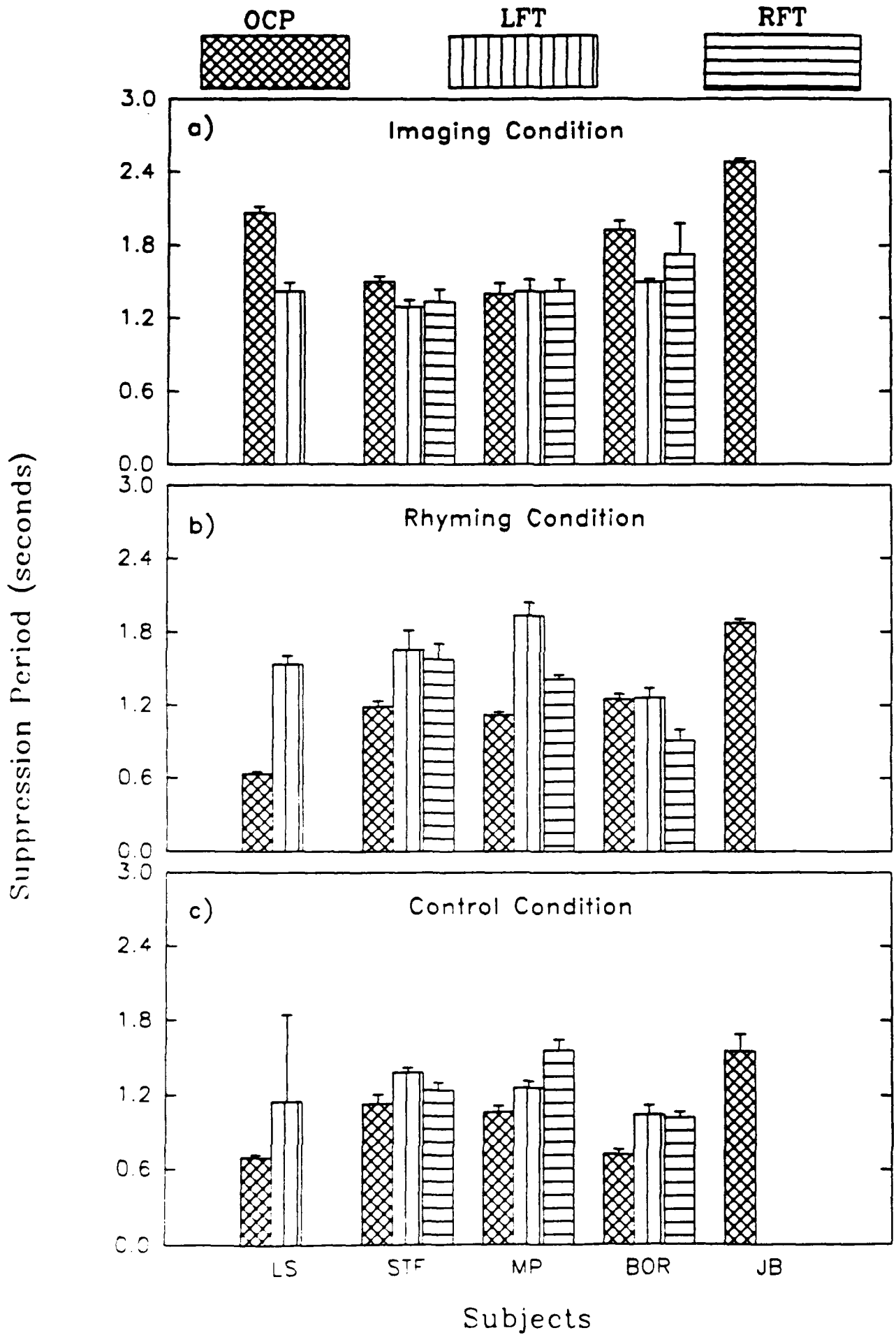
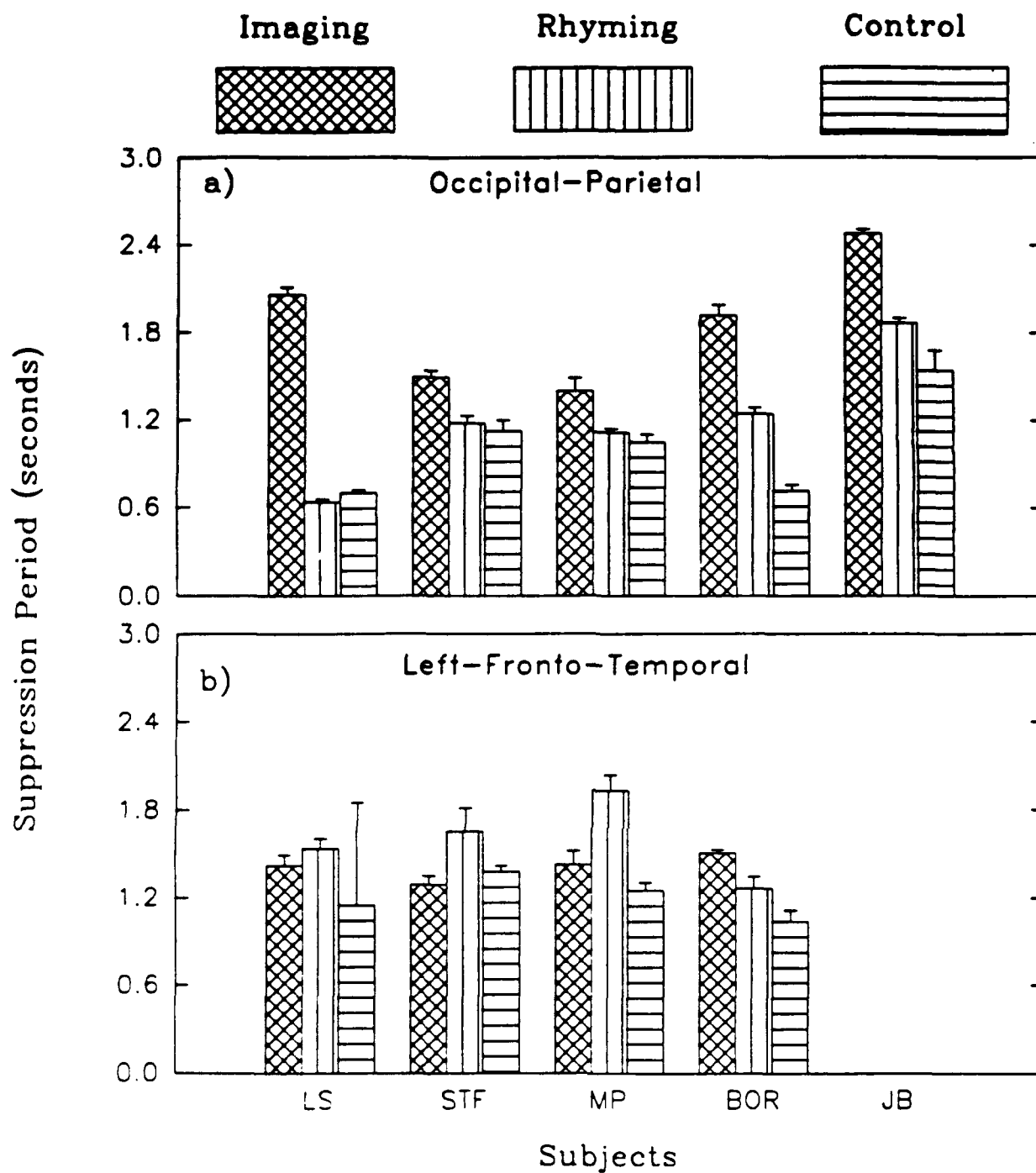


Figure 7



Beta Band Suppression Period (sec)

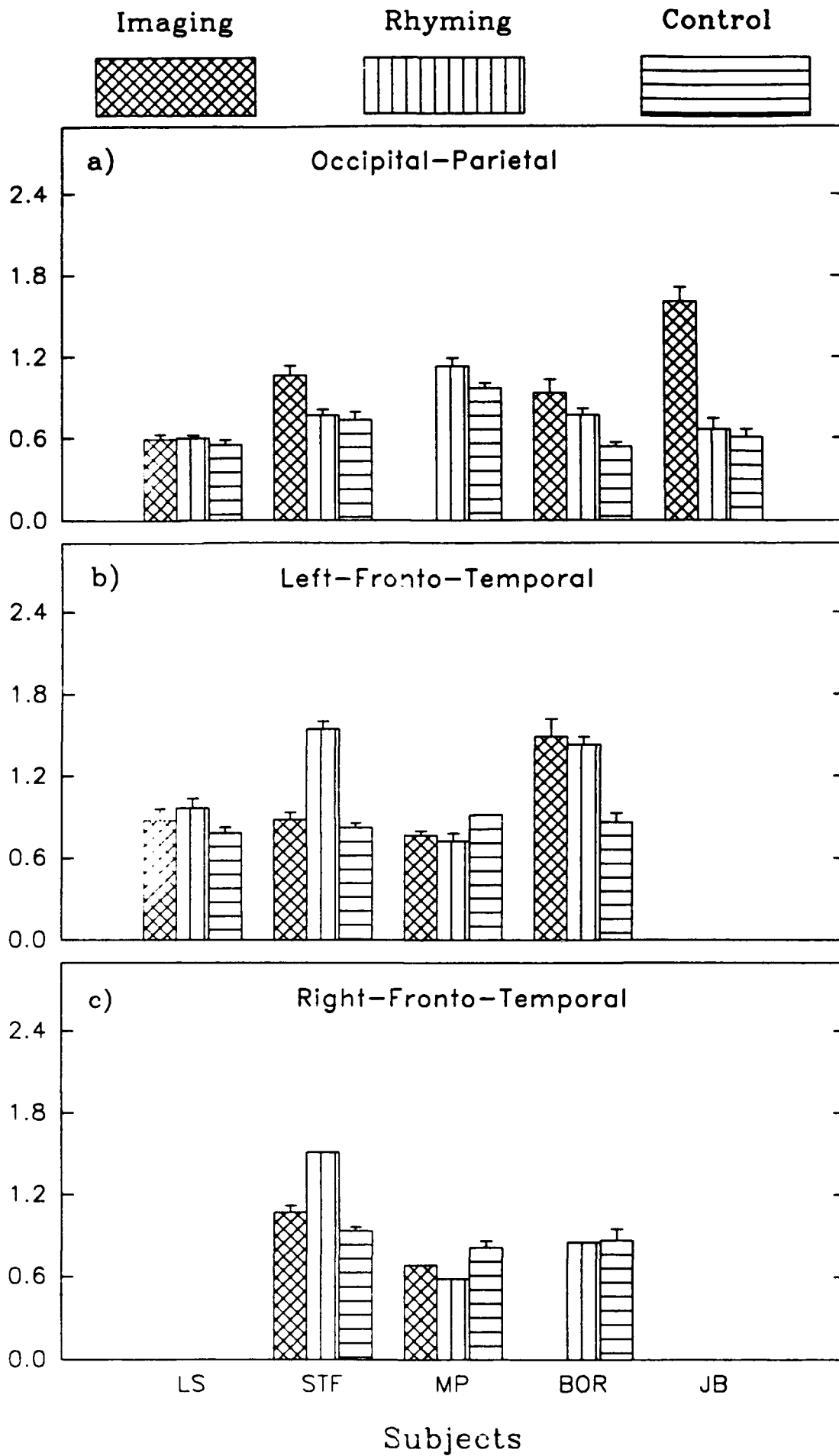
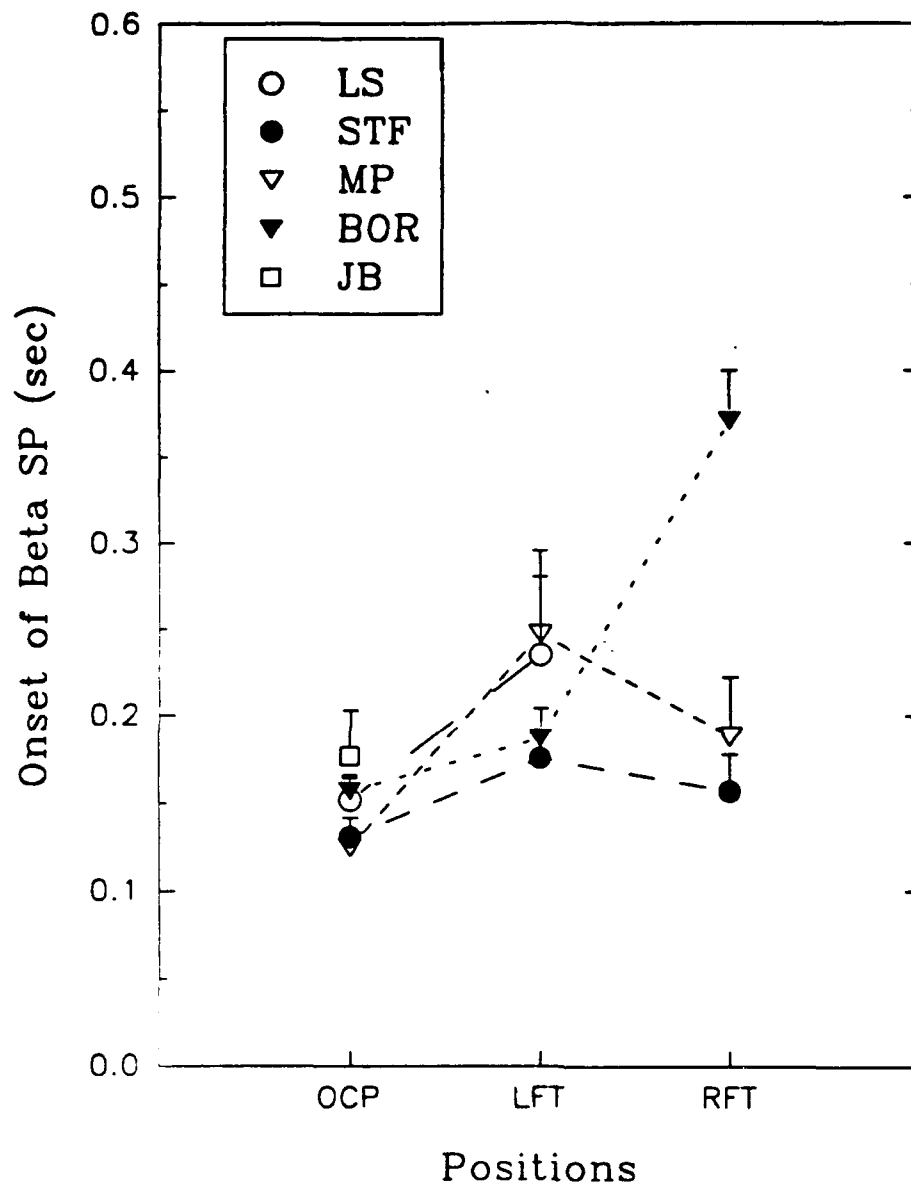


Figure 9:



Advantages and Limitations of Magnetic Source Imaging

Samuel J. Williamson, Zhong-Lin Lü, Daniel Karron, and Lloyd Kaufman

Summary: The term "magnetic source image" (MSI) describes the distribution of neuronal activity in the brain that can be deduced from measurements of the field pattern it produces across the scalp. The signals which provide the basis for an MSI are obtained from the magnetoencephalogram (MEG) which is conventionally recorded with superconducting detectors. Advances in MSI techniques during the past decade have revealed numerous aspects of the functional organization of human sensory systems that were previously unknown. In addition, studies of spontaneous signals, such as those in the alpha bandwidth, have identified specific cortical areas that support rhythmic activity. Extensions of this approach to cognitive research are able to determine the active cortical areas where spontaneous activity is suppressed when a person is engaged in a task such as mental imagery and auditory memory recall. Because only the component of the intracellular current tangential to the overlying skull contributes to the extracranial field, a confined source — modeled as a current dipole — has a characteristic field pattern that simplifies the pattern recognition problem of identifying the underlying sources. This advantage is illustrated by the identification of simultaneously active sources in auditory primary and association cortex. Their separate localization makes it possible to characterize their functional differences. Because the source strength in an MSI may be inferred without knowledge of the electrical conductivities of intervening tissue, it is also possible to estimate the extent of cortical involvement. From the tangential source strength in an MSI, it is possible in most cases to determine the *total* source strength by taking account of the orientation of the cortical surface. This provides an objective, quantitative measure of the strength of neuronal activity. At present, the major limitation in more extensive use of MSI is the cost of instrumentation. While it requires no contact with the head, and measurements can commence within a few minutes of the arrival of the subject or patient, the present cost of a large array of sensors is two to three million dollars.

Key words: MSI (magnetic source image); MRI (magnetic resonance image); Current dipole; Neuronal activation; Habituation; Spontaneous cortical activity.

Introduction

Measurements of voltages across the scalp (EEG) and magnetic fields near the scalp (MEG) provide complementary measures of the underlying neuronal activity. The most pronounced difference between the two approaches in our view does not come from the information that is available in the signals but rather from the different emphasis traditionally placed on how data are analyzed. On the whole, EEG studies emphasize the pattern of electric potential across the scalp, whereas MEG studies emphasize the underlying neuronal ac-

tivity. Indeed, the term "magnetic source image" (MSI) has come to be associated with magnetic analysis. The word "emphasize" is used advisedly, since there are many notable exceptions to this generalization. In part the difference in emphasis comes from the EEG having been exploited earlier, and because of that there are more widespread clinical applications. This fosters a more phenomenological approach for purposes of facilitating classification schemes to identify abnormal functions.

Locating a neuronal source magnetically is easier than electrically, because to good approximation a simpler model can be used for the head. A sphere will suffice, in many cases, fit to the curvature of the inner surface of the skull in the region over the source (Hari and Ilmoniemi 1986). The conductivity of intervening tissue has no effect on the field pattern (Grynszpan and Geselowitz 1973), and thus need not be taken into account when deducing the location and strength of the source (Williamson and Kaufman 1987). By contrast, the values of conductivity enter directly in determining the pattern of electric potential across the scalp. Lack of these data for individual subjects may well be one reason why the EEG literature is practically devoid of values specifying neuronal source strengths, for instance as given by the

Neuromagnetism Laboratory, Departments of Physics and Psychology and Center for Neural Science, New York University, New York, NY, U.S.A.

Accepted for publication: September 16, 1991.

This research was supported by grant AFOSR-90-0221 from the Air Force Office of Scientific Research and by equipment support from Silicon Graphics, Incorporated. We thank Dr. N. Chase for access to the MRI facilities at the NYU Medical Center and J. Stephenson for helping with MR recordings.

Correspondence and reprint requests should be addressed to Prof. Samuel J. Williamson, Department of Physics, 4 Washington Place, New York University, New York, NY 10003 U.S.A.

Copyright © 1991 Human Sciences Press, Inc.

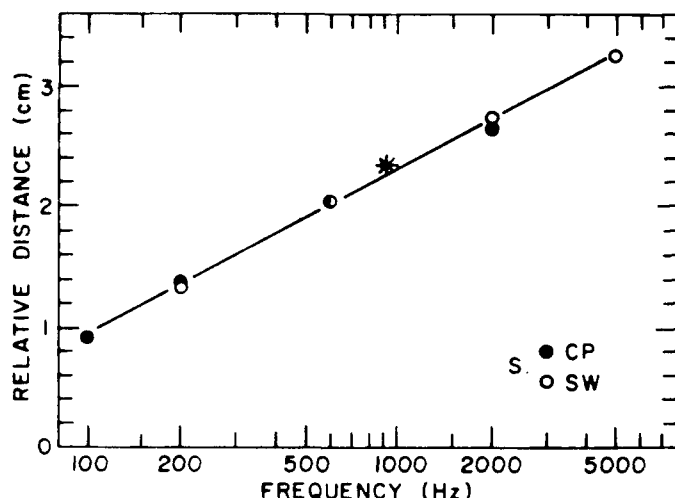


Figure 1. Cumulative distance in 3-D space from the site of one response to the next for steady-state stimuli at the indicated tone frequencies. Only the relative slopes should be compared, because the origins of the best-fitting lines were shifted to a common value of zero for 20 Hz. Stimuli were tones with amplitudes modulated at 33 Hz, and the field patterns for the 33 Hz responses were mapped to obtain the locations for individual sources. All points lie within 1 mm of the best line. The star indicates the relative location of the response to amplitude-modulated noise whose power spectrum peaks at 900 Hz (From Romani et al. 1982b).

current dipole moment of a patch of active cerebral cortex. On the other hand, moments are often quoted in the MSI literature. The value of the moment provides an objective measure of the strength of neuronal activity. In addition, for long-latency components of the event related field (ERF), it can be interpreted to provide an estimate for the spatial extent of the corresponding cortical activity (Lü and Williamson 1991).

For these reasons, there is growing interest in exploiting MSIs to obtain information about the functional organization of the brain. Systematic measurements have been carried out where a current dipole source is placed at a known location inside a spherical or realistic representation of the skull, with a homogeneous conducting medium inside. These have achieved a consistent accuracy of better than 3 mm in locating the dipole when repeated sets of measurements are compared (Yamamoto et al. 1988). Such accuracy can be achieved only if the field pattern is properly sampled, with measurements taken on all sides of areas where the inward or outward directed field is strongest (the "field extrema"). Also, it is important to determine the 3-D position and orientation of the sensor, to take account of the

direction of the measured field component when fitting a source model to the data. Failure to carry out both of these procedures is likely to yield much poorer results (Cohen et al. 1990).

Locating Sources Accurately

The first neuromagnetic study to locate a neuronal source was carried out by Brenner et al. (1978) on the cortical response to stimulation of a finger. The procedure subsequently revealed that response components with latencies as long as 150 msec originate in somatosensory cortex (Kaufman et al. 1981), a feature which had not previously been established in EEG studies. Moreover, the field pattern across the scalp in response to stimulation of various fingers revealed aspects of the somatosensory homunculus (Okada et al. 1984). Detailed measurements also established separate somatosensory and motor contributions in a task involving voluntary movement of a finger (Okada et al. 1982). Similar neuromagnetic techniques applied to auditory evoked responses have identified a feature not previously known about the functional organization of human cortex: the tonotopic organization of the primary auditory cortex (Romani et al. 1982; Pantev et al. 1988). Indeed, the precision — as distinguished from accuracy — for determining the relative positions of the cortical responses may be estimated from the scatter of deduced locations about the best-fitting line that describes the tonotopic progression. All of the locations for two subjects lie within 1 mm of a logarithmic function for the tonotopic sequence for the steady-state response (Romani et al. 1982b), as illustrated in figure 1. High accuracy has also been obtained for the tonotopic organization subsequently observed for the N100m transient response (Iloke 1988) (the 'm' identifies this component as being observed magnetically). In sum, the central motivation for MSI research has been the technique's ability to elucidate brain functions by localizing neuronal activity with high precision and relatively high accuracy (Hari and Lounasmaa 1989).

In less rigorous conditions, the reproducibility in determining the locations of the P50m, N100m, and P200m transient components of the auditory evoked response to a tone burst has been assessed for individual subjects. Positions over the right hemisphere were reproduced to within 3 - 10 mm across sessions on different days in each of 12 subjects (Baumann et al. 1990). From a wide variety of results obtained with careful studies, we conclude that with a favorable geometry (sources at positions where the skull is well-modeled by a sphere), reasonably strong and confined neuronal activity, and intelligent care, it is possible to achieve an accuracy of 3 mm in locating that activity. More general-

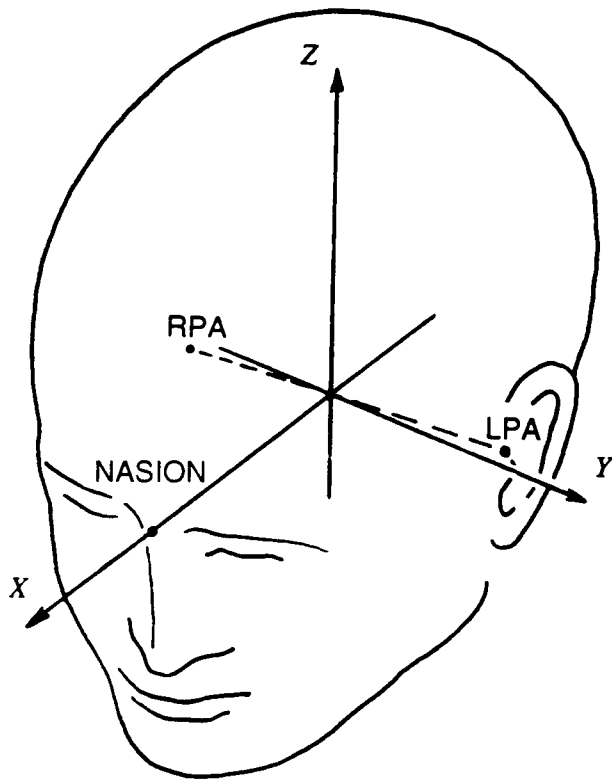


Figure 2. PPN head-based coordinate system for specifying positions within the head or near the scalp of a subject.

ly, it would be reasonable in somewhat less favorable cases to expect an accuracy of better than 1 cm for activity in cortical sensory areas.

Relating Structure and Function

Determining the locations of neuronal activity in space is of little value unless the anatomical substrate can be identified accurately. It is increasingly common to relate deduced positions to features of a magnetic resonance image (MRI) for this purpose. The challenge then is to establish a common coordinate system for specifying MRI pixels and MSI sources. We have chosen the three reference points of the 10-20 system as the "cardinal landmarks" for defining an appropriate system (Williamson and Kaufman 1989). These are the left and right periauricular points and nasion. For convenience, we call this coordinate system the "PPN head-based system". As a short-hand, we refer to coordinates in this system as "PPN coordinates". The coordinate axes of the PPN system are defined in the following way (figure 2). The origin is the mid-point between left and right periauricular points. The x-axis passes through the origin

to emerge from the head at the nasion. The z-axis is oriented perpendicular to both the x-axis and the line between periauricular points, and passes through the origin to emerge near the vertex. It need not pass through the vertex, and if one ear is lower on the head than the other it generally will not lie parallel to the longitudinal fissure. The y-axis is perpendicular to both the x- and z-axes and passes through the origin to emerge from the left hemisphere. Generally it will pass near, but not through, the periauricular landmarks. The PPN System defined this way is a right-handed coordinate system.

To specify measurement positions, as well as the corresponding sensor orientations, this coordinate system can be established for a given subject by using an appropriate 3-D digitizer, such as the Polhemus 3-Space (Polhemus Navigation Corporation), to characterize the relative positions of cardinal landmarks. During measurements, the same system can be employed to register field measurement positions and sensor orientations with respect to the PPN System (Yamamoto et al. 1988). Alternatively, this can be achieved by using the sensors themselves to locate reference coils placed at known locations on the skin (Erné et al. 1987).

Similarly, MRI recordings must contain accurate information about the cardinal landmarks. One traditional method is to place a marker, such as a vitamin-E pill, on the skin at each cardinal landmark for recordings. We have developed a method that achieves registration with higher accuracy, and we believe is easier to use and more convenient (Karron et al. 1991). Three "pointers" are held by a Velcro head-band worn by the subject so that each is directed toward a cardinal landmark, as illustrated in figure 3. The pointer itself consists of 4 thin tubes (called "spokes") filled with vitamin E that are machined so that they cant inward toward a common point in space. That point coincides with the resting spot when the pointer is placed against the skin at one of the cardinal landmarks.

When an MRI is recorded, several additional slices must be registered outside the head to cover the regions of the pointers. An MR slice that intersects the spokes registers one spot for each of them, as shown in figure 4. When the MRI is displayed on a computer monitor, the operator moves a cursor to each spot in turn and a program computes the MRI coordinates for the exact center of the spot. The location is therefore determined with greater accuracy (better than 0.3 mm) than the size of an image pixel (0.8 mm). This procedure of pointing to each spot is repeated for each MR slice that shows them. Then the programed computer computes the best-fitting line for each set of spots belonging to a given spoke, and it determines where the spokes intercept. More specifically, it computes the point in space that lies closest to all the spokes of a given pointer. We find the location where the pointer touches the skin is thereby

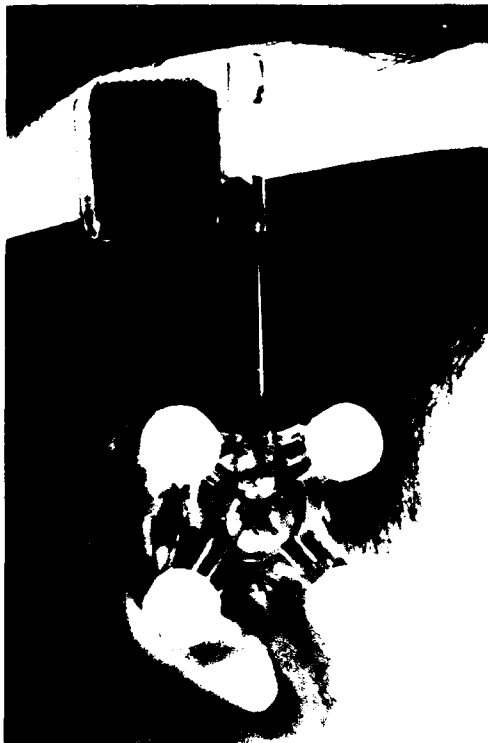


Figure 3. A plexiglas pointer is held against the right periauricular landmark of a subject for an MRI scan. The arrangement of the supporting rod where it is held at the upper end to a plexiglas cube permits adjustments of position and angle. The cube has a piece of Velcro glued to its base so that it can be attached to the subject's Velcro headband in any direction. The yellow spokes of the pointer can be seen directed inward to the periauricular landmark on the scalp.

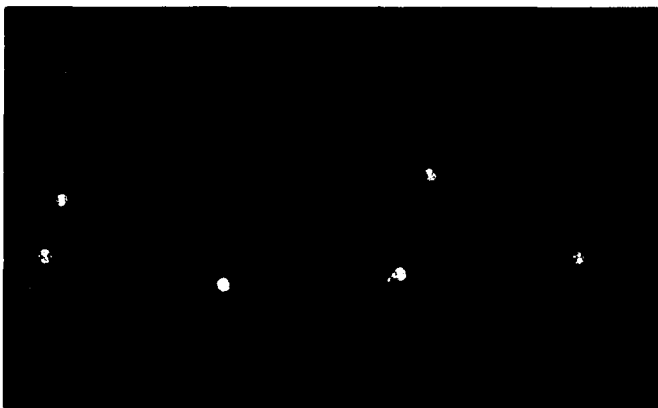


Figure 5. Computer representation of three pointers showing the spokes directed toward cardinal landmarks (yellow). The green axes define the cartesian coordinate system in which MRI pixels are specified. The blue axes define the PPN head-based system, which is defined with respect to the cardinal landmarks.

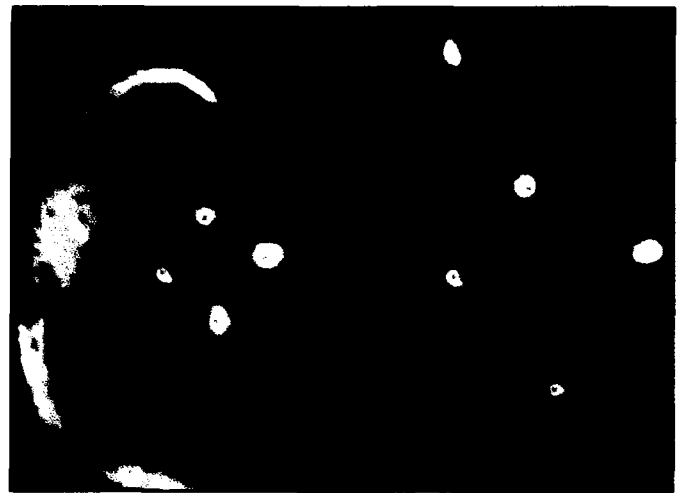


Figure 4. Sagittal MRI scans of a pointer held against the right periauricular point of a subject. (Left panel) Scan closest to the scalp, showing the ear, four spots depicting the four spokes of the pointer, and red dots indicating the pixels closest to the center of each spot. (Right panel) Scan closest to the outer ends of the four spokes. These images were photographed from a Silicon Graphics 85GT computer monitor.

established with an accuracy of better than 0.4 mm. In practice, the accuracy of determining each cardinal landmark is therefore limited by how accurately the pointer can be positioned on the skin for the MRI recording.

This analysis establishes the positions of the three cardinal landmarks with respect to the MR coordinate system. Therefore, the location of each pixel of the MR image can be expressed in the same PPN system as the neuromagnetic measurements (figure 5). By this means, neuronal function can be related to anatomical structure.

Spherical Model for the Head

To interpret the field pattern measured across the scalp, the actual shape of the head must be taken into account. The spherical model has provided a convenient simplification for modeling the pertinent region of the head when interpreting neuromagnetic data (Grynszpan and Geselowitz 1973; Cuffin and Cohen 1977). Hari and Ilmoniemi (1986) provide evidence through a model calculation that the sphere is best when fit to the region of the head overlying the source, where the volume currents are strongest. Because the curvature of the skull differs from one location to another, the spherical model will have a different size than the subject's head. This is illustrated in figure 6 for a fit to the region over the parieto-occipital sulcus. A computer cursor was employed to record the representative locations on the inner surface of the skull on appropriate MR slices, and

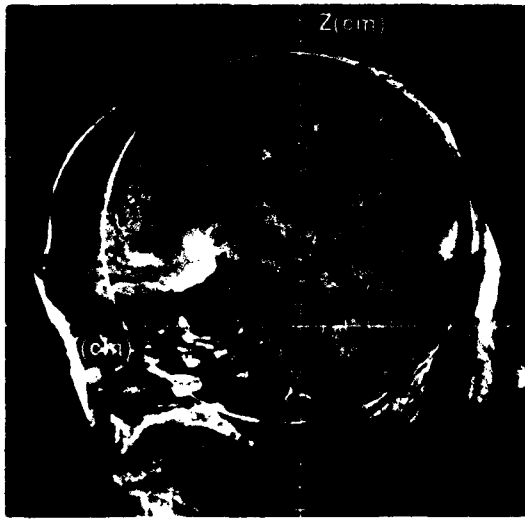


Figure 6. Spherical model (orange) best fitting the parietal region of the inner surface of the skull, shown in relation to a sagittal MRI cross section of the head. PPN axes are depicted in blue.

the computer subsequently computed the location of the center of the sphere whose surface most closely agrees with the locus of points.

Several groups are presently developing realistic conductivity models for the head that can be used with finite element methods to compute the extracranial field and scalp potential for a model source within. Hämäläinen and Sarvas (1989) used a numerical approach to determine the importance of including the currents within the skull and dermis when deducing an MSI within a realistically shaped head. The medium within the skull was assumed uniform in conductivity, and the skull itself was assumed of uniform thickness. They concluded that contributions to the field from the weak currents in the skull and dermis can be neglected for many purposes. Moreover, current patterns produced by departure from sphericity of the inner surface of the skull contribute fields that are generally weak except for sources that are deeper than 4 cm. Considerable improvement in source localization can be achieved by employing numerical models to account for actual volume current patterns (Rose et al. 1989). The effect of using spheres determined by different criteria to model the head when locating a source in the temporal area has been assessed by Lütkenhöner et al. (1990). The most important contributions from non-sphericity are in frontal areas, and they can be appreciable for sources lying more than 2 cm below the skull. Nevertheless, localization accuracies of better than 1 cm can be achieved with numerical modeling to take into account the actual shape of the skull.

Multiple Neuronal Sources in Temporal Cortex

As the quality of MEG measurements improves, interest can be extended to situations where several closely lying sources contribute to the field pattern at any given moment. Weinberg et al. have discussed one example in which several dipoles were placed within a model skull and were activated in various combinations (Weinberg et al. 1985). An ambiguity arises when it is not clear which field extrema are associated with a given source. One method for dealing with the multiple dipole case has been developed by Scherg (1990) for EEG data, when sources are activated in succession. We shall illustrate another method that has proved effective where the individual sources can be separated by exploiting their functional differences.

We shall illustrate the resolution provided by MSI with a difficult challenge that had not previously been met with EEG techniques: resolving the sources in temporal lobe that contribute to the 100-ms component of the auditory evoked response. Näätänen and Picton (1987) suggest that as many as 6 different neuronal sources may contribute in some measure to the event related potential (ERP) detected 100 ms following onset of a tone burst. Evidence for a source of N100 in the supratemporal plane was obtained by Vaughan and Ritter (1970), who observed a polarity reversal in the EEG over that location when the nose was used as reference. Definitive identification of the actual locations was provided by neuromagnetic studies by Hari et al. (1980) and Bak et al. (1981). Contributions from an additional source in the temporal lobe were inferred by Wolpaw and Penry (1975) who reported statistically significant differences in the EEG waveform within the interval of 100 to 200-ms from an electrode over the vertex compared with another over temporal scalp positions T3 and T4. The difference was called a "T" complex, consisting of a positive peak at about 105-110 msec and negative peak at 150-160 msec. More recent studies of scalp potentials also have been interpreted as indicating the presence of a lateral temporal source (Vaughan et al. 1980; Wood 1982). The fact that several neuronal sources contribute differently to the ERP and ERF measured near the scalp was made clear by Hari et al. (1982) who found that the amplitudes of the 100 msec electric and magnetic responses did not increase in the same way with increasing interstimulus interval (ISI). The two would be proportional if they originated from the same source of fixed geometry.

In studies of neuromagnetic responses to tone bursts applied with a constant interstimulus interval (ISI), Lü et al. (submitted) observed that when the ISI is lengthened a second source can be detected with a latency 10 ms shorter than that of the N100m component. In other

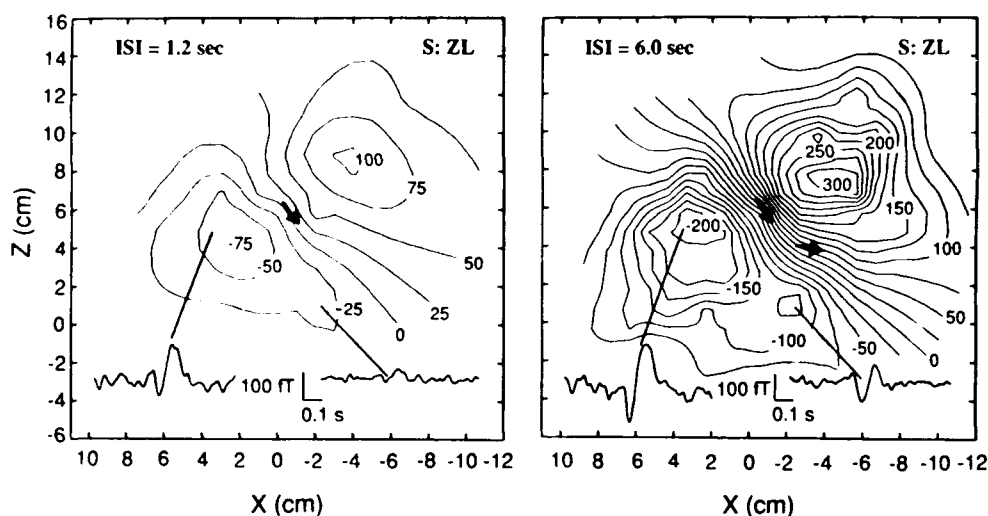


Figure 7. Sagittal view depicting the isofield contours over the left hemisphere for a subject responding to tone bursts presented at a fixed ISI of 1.2 sec and 6 sec.

words, the field map over the temporal and parietal areas indicates the presence of the classic N100m response for an ISI of 1.2 sec (figure 7a), but for an ISI of 6 sec the pattern reveals the presence of a second source as well (figure 7b). For convenience, we shall refer to this new component as the latent component and denote it by L100m. This terminology comes from the dictionary definition of *latent* as "not apparent but capable of being expressed".

The striking differences between the two patterns can be seen in the appearance for long ISI of a region of strong negative field over the area of the ear, and a strengthening and shift to the lower right of the upper right positive extremum, so that it is much stronger than any portion of the negative extrema at the left. A reasonable hypothesis is that neuronal activity appears which produces a positive field extremum at the upper right nearly coinciding with the existing positive extremum of N100m. Its negative extremum lies over the region of the ear, to the lower right of the negative extremum of N100m.

A local sphere model was employed to determine the locations of the two neuronal sources. Its center was

determined by the curvature of the inner portion of the skull, extending over a radius of 5 cm about the point lying about midway between the estimated source positions. Table 1 lists the parameters of the dipole that best account for the N100m pattern at short ISI, for each of 2 subjects. When a second dipole is added to account for the pattern at long ISI, the position and orientation of this N100m dipole were first fixed and then a 6-parameter fit was employed to determine its new strength and the 5 parameters of the L100m dipole. The result for sources in the left hemisphere of one subject is shown in table 1. In a second fitting procedure, we used these dipole parameters as the best initial estimate and carried out a 2-dipole fit, allowing all 10 parameters to vary. The best-fitting positions for the first and second procedures varied by less than 4 mm.









Ambiguities in Identifying Sources

As mentioned earlier, there is an inherent ambiguity in assigning field extrema to individual sources in a 2-dipole model. A positive extremum can be associated

Table 1. Best-fitting parameters for the dipoles that best account for the field pattern at both short and long ISI for the subject characterized in figure 7b. Parameters at short ISI condition for the subject as characterized in figure 7a and for another subject are also shown.

Condition	Subject	Component	x (cm)	y (cm)	z (cm)	ψ (degree)	Q (nA·m)
Short ISI	ZL (Left)	N100m	-0.9	6.3	6.2	-140	3.3
	SW (Left)	N100m	0.8	4.3	5.4	-134	11.4
Long ISI	SW (Left)	N100m	1.2	5.2	5.9	-122	11.4
		L100m	-1.9	6.7	4.2	-94	2.3

Table 2. Successive sets of parameters describing two dipoles in the left hemisphere that are being adjusted to achieve a best fit to the isofield contours of figure 7b for ISI = 6 sec. Orientations of the two dipoles are illustrated schematically at the right by arrows. Between steps 24 and 25 the orientations of the dipoles are switched as are two of the three position coordinates. However, they are switched back to the original assignments between steps 26 and 27. Each step comprises 6 computer iterations.

Step No.	Dipole	Q_x (nA·m)	Q_z (nA·m)	X (mm)	Y (mm)	Z (mm)	Dipole 1	Dipole 2
24	1	-2.5	-8.2	-4.8	-72.3	58.4		
	2	-10.0	-2.3	10.2	-56.0	45.8		
25	1	-2.7	-2.2	-5.5	-77.0	62.7		
	2	-2.7	-10.8	-4.1	-70.4	41.7		
26	1	-3.6	-5.0	-3.7	-73.8	61.5		
	2	-3.9	-7.6	1.3	-65.0	40.1		
27	1	-3.3	-6.8	-2.6	-71.9	60.6		
	2	-6.9	-5.4	3.7	-60.0	40.9		

a priori with either of the negative extrema. To investigate how the program dealt with this, we followed the evolution of the fitting sequence and found instances when an attempt to switch associations was made. Table 2 provides one such example. However, for a variety of starting conditions in which the N100m dipole is close to that providing the best fit to the data of figure 7a the minimization procedure based on chi-square as the cost function yielded similar final values for the parameters. This demonstrates that the fitting procedure is robust.

Figure 8 shows the locations and orientations of the

deduced N100m and L100m dipoles in the left hemisphere with respect to a sagittal MRI recorded near the average depth of the L100m and N100m sources. The N100m source lies 5 mm from the sulcus depicted in this superficial MRI slice. At a greater depth beneath the scalp (e.g., at $y = -5$ cm) the sulcus comes closer to the position of the dipole. Moreover the dipole is oriented perpendicular to the average direction of the nearby sulcus. This can be understood if the neuromagnetic field is produced by intracellular currents within pyramidal cells of the cortical layer forming the floor of

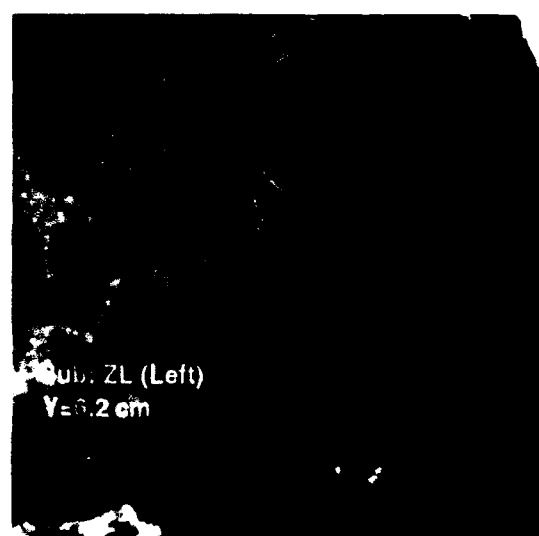


Figure 8. Locations and orientations of dipoles in the left hemisphere accounting for the field patterns in figure 7 (left panel; subject SW), as well for the field pattern of another subject (right panel; subject ZL) are shown as red arrows, where the tip of the stem of each arrow is placed at the respective source. Orange ovals depict the 95% confidence region for each location. Tic marks along the PPN x and z axes are spaced at 1 cm intervals.

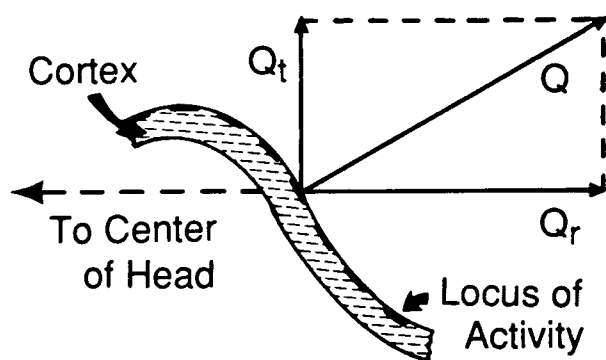


Figure 9. Projection of the tangential component Q_t of a current dipole onto the line that is perpendicular to the cortical surface to predict the total current dipole moment Q .

the lateral sulcus, in primary auditory cortex (Hari et al. 1980; Bak et al. 1981). By contrast the L100m source is found to lie within the supratemporal sulcus, in the region of the auditory association cortex (Pandya and Seltzer 1982), and it is oriented nearly perpendicular to the sulcus at its position.

Lü et al. (submitted) have also observed a second component with approximately 200 ms latency, for tone burst stimuli presented at a long ISI, whose source is located in this same region of the lateral temporal area, but this will not be discussed here.

Total Source Strength

When the pertinent region of the head is well-represented by a sphere, only the component of a current dipole source that is tangential to the sphere contributes to the external field (Grynszpan and Geselowitz 1973). In this sense, what neuromagnetic measurements will not "see" is a precisely radial source. This class of sources is a small proportion of the total. Some two-thirds of cerebral cortex is located within fissures and sulci, where the perpendicular to the cortical surface has an appreciable component lying tangential to the overlying scalp. Thus the majority of the cerebral cortex, as well as subcortical regions, will be accessible for magnetic study.

While only the tangential component Q_t of a dipole will be directly recorded magnetically, it is nevertheless possible to infer the total current dipole moment Q from knowledge of its tangential component Q_t . Anatomical information provides the necessary connection. In cerebral cortex, pyramidal cells are the dominant neuronal populations having a preferred orientation for the axes of their dendritic trees. The corresponding intracellular currents have a net direction perpendicular to

the cortical surface. Therefore, it is only necessary to define the local normal to the cortical surface to infer the direction of the total dipole moment. Figure 9 illustrates how the observed tangential component Q_t is projected onto the direction normal to the surface to predict the total dipole moment Q . This kind of analysis has been applied to obtain the total current dipole moments for steady-state responses to amplitude modulated tone of various frequencies (Romani et al. 1982). While the tangential component Q_t varies considerably with tone frequency, the total moment Q is nearly independent of frequency, suggesting that the same number of neurons respond regardless of frequency.

Once the total dipole moment is obtained, it is possible to take a further step and deduce the areal extent of cortex that responds to the stimulus. An analysis of current source-density measurements for long-latency responses in cat and monkey has shown that the current dipole moment at the moment of peak activity is about $50 \text{ pA} \cdot \text{m}$, to within an uncertainty of about a factor of 2, for each mm^2 of cortical surface area (Lü and Williamson 1991). Therefore, the total active cortical area can be estimated as $Q / (50 \times 10^{-12}) \text{ mm}^2$.

Spontaneous Rhythms of Cerebral Cortex

Because neuromagnetic fields are comparatively well confined near their sources, it is possible to investigate aspects of spontaneous cortical activity that have not yet been studied with EEG measurements. A series of cognitive studies we have carried out is motivated by the research of Pfurtscheller et al. (1977, 1988, 1988b) who found that EEG power in the alpha band between 8 and 13 Hz suffers a sharp reduction ("event related desynchronization") subsequent to visual stimulation as well as during the performance of voluntary acts. Their method is similar to one devised by Kaufman and Price (1967) to study modulation of high-frequency EEG by visual stimulation, and by Kaufman and Locker (1970) to study effects of attention on visual modulation of alpha activity.

We have carried out similar studies with MEG measurements over various areas of the scalp and find that magnetic alpha rhythm during cognitive tasks is sharply suppressed over the areas of cerebral cortex that may be expected to participate. For instance, field maps over the occipital and parietal areas provide evidence that visual cortex plays a role in visual imagery (Kaufman et al. 1990). The strongest source of alpha rhythm is the parieto-occipital sulcus, where sources ("alphons") of individual alpha spindles have been localized (Williamson and Kaufman 1989b). Nevertheless, there is a greater percentage of power suppression near the midline of the occipital area during mental imagery, which is the key

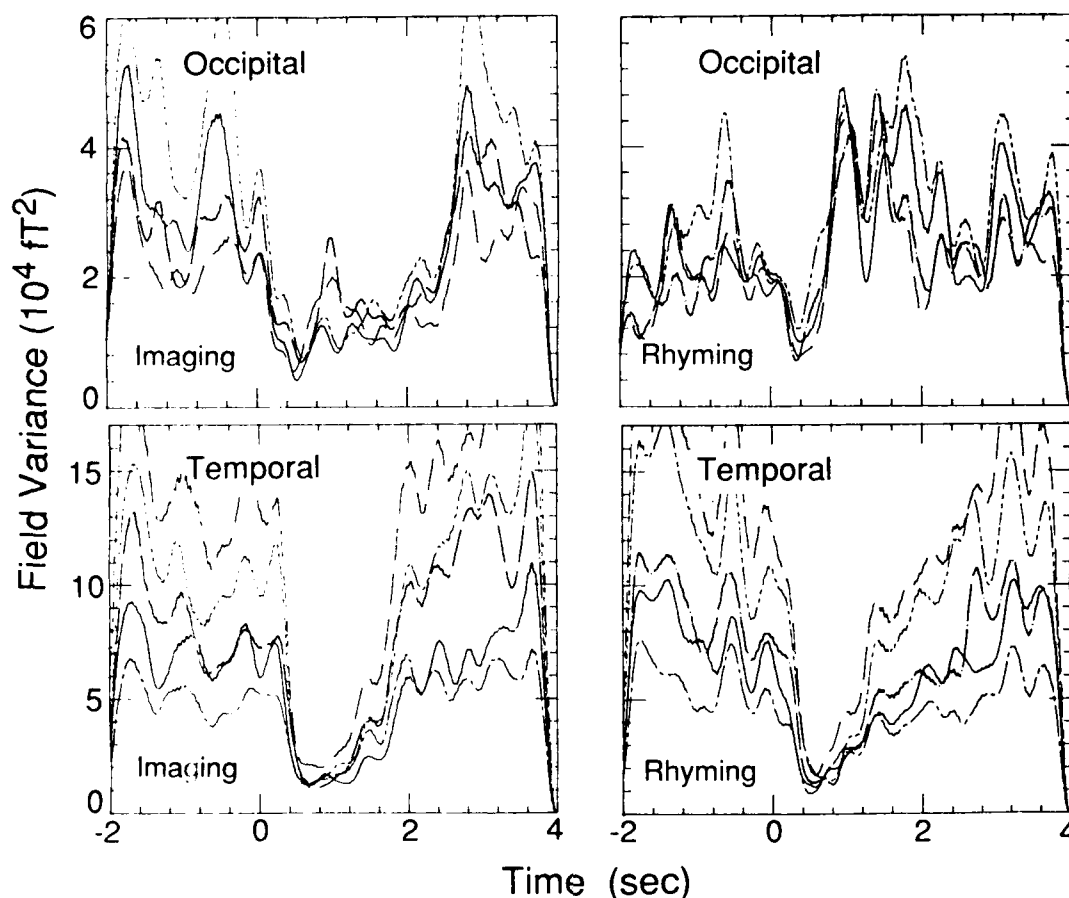


Figure 10. Variance in field power within the alpha bandwidth averaged over 36 trials when an imageable or nonimageable word is shown on a display for 200 msec beginning at the time origin. Data were low-pass filtered to smooth over individual alpha oscillations. Five traces are provided by simultaneous measurements with a probe consisting of four sensors evenly spaced on a circle of 2-cm radius centered on the fifth sensor. The probe was positioned over the occipital scalp (upper panels) or anterior temporal area (lower panels). The left panels show suppression when the subject seeks an image for the object that an imageable word represents, with suppression beginning earlier and enduring longer over the occipital area than temporal. The right panels show the measurements at the same respective locations when the subject seeks a word that rhymes with a non-imageable word displayed. Occipital suppression again begins earlier but is relieved much sooner than for the temporal area.

evidence that indicates the participation of visual cortex. Computer simulations of rhythmic activity in cortical folds, as comprise primary visual cortex, reveal that the average power pattern across the scalp is characteristic of anatomical features of the cortical geometry (Kaufman et al. 1991b).

Moreover, suppression of spontaneous alpha rhythms in the occipital and parietal areas is found to be specific to the task (Kaufman et al. 1989). Figure 10 shows that when a subject seeks a rhyme for a word displayed on a screen, suppression over the visual area begins immediately and is sustained for more than 500 ms. This reflects processing of the visual information in the occipital region. By comparison, after a delay of about 100 ms

suppression begins over the temporal area and is sustained for more than 500 ms as the subject seeks a rhyme. The interplay between the two areas is quite apparent.

As a final example of advantages gained by measuring the neuromagnetic field, we cite a recent study that is the first full use of the Sternberg paradigm to study the relation between short-term memory scanning and the spontaneous activity of the brain. The results support the hypothesis that increases in reaction time with memory set size are reflected in the duration of local changes in the level of spontaneous activity of cerebral cortex. In this study the subject was presented by earphones a series of 1, 3 or 5 tones as a memory set. After a few seconds a probe tone was presented and the subject

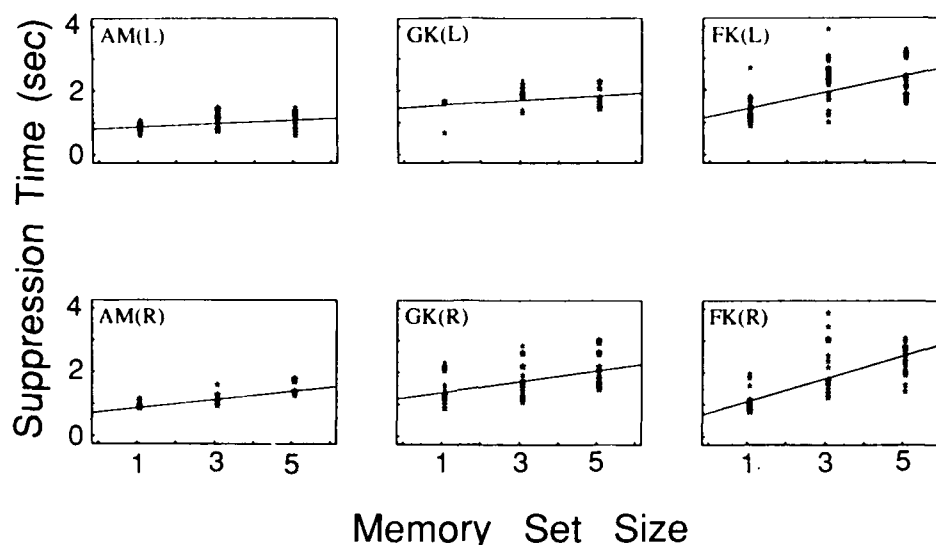


Figure 11. Duration of suppression of alpha rhythm over the left temporal area (L) and right temporal area (R) for each of 3 subjects after hearing a probe tone. The subject is instructed to determine whether it matches a tone previously heard as part of a memory set. Left hemisphere suppression duration is significantly correlated with memory set size for all 3 subjects' right hemisphere data, but for only one subject (FK) in the case of the left hemisphere.

pressed one reaction time button if it was judged to be a member of the memory set and another if it was not. Figure 11 shows that suppression time increases with the number of tones in the memory set (Kaufman et al. 1991), as is true for the reaction time in the classic Sternberg studies (1966). This is conventionally interpreted as reflecting the serial processing of all tones in the memory set, regardless of whether the probe occurs early in the series. Thus the duration of suppression provides a meaningful gauge of the time when a person is accessing memory.

These studies relating suppression duration to memory set size also revealed a strong correlation between the spatial pattern of suppression and the spatial distribution of N100m strength in response to presentation of the individual tones. This provides strong evidence that the alpha rhythm we observe originates in auditory cortex.

Overview

Where MSI techniques have suffered in the past, is the need to carry out sequential measurements because of the lack of a sufficient number of sensors to cover the entire scalp at one time. Determining a field pattern requires a minimum of 30 or so measurements, and often 50 or more need to be obtained for accurate results. These methods are not cost effective for a clinical setting. Moreover, such long measurement sessions may well lead to variability in responses as the state of the subject varies. Fortunately,

this limitation is being overcome by the advent of commercial systems that provide arrays of 37 or more sensors so that the entire field pattern from a given source can be obtained at one positioning. It is reasonable to expect that systems with more than 128 sensors will become available in the next decade to provide simultaneous measurements with proper sampling over nearly the entire head. The virtue of MEG recording being contactless means that the procedure of obtaining data can be efficient. Within five minutes or so of a subject's arrival the measurements can begin. Counterbalancing the obvious advantage in efficiency and effectiveness of large sensor arrays is the likelihood that MSI systems will be expensive, just as for complementary imaging systems, such as positron emission tomography (PET), that provide other measures of local brain function.

MEG has a major advantage over the EEG in the fact that it provides a measurement of the field at one location in space. There is no need for a "reference". The EEG is based on the measurement of a voltage, which necessarily entails a differential measurement of the potential at two separated locations. Eliminating the effect of the reference can be done with the EEG, but it means computing the differences between two voltages, conventionally carried out by computing an approximation to the Laplacian for the data recorded across the scalp. Thus the reference is eliminated, but signals from different sources may be superimposed. Moreover, signals in the area of the scalp at the boundary of the electrode array cannot be characterized by this means, so that complete

coverage is sacrificed. The closeness in spacing of electrodes in an array determines the accuracy with which the Laplacian can be approximated, and correspondingly the extent to which signals of different neuronal sources may be distinguished. The trade-off is that signal strength diminishes as electrodes are brought closer together. Certainly, EEG equipment is much less expensive than MEG systems, but considerable time is required to prepare the subject before, and to clean up after a study. These lengthy procedures are simply not needed for MEG recordings.

We have not discussed another advantage of MEG measurements: the bandwidth extends downward to dc. By moving a subject toward a sensor, the change in dc output indicates the dc field at the final position. Once in place, slow shifts in dc levels can be recorded continuously. This has advantages when characterizing the early stages of migraine, where it is believed that spreading cortical depression may play a role (Barkley et al. 1990).

The illustrations provided in this article demonstrate how MSI can be used effectively in brain research. In the future, we expect to achieve an accurate topographic representation of cortical activity, as distinct from the topography of the MEG and EEG at the scalp. These external phenomena except in simple cases are not related to the underlying activity in any straightforward manner.

References

- Bak, C., Kofoed, B., Lebech, J., Særmærk, K. and Elberling, C. Auditory evoked magnetic fields from the human brain. Source localization in a single-dipole approximation. *Phys. Lett.*, 1981, 82A: 57-60.
- Barkley, G.L., Tepley, N., Nagel-Leiby, S., Moran, J.E., Simkins, R.T. and Welch, K.M.A. Magnetoencephalographic Studies of Migraine. *Headache*, 1990, 30: 428-434.
- Baumann, S.B., Rogers, R.L., Papanicolaou A.C. and Saydjari, C.L. Intersession replicability of dipole parameters from three components of the auditory evoked magnetic field. *Brain Topography*, 1990, 3: 311-319.
- Brenner, D., Lipton, J., Kaufman, L. and Williamson, S.J. Somatically evoked magnetic fields of the human brain. *Science*, 1978, 199: 81-83.
- Cohen, D., Cuffin, B.N., Yunokuchi, K., Maniewski, R., Purcell, C., Cosgrove, G.R., Ives, J., Kennedy, J.G. and Schomer, D.L. MEG versus EEG localization test using implanted sources in the human brain. *Ann. Neurol.*, 1990, 28: 811-817.
- Cuffin, B.N. and Cohen, D. Magnetic fields of a dipole in special volume conductor shapes. *IEEE Trans. Biomed. Eng.*, 1977, BME-24: 372-381.
- Erné, S.N., Narici, L., Pizzella, V. and Romani, G.L. The positioning problem in biomagnetic measurements: A solution for arrays of superconducting sensors. *IEEE Trans. Magn.*, 1987, MAG-23: 1319-1322.
- Grynspan, F. and Geselowitz, D.B. Model studies of the magnetocardiogram. *Biophys. J.*, 1973, 13: 911-925.
- Hämäläinen, M.S. and Sarvas, J. Realistic conductivity geometry model of the human head for interpretation of neuromagnetic data. *IEEE Trans. Biomed. Eng.*, 1989, 36: 165-171.
- Hari, R., Kaila, K., Katila, T., Tuomisto, T. and Varpula, T. Interstimulus interval dependence of the auditory vertex response and its magnetic counterpart: Implications for their neural generation. *Electroenceph. Clin. Neurophysiol.*, 1982, 54: 561-569.
- Hari, R., Aittoniemi, K., Järvinen, M.-L., Katila, T. and Varpula, T. Auditory evoked transient and sustained magnetic fields of the human brain: Localization of neural generators. *Exp. Brain Res.*, 1980, 40: 237-240.
- Hari, R. and Ilmoniemi, R.J. Cerebral magnetic fields. *CRC Critical Rev. in Biomed. Eng.*, 1986, 14: 93-126.
- Hari R. and Lounasmaa, O.V. Recording and interpretation of cerebral magnetic fields. *Science*, 1989, 244: 432-436.
- Hoke, M. SQUID-based measuring techniques — a challenge for the functional diagnostics in medicine. In: B. Kramer, (Ed.), *The Art of Measurement: Metrology in Fundamental and Applied Physics*, VCH Verlagsgesellschaft mbH, Weinheim, 1988, 287-335.
- Karron, D., Lü, Z.-L. and Williamson, S.J. submitted for publication, 1991.
- Kaufman, L. and Price, R. The detection of cortical spike activity at the human scalp. *IEEE Trans. Biomed. Eng.*, 1967, BME-14: 84-90.
- Kaufman, L. and Locker, Y. Sensory modulation of the EEG. *Proc. Am. Psychology Assoc.*, 75th Meeting, 1970.
- Kaufman, L., Okada, Y., Brenner D. and Williamson, S.J. On the relation between somatic evoked potentials and fields. *Intern. J. Neuroscience*, 1981, 15: 223-239.
- Kaufman, L., Glanzer, M., Cycowicz, Y.M., and Williamson, S.J. Visualizing and rhyming cause differences in alpha suppression. In S.J. Williamson, M. Hoke, G. Stroink, and M. Kotani, editors, *Advances in Biomagnetism*, Plenum, New York, 1989, 241-244.
- Kaufman, L., Schwartz, B., Salustri, C. and Williamson, S.J. Modulation of spontaneous brain activity during mental imagery. *J. Cognitive Neuroscience*, 1990, 2: 124-132.
- Kaufman, L., Curtis, S., Wang, J.Z. and Williamson, S.J. Changes in cortical activity when subjects scan memory for tones. *Electroenceph. Clin. Neurophysiol.*, in press, 1991.
- Kaufman, L., Kaufman, J. and Wang, J.Z. On cortical folds and neuromagnetic fields. *Electroenceph. Clin. Neurophysiol.*, 1991b, 79: 211-226.
- Lü, Z.-L., Williamson, S.J. and Kaufman, L. Human auditory primary and association cortex have differing lifetimes for activation traces. Submitted 1991.
- Lü, Z.-L. and Williamson, S.J. Spatial extent of coherent sensory-evoked cortical activity. *Exp. Brain Res.*, 1991, 84: 411-416.
- Lütkenhöner, B., Pantev, C. and Hoke, M. Comparison between different methods to approximate an area of the human head by a sphere. In: F. Grandoli, M. Hoke, and G.L. Romani, (Eds.), *Auditory Evoked Magnetic Fields and Electric Potentials*, Karger, Basel, 1990, 103-118.
- Näätänen R. and Picton, T. The N1 wave of the human electric

- and magnetic response to sound. *Psychophysiology*, 1987, 24: 375-425.
- Okada, Y.C., Williamson S.J. and Kaufman, L. Magnetic field of the human sensorimotor cortex. *Intern. J. Neuroscience*, 1982, 17: 33-38.
- Okada, Y.C., Tanenbaum, R., Williamson, S.J. and Kaufman, L. Somatotopic Organization of the Human Somatosensory Cortex Revealed by Neuromagnetic Measurements. *Exp. Brain Res.*, 1984, 56: 197-205.
- Pandya D.N. and Seltzer, B. Association areas of the cerebral cortex. *TINS*, 1982, 386-390.
- Pantev, C., Hoke, M., Lehnertz, K., Lütkenhöner, B., Anogianakis G. and Wittkowski, W. Tonotopic organization of the human auditory cortex revealed by transient auditory evoked magnetic fields. *Electroenceph. Clin. Neurophysiol.*, 1988, 69: 160-170.
- Pfurtscheller, G. and Aranibar, A. Event-related cortical desynchronization detected by power measurements of scalp EEG. *Electroenceph. clin. Neurophysiol.*, 1977, 42: 817-826.
- Pfurtscheller, G., Steffan, J. and Maresch, H. ERD mapping and functional topography: Temporal and spatial aspects. In G. Pfurtscheller and F.H. Lopes da Silva, editors, *Functional Brain Imaging*, Hans Huber, Toronto, 1988, 117-130.
- Pfurtscheller, G. Mapping of event related desynchronization and type of derivation. *Electroenceph. Clin. Neurophysiol.*, 1988b, 70: 190-193.
- Romani, G.L., Williamson S.J. and Kaufman, L. Tonotopic organization of the human auditory cortex. *Science*, 1982, 216: 1339-1340.
- Romani, G.L., Williamson, S.J., Kaufman, L. and Brenner, D. Characterization of the human auditory cortex by the neuromagnetic method. *Exp. Brain Res.*, 1982, 47: 381-393.
- Rose, D.F., Ducla-Soares E. and Sato, S. Improved accuracy of MEG localization in the temporal region with inclusion of volume current effects. *Brain Topography*, 1989, 1: 175-181.
- Scherg, M. Fundamentals of dipole source analysis. In: F. Grandori, M. Hoke, and G.L. Romani, (Eds.), *Auditory Evoked Magnetic Fields and Electric Potentials*, Karger, Munich, 1990, 40-69.
- Sternberg, S. High-speed scanning in human memory. *Science*, 1966, 153: 652-654.
- Vaughan, H.G. Jr. and Ritter, W. The sources of auditory evoked responses recorded from the human scalp. *Electroenceph. Clin. Neurophysiol.*, 1970, 28: 360-367.
- Vaughan, H.G. Jr., Ritter, W. and Simson, R. Topographic analysis of auditory event-related potentials. In: H.H. Kornhuber and L. Deecke, (Eds.), *Motivation, Motor and Sensory Processes of the Brain*, Elsevier, Amsterdam, 1980, 279-285.
- Weinberg, H., Brickett, P., Coolsma, F., and Baff, M. Magnetic localisation of intracranial dipoles: Simulation with a physical model. *Electroenceph. Clin. Neurophysiol.*, 1986, 64: 159-170.
- Williamson, S.J. and Kaufman, L. Analysis of neuromagnetic signals. In: A.S. Gevins and A. Rémond, (Eds.) *Methods of Analysis of Brain Electrical and Magnetic Signals*, Elsevier, Amsterdam, 1987, Chapter 14, 405-448.
- Williamson, S.J. and Kaufman, L. Theory of neuroelectric and neuromagnetic fields. In F. Grandori, H. Hoke, and G.L. Romani, editors, *Auditory Electric and Magnetic Fields*, Karger, Basel, 1989, 1-39.
- Williamson, S.J. and Kaufman, L. Advances in neuromagnetic instrumentation and studies of spontaneous brain activity. *Brain Topography*, 1989b, 2: 129-139.
- Wolpaw, J.R. and Penry, J.K. A temporal component of the auditory evoked response. *Electroenceph. Clin. Neurophysiol.*, 1975, 39: 609-620.
- Wood, C.C. Application of dipole localization methods to source identification of human evoked potentials. *Ann. N.Y. Acad. Sci.*, 1982, 388: 139-155.
- Yamamoto, T., Williamson, S.J., Kaufman, L., Nicholson, C. and Llinás, R. Magnetic localization of neuronal activity in the human brain. *Proc. Natl. Acad. Sci. USA*, 1988, 85: 8732-8736.

Magnetic Source Images Determined by a Lead-Field Analysis: The Unique Minimum-Norm Least-Squares Estimation

Jia-Zhu Wang, Samuel J. Williamson, *Member, IEEE*, and Lloyd Kaufman

Abstract—The minimum norm least-squares approach based on lead field theory provides a unique inverse solution for a magnetic source image that is the best estimate in the least-squares sense. This has been applied to determine the source current distribution when the primary current is confined to a surface or set of surfaces. In model simulations of cortical activity of the human brain, the magnetic field pattern across the scalp is interpreted with prior knowledge of anatomy to yield a unique magnetic source image across a portion of cerebral cortex, without resort to an explicit source model.

I. INTRODUCTION

A magnetic source image (MSI) specifies the distribution of electric current within a conducting body that can be deduced from measurements of the magnetic field pattern outside its surface. Determining such images is a central focus of biomagnetic research [1]. There is no unique solution to the inverse problem from measurements of the field pattern everywhere outside the body, or for that matter, from measurements of the electric potential across the surface, or from a combination of both [2]. Traditionally, solutions have been achieved by introducing explicit source models such as a current dipole [3], [4] or distribution of a small number of dipoles [5] and determining the values of their parameters to best account for the measured field pattern. When a single dipole is located within a conducting body of planar or spherical symmetry, information about the two field extrema, where the field normal to the surface is strongest, is sufficient to determine its parameter [6]. While field patterns about the human scalp, such as those produced by neuronal activity responding to a sound, often can be accounted for by one or more current dipole sources, the inherent ambiguity of the inverse solutions introduces uncertainty about the validity of multidipole models. This paper provides a means for substantially reducing this uncertainty.

Manuscript received September 14, 1991; revised January 30, 1992. This work was supported by Air Force Office of Scientific Research Grant AFOSR-90-0221.

J.-Z. Wang and S. J. Williamson are with the Neuromagnetism Laboratory, Department of Physics, and Center for Neural Science, New York University, New York, NY 10003.

L. Kaufman is with the Neuromagnetism Laboratory, Department of Psychology, and Center for Neural Science, New York University, New York, NY 10003.

IEEE Log Number 9200694.

A general approach to deduce information about a source current distribution from magnetic data is based on a Fourier analysis and was applied to a geometry in which the current image is confined to a plane [7]–[10]. Spatial filtering models were also developed for two-dimensional current distributions [11]–[13]. A general approach to the 3-D problem was introduced by exploiting lead-field analysis in a linear estimation [14], [15] based on the minimum norm current distribution [16]–[18] as implemented for planar geometries [19]–[21]. The lead field specifies the pattern of sensitivity of a detection coil, and it depends on the coil's geometry and orientation with respect to the conducting body. For axial symmetry, as when the axis of a circular coil is directed perpendicular to the surface of a sphere, the lead field pattern $\vec{L}(\vec{r})$ is identical with the vector potential that would be produced if a current were passed through the coil [6]. In this case, the magnetic flux produced in the coil by a current dipole $\vec{Q}(\vec{r}')$ is the scalar product $\vec{L}(\vec{r}') \cdot \vec{Q}(\vec{r}')$.

It is well known that a current dipole's component lying normal to the surface of a semi-infinite space or sphere of uniform conductivity makes no contribution to the magnetic field outside the surface. The reason is that the boundaries of the conducting medium disturb the pattern of the dipole's volume current in such a way that the normal component of the volume current and dipole fields cancel exactly. For this reason, linear models have a singular feature that adds a family of solutions from the homogeneous equations as the nonunique aspect of the inverse solution. The minimum norm condition eliminates the ambiguity in favor of the solution whose mean square strength integrated over all space has a minimum value. In practice, minimum norm estimates are generally unstable with respect to modeling errors and measurement noise. The spectral expansion [22] is equivalent to the minimum norm approach that permits combinations of lead fields to be used in constructing an orthonormal basis in the vector subspace that they span. One application of these techniques [23] uses a volumetric finite element model with the distribution of primary current expressed parametrically throughout the volume. Other procedures are based on the most probable current distribution in a plane [24] or stack of planes [25], [26].

We report a different approach in which a unique, robust solution is obtained by imposing the natural con-

0018-9294/92\$03.00 © 1992 IEEE

straint of anatomical features. In an earlier work [27], anatomical structure was shown to play an important role in determining the pattern of magnetic field power produced across the scalp. To illustrate the capability of this technique, we carry out computations of direct relevance to applications in neuromagnetism. However, the method is sufficiently general to be applicable for a wide variety of situations, including excitation patterns of the heart. Specifically, we exploit the physiological fact that neuronal sources producing the dominant extracranial magnetic fields are confined to specific regions of the brain. For instance, sensory evoked activity is restricted to the appropriate sensory and association areas of the cerebral cortex. Motor activities originate in specific cortical areas as well, and their coordination involves the cerebellum. Certain cognitive processes are supported by both cortical and subcortical structures such as the hippocampus, where the laminar configuration of aligned neurons can be defined by an appropriate surface. Similar considerations based on surface geometries can be introduced for other applications. Therefore, only the inverse solution for activity on these surfaces need be computed.

In terms of lead field analysis, our approach is to construct a linear model based on a given geometric configuration of the *image surface* where the inverse solution is sought. Field measurements are carried out with sensors placed at various locations on an *observation surface*. The analysis presented here has a trivial generalization to measurements with detection coils placed in any configuration so long as they detect only the field produced by the primary current. The surface specifying the actual location of primary currents is called the *source surface*. Equipped with the theory of the generalized inverse, we exploit the method of computing the minimum-norm least-squares solution (MNLS) for the source current distribution. It is known in mathematics as the Moore-Penrose inverse, or pseudoinverse, which leads to a unique solution to the given linear model. It provides the best estimation in the sense that it has the least residual error between the measured and computed fields, as well as minimum power for the image configuration. It is a unique inverse solution for a given linear model.

We shall illustrate the procedure by computing inverse solutions for sources located within a conducting half space, with field sensors placed across its planar surface. Measurements are performed with the sensors oriented to detect the component of the field that is normal to this observation surface. Therefore, only the component of the primary current lying parallel to the surface need be considered, for the normal component of the primary current produces no external field. The secondary current, which represents the influence that the surface has on the pattern of volume current, produces no field normal to the surface. Solutions will be obtained for the distribution of primary sources across a surface that lies within the conducting medium, with the current everywhere perpendicular to the surface. This represents the portion of cerebral cortex that forms the wall of the fissure or sul-

cus. The image is represented on a corresponding image surface. With correct prior knowledge, we may assume that the image surface and source surface coincide. With this condition, the effects of finite sensor spacing and noise will be assessed for representative conditions. These results indicate that a unique inverse solution is feasible for the general problem of sources limited to a set of surfaces, provided that a sufficient number of sensors is employed and the noise level is not excessive. Thus, knowledge of anatomy, as provided by a magnetic resonance image, overcomes the nonuniqueness of the classic inverse problem in biomagnetism.

The following section provides an explanation of the mathematical basis for the inverse solution. Readers who prefer to skip to applications of the technique can proceed directly to Section III.

II. INVERSE SOLUTION

A. Lead Field Description

The primary current is assumed to be distributed within a finite space Ω . The law of Biot and Savart relates the magnetic inductance $\vec{B}(\vec{r})$ to the current density $\vec{J}(\vec{r}')$ within Ω :

$$\vec{B}(\vec{r}) = \frac{\mu_0}{4\pi} \int_{\Omega} \frac{\vec{J}(\vec{r}') \times (\vec{r} - \vec{r}')}{|\vec{r} - \vec{r}'|^3} d\vec{r}'. \quad (1)$$

The source surface has a known geometrical configuration ($\vec{r}' \in \Omega$). It follows that measurements of the component B_i normal to the observation surface at m positions \vec{r}_i are linearly related to the current source density by

$$B_i = \int_{\Omega} \vec{L}_i(\vec{r}') \cdot \vec{J}(\vec{r}') d\vec{r}' \quad i = 1, \dots, m. \quad (2)$$

The dot product is performed in the ordinary 3-D space and $d\vec{r}'$ is the differential volume element. The vector field $\vec{L}_i(\vec{r}')$ is known in biomagnetism as the lead field and in mathematics as the kernel. The lead field $\vec{L}_i(\vec{r}')$ accounts for the sensitivity of the i th detection coil at measurement position \vec{r}_i to the presence of the source current density at \vec{r}' . The lead field within Ω is determined by the geometry and orientation of the detection coil at its position of observation. In order to concentrate upon the theory and method, we shall restrict ourselves to consider detection coils that have the simple geometry of a magnetometer. This represents a single coil whose diameter is sufficiently small it may be considered a point. Bearing the anatomy of cerebral cortex in mind, it is natural to restrict the source space Ω to a region that can be modeled as a folded surface layer of thickness w . The volume integral is, therefore, reduced to a surface integral. If we further divide the image surface into a grid of n cells of area $\Delta S'_j$ centered at position \vec{r}'_j , and replace the integral by a summation, (2) becomes

$$B_i = \sum_{j=1}^n \vec{L}_i(\vec{r}'_j) \cdot \vec{J}(\vec{r}'_j) w \Delta S'_j \quad i = 1, \dots, m. \quad (3)$$

Note that the combination $\bar{J}(\bar{r}_j) w \Delta S_j$ has the dimension of ampere-meter, which corresponds to that of a current dipole Q_j . In matrix representation, (3) can be written as

$$b = LQ, \quad (4)$$

where b and Q are column vectors and L is an $m \times n$ matrix. If the coordinate system is oriented so that $\bar{J}(\bar{r}_j)$ has a finite projection onto two or three axes, the value of n is correspondingly two or three times greater than the number of image nodes.

B. Least-Squares Solution for an Overdetermined System

We now momentarily turn to consider purely mathematical aspects for dealing with an overdetermined linear system,

$$Ax = y \quad (5)$$

where A is an $m \times n$ rectangular matrix, x is a column vector with n unknown elements, and y is a column vector with m elements of observations. If $m > n$, there are more equations than unknowns, so there is no solution in the traditional sense. Nevertheless, it is possible to obtain a best estimation of x , denoted by \hat{x} . "Best" is understood in the sense of minimizing the Euclidean 2-norm of the residual error e [28] [29] because of its computational convenience:

$$\|e\| = \|A\hat{x} - y\|. \quad (6)$$

Minimizing the norm in (6) is the same as minimizing the square of the norm: $e^T e$. A few steps of derivation lead to the following matrix equation that expresses this condition:

$$A^T A \hat{x} = A^T y \quad (7)$$

where A^T is the transpose matrix of A . Equation (7) is known in statistics as the system of normal equations. The best estimation that minimizes the residual error is given by the solution of this set of equations.

If the square matrix $A^T A$ is non-singular, that is, $\text{rank}(A) = n$, or all the equations are linearly independent, we can define a generalized inverse X :

$$\hat{x} = Xy, \quad (8)$$

$$X = (A^T A)^{-1} A^T \quad (9)$$

However, in real situations found with neuromagnetic measurements, the square matrix $A^T A$ is often singular so that the direct inverse does not exist. This case will be dealt with later in Section II-D.

C. The Minimum Norm Inverse

We now turn to an underdetermined system and first consider only the case where the set of equations is consistent, that is, the equations are all linearly independent:

$$Ax = y. \quad (10)$$

where x is a column vector with n unknown elements, and y is a column vector with m observations. Here A is still an $m \times n$ matrix, but since $m < n$ ($\text{rank}(A) = m$) it has fewer equations than unknowns. For such a case, there exists an infinite number of solutions for x . However, there is a unique solution given by the minimum norm inverse [19], [28], [29]:

$$\hat{x} = Xy. \quad (11)$$

$$X = A^T (AA^T)^{-1}. \quad (12)$$

Let us look at this approach from a different point of view. First we form an $m \times m$ symmetric matrix AA^T , which is nonsingular, since the rank of A is m . Diagonalizing the square matrix, we can obtain m nonzero eigenvalues and corresponding eigenvectors. We can further construct m orthonormal basis vectors in terms of those eigenvalues and eigenvectors, together with the row vectors of matrix A . They form a complete set in this m -dimensional row space of matrix A . Therefore we can expand x in this subspace and find the coefficients for the expansion. This approach is called the spectral expansion [22]. It can be shown that the formulation given by spectral expansion coincides with the minimum norm inverse gain in (12) in the discrete case. give

D. The Unique Minimum-Norm Least-Squares Solution

We now return to the lead field analysis and discuss the realistic situation, where we wish to determine the source current distribution based on a set of measurements. Thus, we are seeking an infinite number of parameters from a finite number of measurements. The inverse solution (2) can never be unique for there may exist a family of functions \bar{J}^* that are the solutions of the corresponding homogeneous equations of (2):

$$\int_{\Omega} \bar{L}_i(\bar{r}') \cdot \bar{J}^*(\bar{r}') d\bar{r}' = 0. \quad (13)$$

If we limit the solution to positions on a grid across an image surface as in (4), we are, in principle, still dealing with an underdetermined system with more unknown parameters than the number of equations. As discussed in Section II-C, for such cases there exist an infinite number of solutions.

Errors contribute further indeterminacy to the inverse solutions. Apart from the additive noise in experimental observations, there are other sources of error such as the lack of accuracy in determining the positions of measurements, etc. Moreover, the mathematical modeling itself introduces error into the problem. One example is the selection of the number of cells for the grid representing a continuous source. Even in the case of a computer simulation, without adding noise there are still machine errors, for roundoff errors are inevitable when using floating-point arithmetic.

Despite these difficulties, it is still possible to find an estimate of the unknown elements of the current image.

$\rightarrow \text{rank}(A)$

For the linear model in (4), what is needed is a type of generalized inverse L^+ that provides the estimation \hat{Q} for the vector Q :

$$\hat{Q} = L^+ b. \quad (14)$$

We claim that the best estimation should always be understood in the least squares sense as it minimizes the residual error: $\|L\hat{Q} - b\|^2$. However, the least squares inverse does not provide a unique solution for the general case with rank $r < \min(m, n)$. Therefore, it is desirable to seek a best estimation that not only minimizes the residual error but also minimizes the norm of the solutions.

Fortunately, this kind of minimum-norm least-square inverse (MNLS inverse) known as the Moore-Penrose [30], [31] generalized inverse¹ or pseudoinverse in mathematics, has been well studied [28], [29]. Because of its importance for the inverse problem, the relevant details of the mathematical description will be reviewed briefly. For a $m \times n$ matrix L with rank $r < \min(m, n)$, it is always possible to factor L into the product of two matrices both with rank r :

$$L = CD \quad (15)$$

where C is a $m \times r$ matrix and D is a $r \times n$ matrix. The MNLS inverse is uniquely given by

$$L^+ = D^T(DD^T)^{-1}(C^T C)^{-1}C^T. \quad (16)$$

Equation (16) reduces to (9) for an overdetermined system ($m > n$) with full possible rank n , and reduces to (12) for an underdetermined system ($m < n$) with rank m .

Some authors have used the expression $L^T(LL^T)^{-1}$ to compute the "minimum norm" inverse. However, as we pointed out above in Section II-C, this simpler expression is correct only when the square matrix LL^T is non-singular. Often it is singular if rank $(L) < m$ when $m < n$, so $(LL^T)^{-1}$ does not exist. In such a case, when a solution in the form of a generalized inverse is sought by the method of singular value decomposition (SVD) [32], this expression is equivalent to the pseudo inverse given in (16). Such a solution is actually the MNLS inverse, which provides not only the minimum norm but also the least square virtue. Therefore, for the solutions presented here, if the number of measurements exceeds the number of unknowns we shall use SVD to obtain $L^+ = (L^T L)^+ L^T$. In the other case, when m is less than n , we shall use $L^+ = L^T(LL^T)^+$. This choice is made to minimize computation time. For either case, the nonzero eigen values of the square matrices LL^T and $L^T L$ are the same, so that the results are equivalent. Alternatively, SVD can be used directly to compute L^+ .

¹E. H. Moore in 1920 generalized the notion of "inverse" to include all matrices, singular or singular. Unaware of Moore's work, R. Penrose showed in 1955 that, for a $m \times n$ matrix A , there exists a unique matrix A^+ satisfying the four relations: $AA^+A = A$, $A^+AA^+ = A^+$, $(AA^+)^T = AA^+$, $(A^+A)^T = A^+A$. Penrose also showed that this generalized inverse possesses the least squares property.

III. SIMULATION WITHOUT NOISE

The human brain is distinguished from that of lower primates by a larger ratio of surface to volume, which enhances the area of cerebral cortex to the extent where two-thirds of it is found in fissures and sulci that penetrate the interior. A small portion of a fissure or sulcus may therefore be modeled as vertical wall extending below a horizontal surface representing the scalp. In general, fissures and sulci do not run in straight lines, so that the local curvature may be modeled in an extreme way by an "L" shaped wall, illustrated in Fig. 1. This kind of model has proved useful in an earlier simulation of spontaneous activity across the surface of visual cortex. In that simulation, the visual cortex was represented by four such pieces, placed so their vertical edges coincide to produce a cruciform-shaped surface [27].

In the present geometrical model, each plane forming the L-shaped wall of cortex is 5×5 cm. This is called the *source surface*, because it specifies the location of neuronal activity. In the examples to be discussed, we assume perfect knowledge of the anatomy so that the *image surface* where the inverse solution will be sought coincides with the source surface. The *observation surface* where field measurements are taken is a horizontal plane located 1 cm above the top edge of the image surface, with its center located +2 cm from the corner of the "L" along the x -axis. For present purposes, it can be considered as the upper boundary of a homogeneous conducting half space. The observation plane has dimensions of 12×12 cm so that it is large enough for the sensor array to extend beyond the locations where the vertical field component has local outward or inward extrema. Each sensor is considered a point magnetometer, so that the finite area of the detection coil can be neglected. The sensors are arranged at nodes of a grid having sides of length s . Computations of the corresponding image on the image surface are carried out for nodes of a grid having sides of length a .

In the simulations, source configurations are defined on the L-shaped walls, and field values are computed for each sensor. Then the MNLS inverse is computed from this set of values. Although (16) provides an explicit expression for the MNLS inverse, it is often impractical for computations. Instead we use the SVD method [32] to construct the inverse solution. We first try to find an orthonormal basis as described in Section II-C and D for the span of lead fields L , as given in (4). If the basis is complete, it is used to expand the source distribution that shares the same domain. If on the other hand the basis is not complete, as is often the case, there exists a null space that corresponds to the zero or near-zero eigenvalues of the symmetric matrix of LL^T or $L^T L$. Using the SVD method we can eliminate the null space. The expansion of the source distribution is then limited to the subspace in the range of L .

When carrying out the above procedures, it is essential to maintain high accuracy in the computations and yet

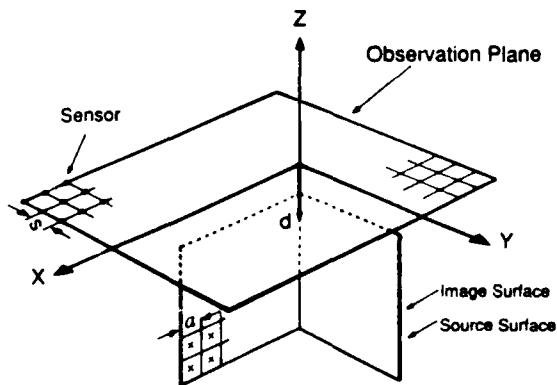


Fig. 1. Horizontal plane where observations of the field B_z are made by point sensors at nodes of a square array of side s . The source space consists of two vertical walls meeting at right angles at 2 cm from the center of the observation plane. The top edge of the image surface locates 1 cm below the observation plane. The image surface coincides with the source surface, and inverse computations are carried out to deduce the source density on node of a square array of side a .

s
image

complete them in a reasonable time. In general, single precision is used for all input values, as well as for output. This procedure reduces computer memory requirements and is adequate in consideration of the uncertainties in practical measurements. Double precision is used only when accumulation of roundoff error will seriously affect the accuracy of the computation. A typical computation, as used to produce the image in Fig. 2, required only 30 s on a Sun Sparc 2 computer with 16 Mb memory size, but for a larger array as used in the lower panel of Fig. 13, 30 min were needed.

A. Single Dipole Source

In the first simulation, a single current dipole is chosen for investigation because it represents the simplest possible source. It is oriented parallel to the y -axis to represent a source in the $x-z$ plane whose primary current flows perpendicular to that surface. Computations were carried out for the dipole placed at $z = -2, -3$, and -4.5 cm beneath the observation plane. Sensors were spaced at intervals of $s = 1$ cm across this plane. The left panel of Fig. 2(a) shows the corresponding magnetic source images represented by a distribution of current dipoles across the image surface, with each dipole at the center of a cell on a square grid of spacing $a = 0.36$ cm. The length of each arrow denotes the current dipole moment provided by a cortical area a^2 centered at the arrow's position. The right panel of Fig. 2(a) represents the image by isodensity contours across the $x-z$ plane. The image density q is expressed as the current dipole moment per unit area (with units $\mu A/m$). In each case [Fig. 2(a)-(c)] the maximum image current density of the MNLS inverse estimation predicts the correct location of the dipole. The shallowest source is better localized, as characterized by the width of the image distribution at half maximum. In addition, a weak side lobe of opposite polarity is evident near the

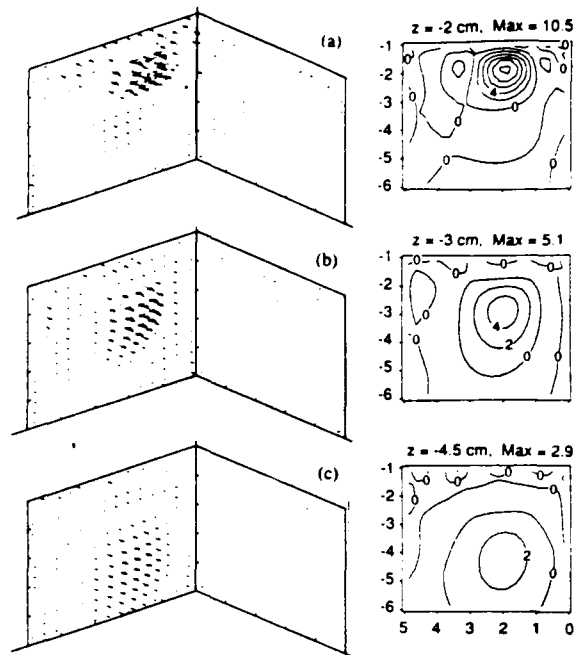


Fig. 2. Magnetic source images (MSI's) of a single current dipole of strength $Q = 1 \text{ nA} \cdot \text{m}$ located on the $x-z$ plane at the indicated depths d , whose coordinates are: $(x, z) = (2, -2), (2, -3),$ and $(2, -4.5)$ cm with its direction normal to the plane. The field sampling interval is $s = 1$ cm. (a) Image represented by current dipoles distributed on a grid of spacing $a = 0.36$ cm, with arrow length proportional to the dipole's strength. (b) Image of the dipole represented by contours of constant current dipole moment density q . The values ($\mu A/m$) for the maxima are indicated in each case. The interval between adjacent contours is $2 \mu A/m$. The values of q in the unit of $\mu A/m$ for the maxima are indicated above each panel.

(
Left
Right

coordinates $(x, z) = (3.5, -2)$. The image density on the $y-z$ plane is everywhere less than $0.1 \mu A/m$, and so is not shown in the figure.

An important property of these images is that the total strength, expressed as the total current dipole moment, is essentially independent of the depth of the maximum and matches that of the source. An integration over the whole image surface provides values that are consistently within 0.1% of the source's dipole moment. Indeed, such a conservation law may be expected if the field pattern across the observation plane is properly sampled and the computation of the SVD is accurate.

To further explore the properties of the point spread function of a current dipole, simulations were carried out for a dipole at a fixed depth $d = 2$ cm, when the field is sampled at different intervals s across the observation plane. The results illustrated in Fig. 3 depict the profile of the image density along a horizontal line passing close to the peak. Finer sampling intervals sharpen the image of the central peak: the full width at half maximum at the 2-cm depth is about 1, 0.75, and 0.5 cm for sampling intervals of 2, 1, and 0.5 cm. This expresses the tradeoff between image sharpness and the number of sensors that record field information across a given area of the observation plane. Because the model source (current dipole)

should be better to keep "s" and "s" together. 30s

009-269

WORK11 A6340SSB1

small
space

A1-5

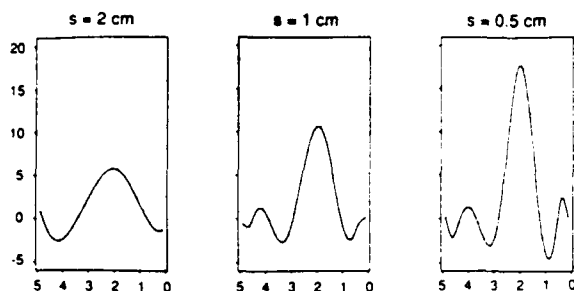


Fig. 3. MSI horizontal profiles at constant depth that pass through the peak image density for a current dipole source $Q = 1 \text{ nA} \cdot \text{m}$ at a depth $d = 2 \text{ cm}$, for field sampling intervals of $s = 2, 1,$ and 0.5 cm .

is a singularity, of zero width, side lobes appear in the image, as noted in Fig. 2. They are more pronounced for finer sampling intervals, because higher spatial frequencies can be represented in the image. We may expect the details of these lobes for a given source depth depend on the geometry of the lead field pattern of the sensors (whether magnetometer, first-order gradiometer, etc.). To investigate this feature, a set of computations was carried out with the observation plane increased to a size of $16 \times 16 \text{ cm}$, compared with the original size of $12 \times 12 \text{ cm}$, with the standard sampling interval maintained at $s = 1 \text{ cm}$. The side lobes do not weaken if the size of observation plane is increased in this way.

B. Two Dipole Sources

We next consider the case of two dipoles of equal strength, 3 cm apart and at the same depth $d = 2, 3,$ or 4.5 cm ($z = -2, -3,$ or -4.5). As a comparison, Fig. 4 shows the corresponding field patterns across the observation plane for sources at depths $d = 2$ and 4.5 cm . As opposing fields from the two parallel dipole sources are largely self-cancelling in the region between, the field pattern resembles that of a single current dipole and only detailed analysis would reveal that it arises from two underlying dipoles. The MNLS inverse solution clearly locates the two dipoles without need to introduce an explicit source model. The dipole images shown in Fig. 5 are well resolved, even at the greatest depth. However, the image peaks for the deepest case lie at a slightly shallower depth of 4.2 cm than the actual source depth of 4.5 cm . The image density in the $y - z$ plane is less than $0.1 \mu\text{A}/\text{m}$ and so is not shown.

Images for dipoles having closer separations are displayed in Fig. 6. With 1.5 cm separation the two are not clearly resolved, but with 2 cm separation two concentrations of strength are evident. To explore less symmetrical situations, we show the MSI's computed for identical dipoles at various positions on the same wall [Fig. 7(a)-(b)] and at positions on adjacent walls [Fig. 7(c)]. The MSI's show that images of sources at nearly the same depth are well resolved with their peaks lying within 0.1 cm of the actual source locations. Fig. 7(b) deals with one of the more difficult challenges in magnetic source imaging: two

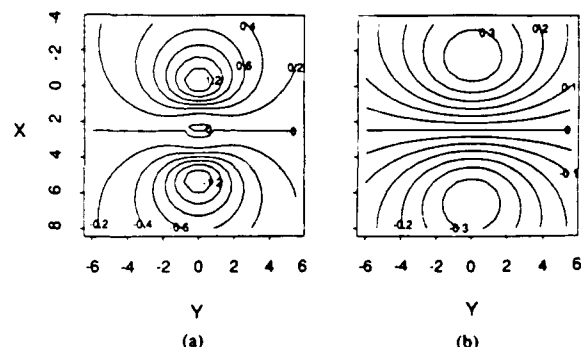


Fig. 4. Isocontours of magnetic field across the observation plane produced by two dipoles 3 cm apart horizontally and at $z =$ (a) -2 cm , (b) -4.5 cm .

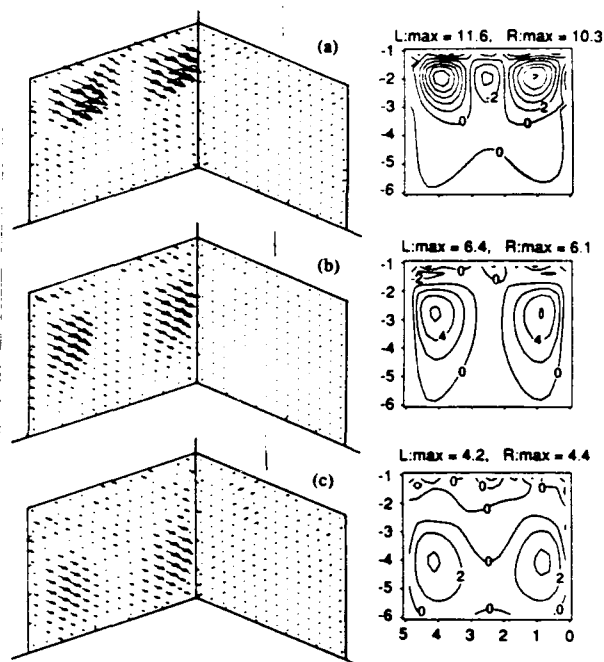


Fig. 5. MSI's of two dipoles, each of $q = 1 \text{ nA} \cdot \text{m}$, separated by 3 cm horizontally and at (a) $z = -2 \text{ cm}$, (b) -3 cm , and (c) -4.5 cm for a field sampling intervals of $s = 1 \text{ cm}$. The values ($\mu\text{A}/\text{m}$) for the left (L) and right (R) extrema are indicated above each panel.

parallel dipoles with one located above the other, and separated by 2.5 cm . Here the two could not be distinguished by separate extrema if the lower dipole were somewhat closer to the upper one.

C. Extended Source

As a particularly interesting example provided by the MNLS inverse, computations were carried out for an extended source, i.e., one having activity distributed over a finite area of the source plane. We chose a configuration having the shape of a crescent moon illustrated in the left panels of Fig. 8. We consider two cases: Fig. 8(a) defines

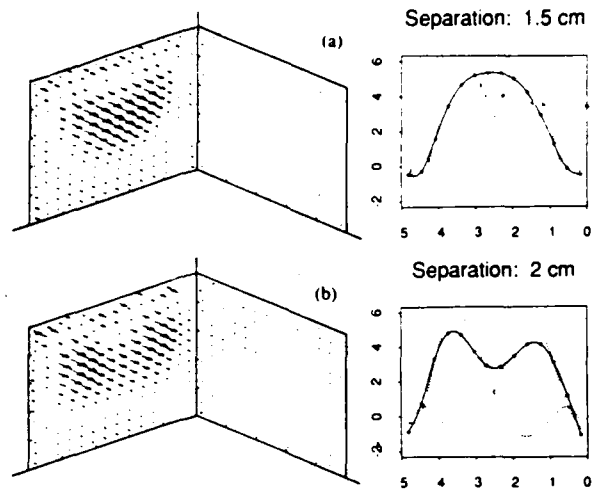


Fig. 6. MSI's for two current dipoles at $z = -3$ cm separated horizontally by (1) 1.5 cm and (b) 2.0 cm. Dotted lines in the right panels are horizontal profiles for individual dipoles, and the solid line is the sum of these profiles. Stars denote the profile computed for the two dipoles when simultaneously present.

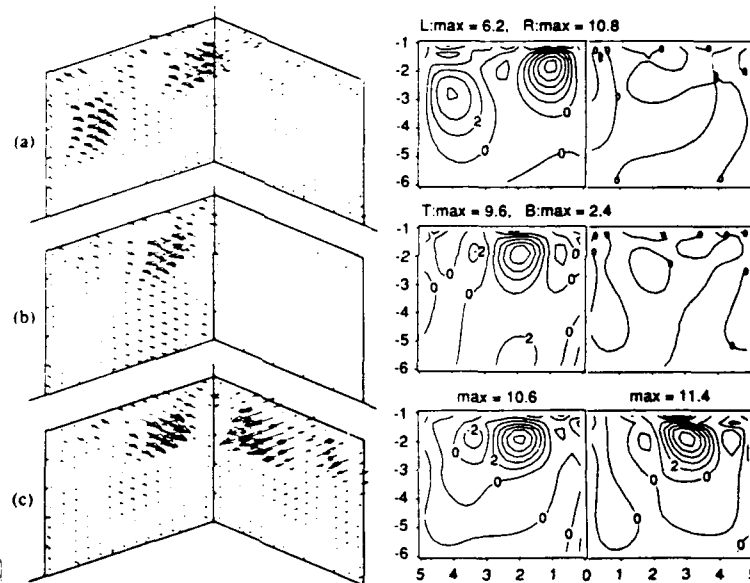


Fig. 7. MSI's of two dipoles of equal strength Q at the following positions on the same wall: (a) $(x, z) = (1, -2)$ and $(4, -3)$; (b) $(2, -2)$ and $(2, -4.5)$; and on different walls: (c) $(2, -2)$ on the left wall and $(2, -2)$ on the right wall. The field sampling interval is $s = 1$ cm. The values ($\mu A/m$) for the left and right extrema in (a), top and bottom in (b) and for each wall in (c) are indicated above each panel.

a continuous current distribution whose top is at a depth of $d = 2.5$ cm and bottom is at $d = 4.5$ cm; and Fig. 8(b) defines a source of the same shape but with source strength increasing linearly with depth to better emphasize the lower region in the field pattern. The dipole distributions in the middle panels generally mimic the overall shape, but exhibit some distortion as more strength is pushed towards the region near the center of gravity.

D. Inclined Source Surface

In general, a sulcus or fissure of the brain is inclined to the overlying skull. When the relevant volume of the head is well-modeled as a sphere, only the component of the source current lying tangent to the skull contributes to the external field. To represent this, we consider two current dipoles at the same depth separated by 3 cm and oriented

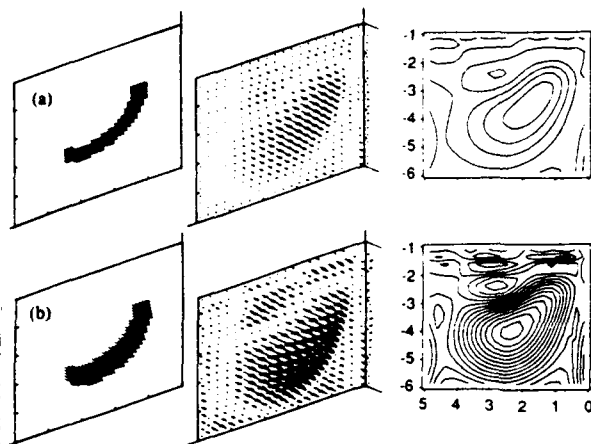
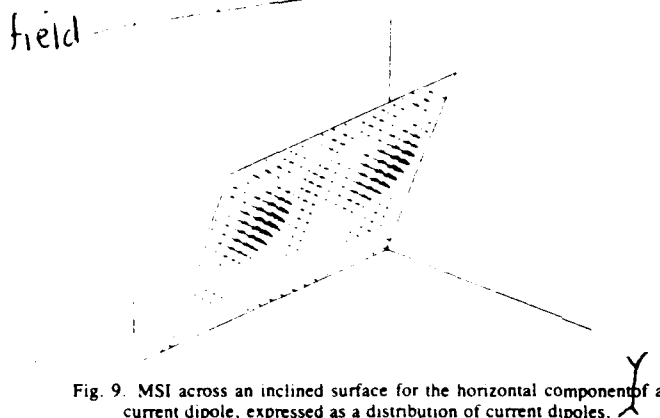


Fig. 8. (a) Extended source of uniform source density with upper edge at $z = -2.5$ cm and lower at -4.5 cm; (b) source of the same outline but with the source density at the bottom quadruple that at the top. With a file sampling interval of $s = 0.5$ cm, and measurements across an observation plane of boundaries 14×14 cm, the corresponding MSI's are shown in the middle and right panels.



parallel to the observation plane. There is no change in procedure when applying the MNLS approach, except in specifying the new locations in space that define the image surface.

The MSI for this geometry is illustrated in Fig. 9

We point out, however, that these solutions can be carried one step further to determine the *total* current dipole moment at each location, not just the component that is tangential to the overlying surface of the conducting volume. This is achieved by exploiting the physiological fact that, on average, the net intracellular current within cerebral cortex is oriented perpendicular to the cortical surface. To take this into account, the dipole moment in each cell should be divided by the cosine of the angle by which the source plane is tipped from the vertical [33].

IV. INFLUENCE OF NOISE

The practical limit in determining the quality of a magnetic source image in neuromagnetic measurements is

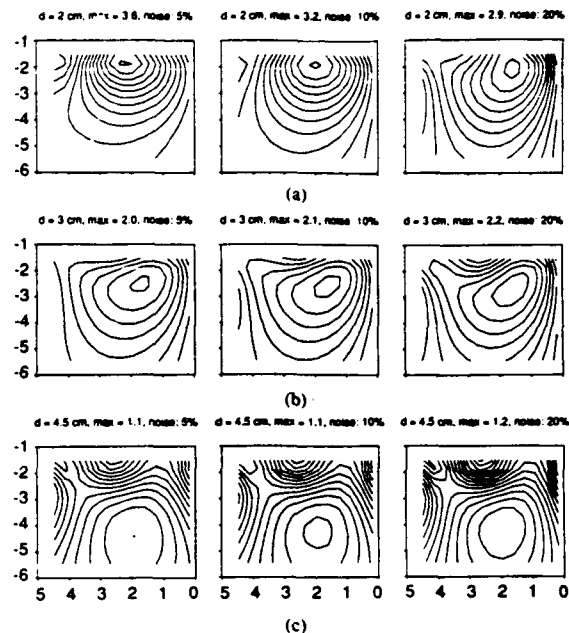


Fig. 10. Isocontours for MSI's representing the single dipole at positions (a) $(x, z) = (2, -2)$; (b) $(2, -3)$; and (c) $2, -4.5$ for noise levels of 0, 10, and 20% of 0.707 times the strongest field at the observation plane.

generally noise. This may originate in the sensing instruments, but in many cases the dominant contribution comes from biological activity in adjacent regions of the subject. In the following simulations we assume that the noise in each sensor has a Gaussian distribution with no coherence across sensors. This is generally an appropriate representation for sensor noise, but it is inadequate for biomagnetic noise because of its long range characteristics.

To treat noise, we modify (4) by normalizing both sides with the standard error σ_i of each measurement:

$$b' = L'Q \quad (17)$$

where b' is the column vector with element B_i/σ_i and L' is the normalized matrix of lead field with element L_{ij}/σ_i . The corresponding generalization of (6) can be recognized as the form that minimizes the chi square statistic,

$$\sum_i \left(\frac{\hat{B}_i - B_i}{\sigma_i} \right)^2 \quad (18)$$

where \hat{B}_i is the computed field value from the estimated sources.

A. Single Dipole

As the simplest example, we consider a current dipole that is imaged in the presence of 5, 10, and 20% rms noise levels compared with $\sqrt{2}$ times the maximum signal at the observation plane. As illustrated in Fig. 10, a low level of 5% noise markedly suppresses the side lobes that appear in the noise-free image of a current dipole. Higher noise levels have relatively little additional effect on the width of the image peak until reaching levels of about

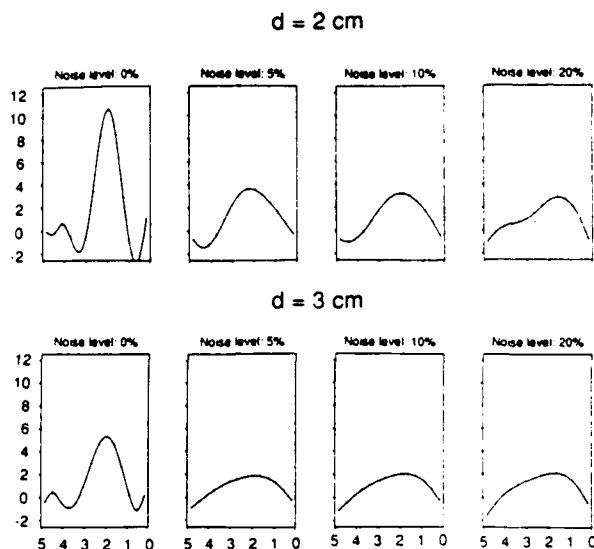


Fig. 11. Horizontal MSI profiles passing through the peaks of the current dipole density plots of the previous figure at the depth of the source positions $d = 2$ cm and $d = 3$ cm with different noise levels.

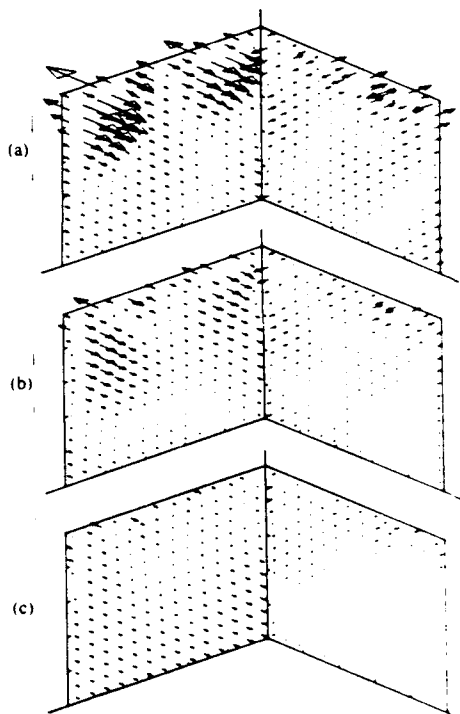


Fig. 12. The MSI for two dipoles at positions (a) $(1, -2)$, $(4, -2)$, (b) $(1, -3)$, $(4, -3)$; and (c) $(1, -4.5)$, $(4, -4.5)$ for a 20% noise level.

20%. Similarly, the peak location is not appreciably affected until reaching comparable noise levels. This is illustrated by the MSI's in Fig. 11 for dipoles at $x = 2$ cm and different depths.

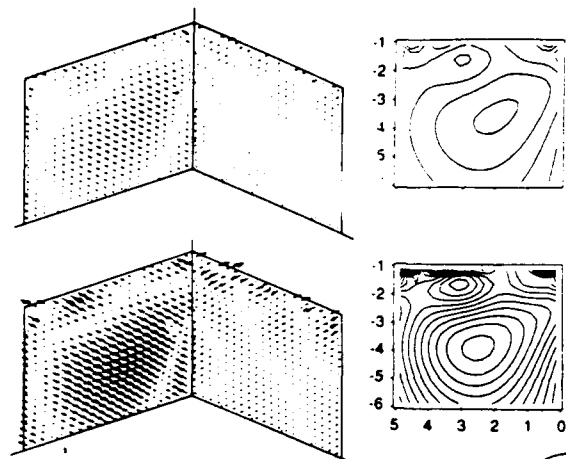


Fig. 13. MSI's for the extended uniform and non-uniform sources, for 10% noise level.

B. Two Dipoles

The effect of noise on MSI's of two dipoles separated by 3-cm horizontally has been assessed for $z = -2, -3$, and -4.5 cm. In comparison with the noise-free case of Fig. 5, the dipole images in Fig. 12 for the two shallow cases with 20% noise are still well-resolved. Their individual features are in accordance with MSI's obtained for single dipoles. As a consequence, there is serious deterioration of image quality for the deepest pair of dipoles. The image is more widespread, and correspondingly the current dipole density q is weaker in the regions of greatest strength.

C. Extended Source

The same uniform and nonuniform extended sources of Fig. 8 were evaluated in a simulation with noise. The sampling interval $s = 0.5$ cm and dimension of observation plane 14×14 cm are identical to those of the noise-free examples. With 10% noise level, the MSI given by the MMLS inverse solutions reveals the existence of an extended source and provides an indication of its shape (Fig. 13). However, the quality of the image is markedly degraded at this noise level. One prominent feature of the image is a series of sharply localized fluctuations in q across the top edge of the image plane.

V. DISCUSSION

The preceding sections illustrate unique solutions obtained by the MMLS procedure for a variety of inverse problems of relevance in biomagnetism. The procedure involves no *a priori* assumption about the nature of the current source, except that it is normal to a specified surface. The spatial resolution for a localized source, in the noise-free case, depends on the field sampling interval s , the source depth d , and the grid size a on the image surface. In general, the resolution is better for shallower sources than deeper. This can be understood from the fact

① its? this

that the field pattern of the former is more confined across the observation plane and therefore a correspondingly smaller number of magnetometers contribute significantly to the image. A complementary explanation, based on lead field theory, is that the lead field pattern for a given magnetometer varies more sharply with distance near the magnetometer, and therefore each magnetometer is more sensitive to the position of a source when close by.

One feature revealed by these simulations is a "conservation" law whereby the total image strength integrated over the image surface matches the total source strength. We view this property of the solution as providing an important empirical check on whether a given computation is correct. For example, if the threshold chosen to eliminate near-zero eigen values in the SVD is not appropriate, conservation of overall source strength will not be preserved.

The accuracy of an image will be degraded if the array of sensors across the observation plane does not record all of the essential features of the field pattern, (e.g., locations of field extrema, regions of field reversal, and the asymptotic behavior of the field far from the source). A proper characterization therefore relies on simultaneous measurements at a large number of locations, or on carrying out sequential measurements at many positions with a smaller array assuming stationarity in the signal being monitored. In the noise-free case, this requirement differs from the traditional procedure of accounting for the field pattern by employing a model source, in that fewer measurements are required for the latter procedure. For instance, a current dipole model requires only that five nonequivalent measurements be registered.

The quality of the image improves when the field sampling interval s is decreased to capture information about details. This is illustrated in Fig. 3, which shows that the central peak of the image of a current dipole sharpens as s is made smaller. A similar feature is found in the presence of noise. In the latter case, the effect of noise in adjacent sensors tends to average out when s is small, because the greater similarity in lead field patterns of adjacent sensors permits appreciable cancellation of their incoherent sensor noise.

A prominent feature that emerges from these calculations is the appearance of side lobes of opposite polarity to the main peak when a sharply localized source (e.g., current dipole) is represented (e.g., Fig. 2). We attribute this to an insufficient representation of basis functions of high spatial frequency in the procedure for SVD. Side lobes are also evident in the presence of noise.

Another artifact of several images is the series of intense fluctuations in current dipole density localized across the edges of the image surface (right panels of Fig. 8, Fig. 12(a) and (c) and right panels of Fig. 13). This is especially pronounced at the top edge (Fig. 12) in the presence of noise. Evidently, sensors are not spaced sufficiently close together for their lead fields to produce a net cancellation of image current when incoherent noise is present. As a means of avoiding false interpretations, any such

features of an image should be disregarded unless confirmed by additional measurements with the observation surface placed further above the source surface.

Our approach has a natural extension to a conducting body of spherical geometry, the details of which will be presented in a future publication. The procedure is identical to that described above. Only the geometry file describing the lead fields need be changed.

In order to establish the MNLS approach as a practical technique in the future, more studies are needed to establish the relationship between the optimal sampling interval for a given type of sensor and the effect of noise on the image quality. In particular, much of the noise in present recordings has spatial coherence, and this will degrade the image more dramatically than random noise. Spatially coherent noise will distort the image shape in addition to causing it to broaden. However, in the case of focal sources where field patterns are recovered after signal averaging [27], this effect of spatially coherent noise is largely attenuated. Attention should also be directed to the possibility that there well may be advantages in using combinations of sensors having differing lead field configurations, e.g., some magnetometers, first-order gradiometers, and second-order gradiometers [34]. The former would be more sensitive to distant sources than the latter, and so the differential sensitivity to sources at varying depths may be improved. The present simulations indicate that a variety of source configurations can be deduced by the MNLS method without resort to an explicit source model.

REFERENCES

- [1] S. J. Williamson, M. Hoke, G. Stroink, and M. Kotani, Eds. *Advances in Biomagnetism*. New York: Plenum, 1989.
- [2] H. Helmholtz, "Über einige Gesetze der Vertheilung elektrischer Ströme in körperlichen Leitern, mit Anwendung auf die thierisch-electrischen Versuche," *Ann. Phys. Chem.*, vol. 89, pp. 211-233, 353-377, 1853.
- [3] F. Grynszpan and D. B. Geselowitz, "Model studies of the magnetocardiogram," *Biophys. J.*, vol. 13, pp. 911-925, 1973.
- [4] B. N. Cuffin and D. Cohen, "Magnetic fields produced by models of biological current sources," *J. Appl. Phys.*, vol. 48, pp. 3971-3980, 1977.
- [5] D. B. Geselowitz and W. T. Miller, III, "Extracorporeal magnetic fields generated by internal bioelectric sources," *IEEE Trans. Magn.*, vol. MAG-9, pp. 392-398, 1973.
- [6] S. J. Williamson and L. Kaufman, "Magnetic fields of the cerebral cortex," in *Biomagnetism*, S. N. Erné, H.-D. Hahlbohm, and H. Lubbig, Eds. Berlin: Walter de Gruyter, 1981, pp. 353-402.
- [7] W. J. Dallas, "Fourier space solution to the magnetostatic imaging problem," *Appl. Opt.*, vol. 24, pp. 4543-4556, 1985.
- [8] W. J. Dallas, W. E. Smith, H. A. Schlitt, and W. Kullman, "Bioelectric current image reconstruction from measurement of the generated magnetic fields," in *Medical Imaging*, R. H. Schneider and S. J. Dwyer III, Eds., SPIE—The Internat. Soc. Opt. Eng., 1987, pp. 2-10.
- [9] W. Kullmann and W. J. Dallas, "Fourier imaging of electrical currents in the human brain from their magnetic fields," *IEEE Trans. Biomed. Eng.*, vol. BME-34, pp. 837-842, 1987.
- [10] M. Singh, D. Doria, V. W. Henderson, G. C. Huth, and J. Beatty, "Reconstruction of images of neuromagnetic fields," *IEEE Trans. Nucl. Sci.*, vol. NS-31, pp. 585-589, 1984.
- [11] J. P. Wikswo, Jr. and B. J. Roth, "Magnetic determination of the spatial extent of a single cortical current source: A theoretical analysis," *Electroenceph. clin. Neurophysiol.*, vol. 69, pp. 266-276, 1988.

- [12] B. J. Roth, N. G. Sepulveda, and J. P. Wikswo, Jr., "Using a magnetometer to image a two-dimensional current distribution," *J. Appl. Phys.*, vol. 65, pp. 361-372, 1989.
- [13] S. Tan, B. J. Roth, and J. P. Wikswo, Jr., "The magnetic field of cortical current sources: the application of a spatial filtering model to the forward and inverse problem," *Electroenceph. clin. Neurophysiol.*, vol. 76, pp. 73-85, 1990.
- [14] W. E. Smith, W. J. Dallas, W. H. Kullmann, and H. A. Schlitt, "Linear estimation theory applied to the reconstruction of a 3-D vector current distribution," *Appl. Opt.*, vol. 29, pp. 658-667, 1990.
- [15] J. Sarvas, "Basic mathematical and electromagnetic concepts of the biomagnetic inverse problem," *Phys. Med. Biol.*, vol. 32, pp. 11-22, 1987.
- [16] M. S. Hämaläinen and R. J. Ilmoniemi, "Interpolating measured magnetic fields of the brain: Estimates of current distributions," *Tech. Rep. TKK-F-A559*, Helsinki Univ. Technology, 1984.
- [17] W. H. Kullmann, K. D. Jandt, K. Rehm, H. A. Schlitt, W. J. Dallas, and W. E. Smith, "A linear estimation approach to biomagnetic imaging," in *Advances in Biomagnetism*, S. J. Williamson, M. Hoke, G. Stroink, and M. Kotani, Eds., New York: Plenum, 1989, pp. 571-574.
- [18] Y. C. Okada and J. C. Huang, "Current-density imaging as method of visualizing neuronal activities of the brain," in *Proc. Ann. Meet. Soc. Neurosci.*, St. Louis, MO, 1990.
- [19] M. S. Hämaläinen and R. J. Ilmoniemi, "Interpreting magnetic fields of the brain: Minimum norm estimates," *IEEE Trans. Biomed. Eng.*, vol. 38, 1991.
- [20] W. H. Kullmann, "Can volume conductor modeling improve biomagnetic distributed source imaging?" in *Biomagnetic Localization and 3D Modeling*, J. Nenonen, H.-M. Rajala, and T. Katila, Eds., Helsinki University of Technology, Dep. Technical Physics Rep. TKK-F-A689, Otaniemi, 1991, pp. 137-153.
- [21] R. Graumann, "The reconstruction of current densities," in *Biomagnetic Localization and 3D Modeling*, J. Nenonen, H.-M. Rajala, and T. Katila, Eds., Helsinki University of Technology, Dep. Technical Physics Rep. TKK-F-A689, Otaniemi, 1991, pp. 172-186.
- [22] R. L. Parker, "Understanding inverse theory," *Annu. Rev. Earth Sci.*, vol. 5, pp. 35-64, 1977.
- [23] C. W. Crowley, R. E. Greenblatt, and I. Khalil, "Minimum norm estimation of current distributions in realistic geometries," in *Advances in Biomagnetism*, S. J. Williamson, M. Hoke, G. Stroink, and M. Kotani, Eds., New York: Plenum, 1989, pp. 603-606.
- [24] C. J. S. Clarke, A. A. Ioannides, and J. P. R. Bolton, "Localised and distributed source solutions for the biomagnetic inverse problem I," in *Advances in Biomagnetism*, S. J. Williamson, M. Hoke, G. Stroink, and M. Kotani, Eds., New York: Plenum, 1989, pp. 587-590.
- [25] A. A. Ioannides, J. P. R. Bolton, R. Hasson, and C. J. S. Clarke, "Localised and distributed source solutions for the biomagnetic inverse problem II," in *Advances in Biomagnetism*, S. J. Williamson, M. Hoke, G. Stroink, and M. Kotani, Eds., New York: Plenum, 1989, pp. 591-594.
- [26] A. A. Ioannides, J. P. R. Bolton, and C. J. S. Clarke, "Continuous probabilistic solutions to the biomagnetic inverse problem," *Inverse Problems*, vol. 6, pp. 1-20, 1990.
- [27] L. Kaufman, J. Kaufman, and J. Z. Wang, "On cortical folds and neuromagnetic fields," *Electroenceph. clin. Neurophysiol.*, vol. 79, pp. 211-226, 1991.
- [28] A. Ben-Israel and T. N. E. Greville, *Generalized Inverses: Theory and Applications*, New York: Wiley, 1974.
- [29] S. Barnett, *Matrices. Methods and Applications*, Oxford: Clarendon, 1990.
- [30] E. H. Moore, "On the reciprocal of the general algebraic matrix," *Bull. Amer. Math. Soc.*, vol. 26, p. 394-395, 1920.
- [31] R. Penrose, "A generalized inverse for matrices," in *Proc. Cambridge Philos. Soc.*, vol. 51, pp. 406-413, 1955.
- [32] G. Dahlquist and A. Björck, *Numerical Methods*, Englewood Cliffs, NJ: Prentice-Hall, 1974.
- [33] G. L. Romani, S. J. Williamson, L. Kaufmann, and D. Brenner, "Characterization of the human auditory cortex by the neuromagnetic method," *Exp. Brain Res.*, vol. 47, pp. 381-393, 1982.
- [34] G. L. Romani, S. J. Williamson, and L. Kaufman, "Biomagnetic instrumentation," *Rev. Sci. Instrum.*, vol. 53, pp. 1815-1845, 1982.



Jia-Zhu Wang was born in Chongqing, China. She received the B.Sc. degree in physics from Fudan University in Shanghai, China, the M.S. degree in physics from the International School of Advanced Studies, Trieste, Italy, in 1982, and the M.S. and Ph.D. in physics from New York University, in 1985 and 1986, respectively. Her area of specialization was in theoretical aspects of general relativity.

In December 1986, she joined the Neuromagnetism Laboratory of the Departments of Physics and Psychology and Center for Neural Science, New York University. She is currently Associate Research Scientist. Her research interests include modeling and simulation of neuronal activity of the cerebral cortex, as well as signal and image processing for neuromagnetic applications. She is also developing applications of estimation and inverse theory to several areas of magnetic source imaging.



Samuel J. Williamson (M'81) was born in Reading, PA. He received the S.B. degree in physics from M.I.T., Cambridge, in 1961 and the Sc.D. in 1965.

After a year as a Staff Member at the Francis Bitter National Magnet Laboratory at M.I.T., he became a National Academy of Sciences Postdoctoral Fellow, at the Université de Paris (Orsay). From 1967 to 1970 he was a Member of the Technical Staff at the Science Center of North American Aviation, and in 1970 became Lecturer at the University of California, Santa Barbara. In 1971 he joined the New York University as Associate Professor of Physics in the Faculty of Arts and Sciences. He became Professor of Physics in 1977 as well as Adjunct Professor of Physiology and Biophysics in the School of Medicine, and in 1991 he was appointed University Professor. During the period 1979-1980, he was a Fulbright Senior Research Scholar at the Université de Paris (Orsay). He is Co-Director of the Neuromagnetism Laboratory of the Departments of Physics, Psychology, and Center for Neural Science, and his interests focus on the use of neuromagnetic investigations to relate human physiology to the processes of perception and cognition. He received the Sc.D. honors causa from New Jersey Institute of Technology and is a Fellow of the American Physical Society. He is a member of the Editorial Boards of *Biophysical Journal* and *Brain Topography* and is author of the textbook *Fundamentals of Air Pollution* (Addison Wesley) and coauthor of the textbook *Light and Color in Nature and Art* (Wiley).



Lloyd Kaufman was born in New York, NY. He received the B.A. degree in (1950) from San Diego State College, and the M.A. degree in 1959, and the Ph.D. degree in 1961 in experimental psychology from the New School for Social Research.

He worked successively as an Engineer, Section Head for Human Factors, and Member of the Research Staff for the Sperry Rand Corporation (1951-1967). In 1967 he became Associate Professor of Psychology at Yeshiva University in New York City. He joined New York University as Professor of Psychology in 1969 and is currently also Professor of Neural Science in the Faculty of Arts and Science and Adjunct Professor of Physiology and Biophysics in the School of Medicine. He is Co-Director of the Neuromagnetism Laboratory of the Departments of Physics, Psychology, and Center for Neural Science. In 1990 he was awarded the D.Sc. *honoris causa* from Long Island University. He is the author of *Sight and Mind* (Oxford University Press, 1974), and of *Perception: The World Transformed* (Oxford University Press, 1978), and was a general editor of the *Handbook of Perception and Human Performance* (Vols. I and II) (Wiley, 1986). He is the author or coauthor of numerous papers on neuromagnetism and on visual perception.

Imaging regional changes in the spontaneous activity of the brain: An extension of the unique minimum-norm least-squares estimate

Jia-Zhu Wang, Lloyd Kaufman, Samuel J. Williamson

*Neuromagnetism Laboratory, Departments of Physics and Psychology
and Center for Neural Science
New York University, New York, NY 10003, U.S.A.*

Manuscript submitted: December 26, 1991

Manuscript revised: April 2, 1992

Summary This paper describes methods for inferring mathematically unique local distributions of primary cortical current that underly changes in the average pattern of power of the ongoing ("spontaneous") extracranial magnetic field of the brain. In previous work we demonstrated that mathematically unique solutions to the inverse problem are possible for current sources of the brain's field, without any assumed source model, e.g., an equivalent current dipole. Thus, in principle it is possible to locate and delineate patterns of current of any configuration. In practice this approach applies to synchronized neuronal activity, e.g., activity which is known to underly average evoked or event related brain responses. This paper extends that approach to local changes in incoherent activity, e.g., activity yielding fields or potentials that tend to be self-canceling when averaged over time. This includes the spontaneous brain activity normally treated as background noise when it accompanies event related responses. We demonstrate that local changes in this ongoing incoherent activity may also be uniquely delineated in space and time. Evidence is reviewed indicating that the distribution of the brain's magnetic field, due to *both* its synchronized and incoherent neural activity, is affected by early sensory-perceptual processes and by higher cognitive processes. Hence, in principle, the ability to delineate both kinds of sources in space and time makes it possible to form more comprehensive dynamic functional images of the human brain.

Key words: Inverse solution, Minimum-norm least-squares inverse, Neuromagnetic measurements, Magnetic source image

This work was supported in part by AFOSR Grants Nos. AFOSR90-0221 and F49620-88-0004. Address reprint requests to Dr. Jia-Zhu Wang, Department of Physics, New York University, 4 Washington Place, NYC, NY 10003, USA.

Ionic currents flowing within the brain's neurons are accompanied by superimposable magnetic fields that encircle entire populations of concurrently active neurons. Where the coherent (synchronized) activity of the neurons is limited in area - so that the extent of cortex involved is small relative to the distance at which its field is measured - the external field is essentially indistinguishable from one produced by a current dipole. Field measurements make it possible to determine the 3-dimensional location, orientation and strength of this equivalent current dipole (Cuffin and Cohen, 1977; Williamson and Kaufman, 1981; 1987). Typically, a statistical method is used to fit the observed field pattern to one that would be produced by a hypothetical underlying current dipole. However, a dipolar source deduced from an observed field is but one of many possible solutions to the so-called *inverse problem*, which, in general, has no unique solution. Many different source configurations could produce virtually the same dipolar field pattern.

Generally, the inherent ambiguity of inverse solutions makes it impossible to be certain of the actual generator of an observed field pattern, as the field may be due to the activity of an assemblage of dipoles distributed throughout the intracranial space. However, it is not necessary to restrict solutions to those predicated on specific source models, e.g., dipoles. For example, in recent work on magnetic source imaging it was assumed that the current to be imaged flowed parallel to a plane or to each of several parallel planes, but no particular configuration was assumed. In some of these studies (Dallas, 1985; Kullmann and Dallas, 1987) the shape of an arbitrary planar current distribution producing an observed external field was computed from the inverse of the Fourier transform of the field. However, this approach does not provide a unique solution to the inverse problem, as magnetic field measurements alone do not contain enough information to assure uniqueness. Nevertheless, within constraints due to limited bandwidth of the spatial frequency content of the field (because of the distance between the source and the sensor), and errors due to additive noise, the method does yield a current distribution in any arbitrarily selected plane or subspace within a volume. What is lacking is unambiguous knowledge of the space actually occupied by the primary current distribution within the volume. Other authors describe similar approaches (Dallas et al., 1987; Kullmann and Dallas, 1987; Singh et al., 1984; Roth et al., 1989; Tan et al., 1990).

Another related approach is that of Hämäläinen and Ilmoniemi (1984; 1991), Kullmann et al. (1989), Okada and Huang (1990), and Graumann (1991), who used linear estimation methods to determine the current distributions from their field patterns. We should also note the recent works of George et al. (1991), Greenblat (1991), Okada et al. (1991), Robinson (1991), Szinger & Kuc (1991), etc. who employed related methods to form magnetic source images. Kullmann (1991), summarizing much of the work based on this approach, claims that (within the bounds of precision due to noise and spatial filtering of the observed field) the linear estimation method also gives recognizable images of the distributions when they are projected onto an arbitrary plane within the conducting volume. However, he concludes that the non-uniqueness of inverse solutions proscribes unambiguous image formation. Similar problems are associated with probabilistic approaches described by Clarke et al. (1989), and by Ioannides et al. (1989; 1990) although in principle they too can deal with current configurations on a plane or stacks of planes within a conducting volume.

Most of these authors seem to have missed the simple point that the actual surface on which the primary current configuration may exist is knowable. Furthermore, ample electrophysiological evidence supports the assumption that the primary current flow is, on average, normal to the surface and not parallel to it (Kaufman, Kaufman and Wang, 1991; George et al., 1991; Wang et al., 1992). This *a priori* information is one vital ingredient of methods for finding mathematically

unique solutions to the inverse problem.

The geometry of the surface containing the primary sources needed to achieve a mathematically unique solution to the inverse problem may be obtained from high-resolution MRI scans. Moreover, basic electrophysiology teaches us that post synaptic potentials leading to axial intracellular current flow, e.g., in pyramidal cells within cortical macrocolumns, is predominantly normal to the surface of the cortex. These axial (primary) currents make the major contribution to the field measured normal to the surface of the scalp. Thus, according to Wang et al. (1992), any arbitrary pattern of current would consist of elements of current flowing in the same direction normal to the surface of some region of cortex. The problem is thus constrained to discovering the net strength of this current flow and the area of cortex it occupies.

The linear estimation method of Hämäläinen and Ilmoniemi (1984; 1991), Crowley et al. (1989) employ a so-called *minimum-norm* criterion, which refers to the fact that the accepted solution is one in which the net squared current (the square of the current integrated over the surface) predicting the observed field is a minimum, as compared with the net squared current of all possible candidate source configurations. However, even when supplemented with prior knowledge of the source surface, the minimum-norm criterion is still insufficient to produce a solution that qualifies as mathematically unique. Wang et al. (1992) recognized that the minimization of the sum of the squares of the differences between the observed or measured field pattern external to the scalp and a theoretical pattern computed from the source configuration meeting the minimum-norm criterion leads to a unique solution. This minimum-norm least-squares (MNLS) criterion falls naturally out of the specific type of the generalized inverse Wang et al. adopted for this problem (Penrose, 1955). While earlier investigators adopted this same generalized inverse, they failed to recognize its least-squares feature and that it makes a unique solution possible. The MNLS solutions were found to be robust in the presence of typical noise levels (Wang et al. 1992).

MNLS solution for coherent sources

Review of Basic Concepts

The MNLS approach can be simply explained by considering a geometry illustrated in Fig. 1 which shows a *source surface* composed of two planar surfaces at right angles to each other, and an *observation surface* above and at right angles to the source surface. Since the source surface is presumed to be known, it coincides with the *image surface* on which the inferred current pattern, flowing normal to it, is to be located. Fig. 2 illustrates a field pattern on the observation surface generated by single dipole on the source surface. The image of the source computed from the field is shown on the image surface. Fig. 3 shows a region of one plane of the source surface containing a crescent-shaped pattern of current elements. These currents are all flowing in the same directions at once. Thus, we say that they are coherent or synchronized. The plots in the middle panels of Fig. 3 show the inverse solutions across the image surface. The inverse solution clearly resembles the original source. Wang et al. (1992) provide several examples of this type of result, proving that unique inverse solutions are possible given the conditions specified above.

Thus far we have said little about the actual measurements made on the observation surface. At every position where a measurement of the field is made, the actual measure depends upon the contribution of each current element of the source, which in turn is dependent upon the strength of the element, its orientation relative to the sensing coil, and its distance from the coil. Further, it

depends upon the geometry of the coil itself and the orientation of the coil with respect to the observation surface. The effects of all of these factors may be taken into account through the concept of coil's lead field (see below). Points on the image surface are taken to represent elements of a current configuration that would produce the values of \vec{B}_i measured at positions \vec{r}_i , $i = 1, \dots, m$, on the observation surface, where the measures are weighted by the sensitivity of the respective detection coil at the various positions. The distribution of the current across the cortex can be represented as an array of closely spaced current dipoles of suitable strength Q_j at the positions \vec{r}_j on the source surface, the values of \vec{Q}_j , where $j = 1, \dots, n$ determine the observed field pattern. The matrix relating the values \vec{B}_i at \vec{r}_i to a current dipole of unit strength ($|Q_j| = 1 \text{ A}\cdot\text{m}$) at \vec{r}_j is referred to as the lead field matrix L . A more technical account of the lead field concept and that of the minimum-norm least-squares (MNLS) approach follows. The non-mathematical reader may skip the equations in the sections with a leading asterisk, but much of the text is understandable without them.

*Lead Field Analysis

In common with all of the other linear estimation and related methods, the approach of Wang et al. (1992) assumes that the primary current underlying the observed field is intracellular and that the secondary (volume) currents make a negligible contribution. Further, the primary current is assumed to be distributed within a finite space Ω . The law of Biot and Savart relates the magnetic induction $\vec{B}(\vec{r})$ to the current density $\vec{J}(\vec{r}')$ within Ω

$$\vec{B}(\vec{r}) = \frac{\mu_0}{4\pi} \int_{\Omega} \frac{\vec{J}(\vec{r}') \times (\vec{r} - \vec{r}')}{|\vec{r} - \vec{r}'|^3} d r'^3 \quad (1)$$

In reality, the number of observations of magnetic field is finite. While the brain anatomy is complicated, as pointed out earlier, in principle, it has a known geometrical configuration Ω . It follows that the observations of the normal components of field B_i are linearly related to the current source density by

$$B_i = \int_{\Omega} \vec{L}_i(\vec{r}') \cdot \vec{J}(\vec{r}') d r'^3, \quad i = 1, \dots, m, \quad (2)$$

where \vec{r}' is the position vector within the source region Ω , ($\vec{r}' \in \Omega$). The vector form $\vec{L}_i(\vec{r}')$ is known as the lead field (Plonsey, 1972; Williamson and Kaufman, 1981). The lead field $\vec{L}_i(\vec{r}')$ accounts for the sensitivity to the magnetic flux of the i th pickup coil at position \vec{r}_i produced by unit source current density at \vec{r}' . The lead field within Ω is determined by the geometry and orientation of the detection coil. For the present we make the simplifying assumption that the detection coil is so small that it may be considered to be a point.

To prove the principles presented here, it is not necessary to employ the actual convoluted cerebral cortex as a source surface. Instead, in the interest of clarity, we employ as a source space Ω a simple folded surface layer of uniform thickness w . Therefore, the volume integral is reduced to a surface integral. If we further divide the surface into a grid of n cells with area $\Delta S_j'$, centered at position \vec{r}_j and assume that current density is constant within each small area, we can replace the integral of Eq. 2 with a summation sign. Eq. 2 becomes

$$B_i = \sum_{j=1}^n \vec{L}_i(\vec{r}_j) \cdot \vec{J}(\vec{r}_j) w \Delta S_j', \quad i = 1, \dots, m. \quad (3)$$

Note that $\vec{J}(\vec{r}_j) w \Delta S_j'$ bears the dimension of current dipole: ampere-meter. In matrix representation Eq. 3 can be written as

$$b = L Q, \quad (4)$$

where b and Q are column vectors and L is a $m \times n$ matrix.

As stated earlier, it is well known that the inverse solution of Eq. 4 is not unique. Mathematically, this is because there may exist a family of solutions Q^* of the following homogeneous equation corresponding to Eq. 4

$$L Q^* = 0. \quad (5)$$

We know that the solutions of Eq. 5 may have an infinite number of elements. If \hat{Q} is an estimated source of Eq. 4 then any combination of $\hat{Q} + Q^*$ could be the solution of Eq. 4. The component Q^* represents the "magnetically silent" sources, which produce no magnetic field on the observation plane.

**The Unique Minimum-Norm Least-Squares Inverse of the Field*

Despite the obstacle posed by the nonuniqueness of inverse solutions, we claim that the source can be estimated by minimizing the square of the residual error between the measurements and theoretical computations from the estimated sources. In the presence of noise, we minimize the weighted least-squares error (or the χ^2 statistic)

$$\text{Minimum of } \sum_{i=1}^m \left[\frac{\hat{B}_i - B_i}{\sigma_i} \right]^2 \quad (6)$$

where \hat{B}_i represents values of the field computed from the estimated source, B_i the measured values of the field, and σ_i the rms noise. The corresponding matrix expression of Eq. 6 is

$$\text{Minimum of } \| L' \hat{Q} - b' \|^2. \quad (7)$$

where $\| \cdot \|$ is the Euclidean norm of a vector, L' the weighted matrix with element L_{ij}/σ_i , and b' the weighted vector with element B_i/σ_i in the presence of noise. In what follows we will drop the prime in L and b for simplicity. However, it is understood that they refer to the weighted matrix and vector whenever noise is present.

In statistics one generally deals with cases where the number of measurements, and therefore the number of equations, is greater than number of unknowns ($m > n$), and the unknowns are always linearly independent. It is only in such conditions that the least-squares fit will give a unique estimate.

In reality the number of unknowns may exceed the number of equations. Also, the n unknowns may not all be linearly independent of each other because of noise or an accumulation of round-off errors. In this case the least-squares criterion will not lead to a unique estimate. That is to say, there may exist a set of solutions which all fulfill the least-squares criterion. If we further select one solution from such a set and require that the square of the image current ("power") integrated over the image surface also be a minimum, the resulting estimate has the

least residual error and has itself the minimum power amongst all least-squares solutions

$$\text{Minimum of } \|\hat{Q}\|^2 = \text{Minimum of } \sum_j^n \hat{Q}_j^2 \quad (8)$$

Equivalently, we seek the solution that minimizes the following Euclidean norm of the vector Q

$$\text{Minimum of } \|\hat{Q}\| = \text{Minimum of } \left(\sum_j^n \hat{Q}_j^2 \right)^{1/2}. \quad (9)$$

The above equation is the so-called *minimum-norm*, which, as we pointed out earlier, together with Eq. 6 (or 7) represent both the least-square residual error and the minimum power of the inverse solution.

There exist many different types of generalized inverses in mathematics. This particular type which has the feature of the least residual error of the measurements and the minimum power of the source is known as the Moore-Penrose inverse, or pseudo-inverse (Barnett, 1990; Ben-Israel and Greville, 1974). We have adopted the terminology of minimum-norm least-squares (MNLS) inverse because the name implies its properties. More importantly, the MNLS inverse is proven to be mathematically unique.

The unique MNLS inverse estimate of Eq. 4 is given by

$$\hat{Q} = L^+ b, \quad (10)$$

where L^+ is the MNLS inverse matrix of L . The structure of L^+ and how to compute it are discussed in detail in Wang et al. (1992). Here we mention only that the method of singular value decomposition (SVD) is used in computing L^+ (Press et al., 1986; Ciarlet, 1991). Nevertheless, we list a few properties of the MNLS inverse which could be useful to the reader in actual computations (Ben-Israel and Greville, 1974; Ciarlet, 1991).

$$(L^T)^+ = (L^+)^T \quad (11a)$$

$$L^+ = (L^T L)^+ L^T \quad (11b)$$

$$L^+ = L^T (L L^T)^+ \quad (11c)$$

MNLS solution for incoherent sources

Incoherent versus Coherent Distributed Sources

It is important to emphasize that the MNLS method discussed thus far applies only to coherent (synchronous) patterns of primary current. Synchronous currents flowing normal to the surface of the cortex was demonstrated by Kaufman et al. (1991a) to be a reasonable model of sources of evoked responses. Time averages are dominated by fields of the coherent activity, while those of the incoherent background activity tend to be self canceling. Evoked fields are stable in space, while the spatial distributions of the fields of the incoherent background activity change with time. However, if the fields due to ongoing incoherent activity are squared to obtain *field power*, and the resulting spatial patterns of power are averaged, then the configuration of the averaged power pattern is determined by the underlying geometry of the source surface, as well as by the statistics of the elements of current of which its source is composed (Kaufman et al., 1991a). Also, if, on average, a region of the source surface exhibits either more or less

asynchronous activity than its surroundings, the average field power pattern is affected and is related to the location and shape of the region in question. This suggests that it is possible to locate and delineate differentially active regions of cortex, even when that activity is incoherent. In fact, simple methods previously applied to dipole localization (Williamson and Kaufman, 1981) were successfully extended to apply to the localization of the center-of-gravity of a region of incoherent activity that was either stronger or weaker than that of its incoherently active surroundings (Kaufman et al., 1991a).

Many experiments now show that incoherent activity revealed by power patterns of extracranial fields are differentially affected by the performance of cognitive tasks. Such differential effects are localized to different regions of the scalp, depending on the nature of the cognitive task. These experiments motivated the present theoretical study. For example, Kaufman et al. (1991b) demonstrated that power of the spontaneous alpha activity originating in the right temporal lobe is suppressed while subjects scan memory for previously heard musical tones. The duration of this suppression increases linearly with the size of the memory set, as does reaction time when performance is relatively free of errors (Sternberg, 1966). Further, while suppression is detected elsewhere, its duration is not related to the time required to scan memory. The interhemispheric differences among these effects are far more profound than those encountered in event related potential studies (Regan, 1989). The N100 component evoked by the same tones and detected electrically at Cz does not covary systematically with RT. Further, the magnetic counterpart to N100 does not vary consistently with set size either, and changes in its amplitude with set size differ dramatically across the hemispheres. N100 is due to the activity of neurons synchronized by the stimulating event, and may well reflect different attentional strategies, but it does not reflect operations on short-term memory. Similarly, Kaufman et al. (1991b) reviewed an extensive P300 literature on this subject and found that neither the latency nor the amplitude of P300 (which is also due to coherent activity of neurons) varies linearly with set size. Further, sometimes there is no change at all in P300 with set size, although the RTs of the same subjects increase with set size.

Kaufman et al. (1990) also found suppression of alpha frequencies when subjects scanned memory for visual forms. However, in this case the effect was measured over the visual areas. This result was recently confirmed by Cycowicz et al. (1992). Also, when subjects engage in verbal tasks in response to visually presented words, the suppression related to performing the task is not present over the visual areas (Kaufman et al., 1989), but it is over the left frontotemporal areas (Cycowicz et al., 1992).

Pfurtscheller et al. (1977; 1988a; 1988b) observed dramatic changes in alpha power in the EEG over different cortical regions, depending upon the nature of the task. These effects were often bilateral and difficult to localize from the EEG data. However, the reference-free MEG clearly establishes that these suppression effects are local, and not merely due to generalized arousal.

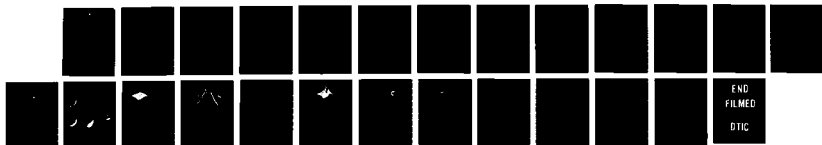
All of this serves to motivate the present paper. It is clear that early sensory-perceptual and some cognitive processes are reflected in the coherent event-related responses. It is equally clear that local changes in incoherent activity reflect other cognitive processes and may even be related to perceptual processes as well. The two measures complement each other, and neither alone is an adequate basis for building a cognitive neuroscience. The MNLS method has now made it possible to delineate the cortical areas involved in the coherent aspect of brain activity. To complete the picture we now extend the MNLS method to make it possible to find unique inverse solutions to the problem of delineating the cortical areas exhibiting changes in incoherent activity.

AFM-92-003 483

COGNITION AND THE BRAINCUS NEW YORK UNIO NY
S J WILLIAMSON ET AL. 23 MAY 92 AFOSR-TR-92-05446
AFOSR-90-0221

UNCLASSIFIED

ML



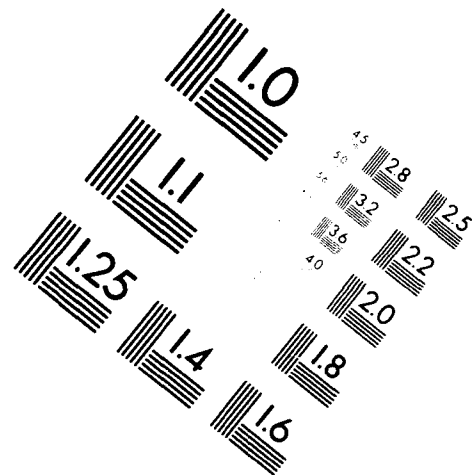
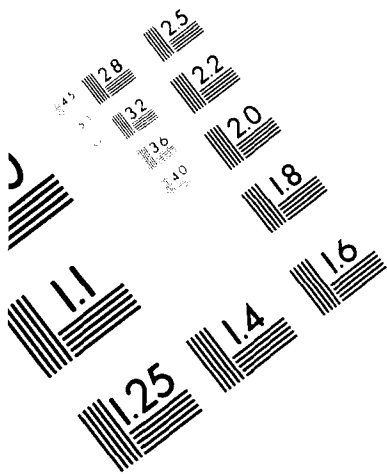


AIM

Association for Information and Image Management

1100 Wayne Avenue, Suite 1100
Silver Spring, Maryland 20910

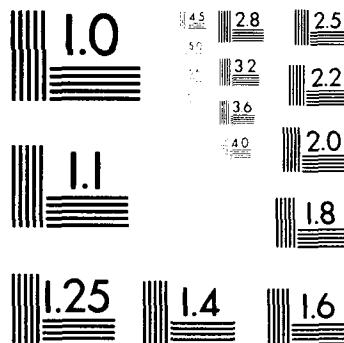
301/587-8202



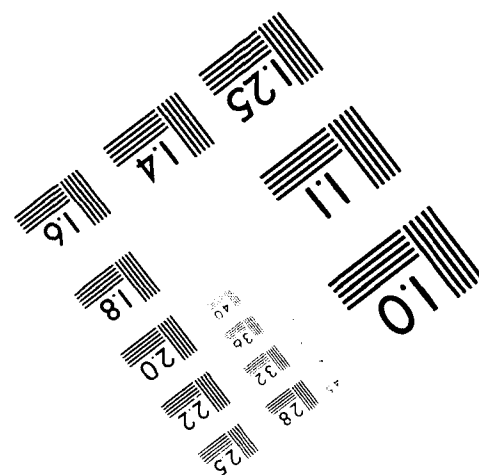
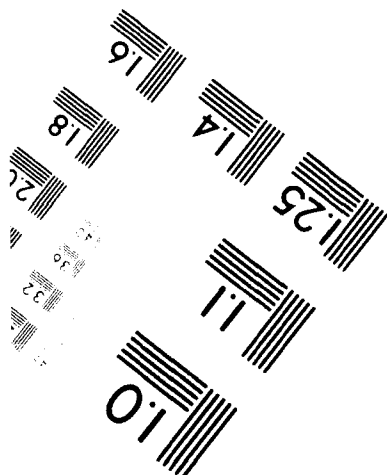
Centimeter



Inches



MANUFACTURED TO AIM STANDARDS
BY APPLIED IMAGE, INC.



**The Unique Minimum-Norm Least-Squares Inverse of the Power*

The basic problem attendant upon identifying differentially active regions is that we deal with average field power as the basic measure and not field *per se*. We introduce a novel mathematic development for solving the inverse problem for such measures.

Previously the values of the field B_i measured normal to the observation surface at m positions were used to form a column vector \mathbf{b} of m elements. If we now introduce an auto-correlation matrix \mathbf{B}_p in terms of the vector \mathbf{b} , we obtain

$$\mathbf{B}_p = \mathbf{b} \mathbf{b}^T, \quad (12)$$

with elements $(\mathbf{B}_p)_{ij} = B_i \cdot B_j$, where $i, j = 1, 2, \dots, m$. Therefore, the diagonal elements of \mathbf{B}_p are the field power B_i^2 , rather than field.

Manipulations of Eq. 4 reveal a new linear model which relates field power to the source power, as opposed to a linear relation between field *per se* and source strength as given by Eq. 4. Thus,

$$\mathbf{B}_p = \mathbf{L} \mathbf{Q}_p \mathbf{L}^T, \quad (13)$$

where \mathbf{Q}_p is the auto-correlation matrix of source image, $(\mathbf{Q}_p)_{kl} = Q_k \cdot Q_l$, $k, l = 1, 2, \dots, n$, with the diagonals as the power of the source. Note the difference between Eq. 4, which has a matrix and two vectors, and Eq. 13, which contains all matrices. Fortunately, for the matrix equation Eq. 13 there also exists a unique MNLS inverse. With the help of the MNLS inverse theory (Penrose, 1955; Ben-Israel and Greville, 1974) and the property given in Eq. 11a, we are able to derive the MNLS inverse of the source power for a given field power distribution

$$\hat{\mathbf{Q}}_p = \mathbf{L}^+ \mathbf{B}_p (\mathbf{L}^+)^T \quad (14)$$

Applying this equation makes it possible to delineate regions of cortex whose levels of incoherent activity deviate from a baseline because of some ongoing cognitive process, or even because of effects of transient ischemia, cortical hyperactivity, abnormally low metabolic level, etc.

If we use $\langle \rangle$ to denote the time average, and take the time average of the field power given by Eq. 14, we obtain

$$\langle \hat{\mathbf{Q}}_p \rangle = \mathbf{L}^+ \langle \mathbf{B}_p \rangle (\mathbf{L}^+)^T. \quad (15)$$

Note that, the lead field matrix \mathbf{L} is time invariant, and so is its MNLS matrix \mathbf{L}^+ , provided that the measures made at different times are made at the same positions. This is the basis for the extended MNLS inverse.

It is important to note that the concept of direction of current flow is totally meaningless when dealing with field power related to such phenomena. These differ from evoked responses and similar time-evoked events where direction of underlying current flow is of considerable importance.

Methods and results

Image Representation

An inverse solution for a set of field measurements can be represented in two convenient ways. One is by an array of current dipoles oriented perpendicular to the image surface, each dipole placed at the center of a cell of area a^2 . The image is thus represented by the distribution

of strengths of the dipoles, each representing the current dipole moment per cell (as shown in Fig. 2b). Another representation is the pattern of isocontours on the image surface that describe the dipole moment density (as shown in Fig. 2c). Both of these are sometimes referred to as the "current image" obtained from the data.

An inverse solution for a set of time-averaged field power measurements can be represented in analogous ways. Instead of an array of current dipoles across the image surface whose moments are specified, we use an array whose time-averaged square moments are specified (as shown in Fig. 6b). Arrows directed toward the viewer indicate positive strength for the inverse solution. Also, the image can be specified by the pattern of isocontours that describe the mean square moment density. Both of these can be referred to as the "current power image".

Simulations

The results of this theoretical work are in the form of simulations in which surfaces representing the cerebral cortex (or any other thin layer of spontaneously active neural tissue within the brain) are populated by a large number of perpendicular primary current elements (dipoles) of random orientation and magnitudes. Subsets of these elements are either incremented or decremented in magnitude, and the net fields of all of the elements are summed at the observation surface (Fig. 1). In the simulation, the current dipole moments populating the source surface are sampled from a uniform distribution, and a new random seed is applied to the random number generator prior to the selection of any array. This assures an ever-changing field pattern at the observation surface. The field at each detector is squared to obtain field power (Eq. 12). One hundred such plots representing different time series are averaged together to form the average power plot. Then the extended MNLS method is applied to deduce the image of the source. This image is compared with the configuration of the original source to determine whether the inverse solution is a reasonable estimate of the actual source which, in this case, is either the incremented or decremented region of incoherent activity.

In the various simulations carried out here, the background activity is spread over the entire source surface (the L-shaped wall of Fig. 1). Each wall of the surface is assumed to be 5 cm x 5 cm. The randomized magnitudes and directions of current flow (to simulate background "noise"), are given values that range from -1 to +1. It is important to note that there is one major difference between the walls of our source model and the actual cortex. The contours of the latter are rounded and not sharply terminated. Rounded contours of the actual cortex insure a gradual rotation of its macrocolumns, with those in a sulcus being largely tangential in orientation with respect to the surface, and those approaching a gyrus tending to become more nearly radial in orientation. Since the latter produce much weaker fields at the surface than do the tangential current elements within the wall of a sulcus, there is a graduated fall-off of the contributions of elements nearer the skull. To simulate this in our model we allow a smooth attenuation of the magnitudes of the still randomly selected dipoles beginning about 0.5 cm away from the top and side edges of the L-shaped wall and reaching zeros at the edge.

As indicated above, using different initial random seeds, 100 samples of source configurations were generated. The bottom of Fig. 4 is one of the samples. Field values are computed for each sensor on the 12 cm x 12 cm observation plane, which is 1 cm above the top edge of the source surface. In this simulation the sensors are spaced about 1 cm apart. As indicated, the 100 plots of field power thus generated are averaged. This is illustrated by the 3-D power plot in Fig. 4a. It is of some interest to compare this plot with one of those depicted in Kaufman et al. (1991a) shown here as Fig. 5, where the underlying cortex was simulated by a cross-shaped

arrangement of sulci. There was clearly a four-lobed power pattern which was topologically related to the shape of the underlying structure. In this case the average power pattern resembles the shape of the underlying L-shaped structure - once again demonstrating the dependency of average field power on structure. It is worth noting in passing that this confirms our earlier conclusion that the actual geometry of the cortex must be explicitly taken into account if one is to understand scalp-detected phenomena, whether they be potentials or fields. In any event, in this case the average field power plot reveals the existence of the underlying L-shaped source surface when the incoherent background activity is uniform on average over time. As we shall see below, departures from uniformity also affect the shape of the pattern.

Incremented Incoherent Activity

As a first test of the method, on average, the current dipole moment (amplitude) of a small circular region of radius 0.6 cm on one wall is enhanced by a factor of 10 as compared with the otherwise uniformly distributed activity of its surroundings, which is as described above. Fig. 6a shows one sample of 100 such source distributions. Note that the arrows signify current elements where the directions of current flow are randomly related to each other, unlike the sources of evoked responses. We first computed the average field power distribution at the sensors on the observation surface and the correlations among different sensors (Eq. 12). Then, in a one-step process, we computed the extended MNLS inverse over the entire image surface. According to Eq. 15, if the time average of field power is used, rather than field, the resulting inverse solution gives the time-averaged current power image.

Since the extended MNLS approach guarantees that the result is the best (in the sense of the least-square residual error between the measurements and the estimated field values) an iterative search process in which residual errors are compared at each step to find a minimum is unnecessary (as in a typical non-linear least-squares method)[†]. Fig. 6b. is a perspective view of the current power image derived from the extended MNLS inverse. The power at each location is indicated by the length of an arrow, whose direction is arbitrarily chosen to be toward the reader. Heads are included to better illustrate their length. Fig. 6c is an isocontour plot representing the same inverse. Note that the contours are centered on a point at the coordinates $(x, z) = (2, -3)$ cm, which was the exact center of the original incremented current distribution of the source surface.

We next consider the case of two incremented circular regions, located on the source surface at the coordinates $(x, z) = (2, -3)$ cm, and $(y, z) = (2, -3)$ cm. While the current elements vary at random over time inside as well as outside the incremented regions, the ratio of averaged amplitude of the two incremented regions relative to their surroundings is 10:1. One of the 100 source samples is shown in Fig. 7b. Fig. 7a is the plot of the field power averaged over all 100 samples. It is of some interest to compare this plot with the L-shaped plot of Fig. 4, which is based on an average of 100 samples of randomly selected current elements where there is no net increment or decrement of any region. When two regions are, on average, more "active" than their surrounding, the L-shaped plot is transformed into one with three lobes, thus illustrating how both the geometry of the source surface and the statistics of its activity affect the distribution of field power at the observation plane. Fig. 7c is the inverse solution computed using the extended MNLS.

[†] However, technical problems arise in practice because, numerically, the lead field matrix is often ill-conditioned, that is to say, small errors in the data will lead to large errors in the solutions.

To illustrate the potential power of this method in delineating the shape of a region of differential incoherent activity, a crescent shaped portion of the source surface similar to that of Fig. 3 contains current elements which, on average, are 10 times stronger than those of the surrounding region of the surface. The top of the enhanced region is at $z = -2.5$ cm and the bottom at $z = -4.5$ cm. Fig. 8a shows two of the 100 samples of the random distributions used in computing the average field power at the observation plane. As before, each of these samples was created by applying different initial seeds to the random number generator. However, the current power image (Fig. 8b) provides a reasonable rendition of the crescent shape. This is made clearer in Fig. 8c by the isocontours of the current power image.

While the enhanced region in the preceding example was, on average, always 10 times that of its surroundings, we also experimented with different ratios. Thus, the three plots in Fig. 9 are current power images in which a circular region 0.6 cm in radius is incremented, but the amplitude enhancement is 5 times (Fig. 9a), 4 times (9b), and 3 times (9c) that of the surroundings. Note, these are all drawn with the same scale, while the 10:1 plot of Fig. 6 is shown with a different scale.

If the circular region is moved downward away from the observation plane by 1.5 cm, the center of the region is now at $z = -4.5$ cm and the magnetic field at the observation plane is greatly weakened. In this case, if the incremented region's strength is less than 5 times that of its surroundings, the incremented region is no longer discriminable in the current power image (Fig. 10). The gradual deterioration in the ability to visualize current power images for incremented regions of a particular size is illustrated in Fig. 10 where the ratios, from top to bottom are 7:1, 6:1, 5:1, respectively. Note that Figs. 9 and 10 were plotted at the same scale. These examples are meant merely to illustrate the fact that inverse solutions may not be successful for regions with levels of differential activity that are too small considering the distance of the detection coil from the source area, or when the area is smaller than some minimum size. The degree to which these interacting parameters will affect the application of the extended MNLS method in real situations is clearly an empirical question.

Because of these potential problems we devised a variation on the basic method described thus far. This variation significantly enhances the ability to visualize "target" areas in current power images when signal-to-noise ratio, area, and distance were not favorable, as in the foregoing examples. In this variation we first evaluate the field power associated with the overall background when the target area is absent (as shown in Fig. 4). An example of this in a real situation would be to plot the power of the component of the field normal to the surface of the scalp of a resting human subject. We then find the extended MNLS solution for the current power image to define a *baseline* image of the background. Then the localized area is imposed on this background as, for example, when the subject becomes engaged in a mental task of some kind, thus altering the level of activity of one or more regions of the cortex. We then find the extended MNLS for the current power image with this target area or areas present. Subtracting the image of the baseline distribution from the image containing the target area gives a current power image difference plot, such as those illustrated in Fig. 11. The directions of the arrows in the image surface reflect the sign of the difference between the suppressed and baseline activity. Positive values are indicated by arrows directed toward the reader. Note that the target in Fig. 11a is one that is difficult to visualize in Fig. 10c. Note also that the noise in the surroundings is much improved, even though accentuated by the greater magnification of a factor of 2.5, the scale used to plot the image strength in Fig. 11. It is very important to emphasize that different initial seeds were used for simulating the baseline activity and for simulating the activity containing the

targets. This indicates that a similar approach may be used in real situations where neuronal activity is simply not going to have a constant distribution over long periods of time, despite the long-term stability of average MEG and EEG power.

Decrementing Incoherent Activity

Thus far we have dealt only with target areas whose activity has a somewhat higher level than that of the surroundings. However, this is a distinction based on an assumed convention. It is equally logical to consider these patterns as those in which the so-called surroundings is decremented as compared to the smaller target areas. So, if very large areas of cortex should exhibit alpha suppression, for example, then the methods we have used would be able to delineate those areas. Moreover, we may also consider the reverse situation, in which the suppressed target region is small relative to the surroundings, since this may have important applications. For example, relatively small cortical regions affected by ischemia may exhibit less overall activity than their surroundings. Also, as implied in the work of Kaufman et al. (1991b), relatively circumscribed areas may exhibit suppression as subjects engage in scanning short-term memory for tonal stimuli. It would be of considerable value to locate and delineate such areas.

One of the difficulties associated with detecting small decremented target areas is that the extracranial field is dominated by the background activity which originates in a relatively much larger area of cortex. This could result in an extremely disadvantageous signal-to-noise ratio which may make it difficult to detect any change simply by examining at the inverse plots of current power image. While in actual suppression data studied by Kaufman et al. (1990; 1991a) the empirically observed suppression is very pronounced and may often be seen in single trials, this problem could arise in the case of subtler effects. To deal with this in our simulation, we begin with a circular target area having a radius of 1 cm. On average, the strength of activity within this target is 1 : 10 that of its surroundings. A single sample of a source distribution is shown in Fig. 12a. In our computations, 100 such samples with different initial seeds were used in the simulation. The current power image when the source was decremented was subtracted from the current power image of the baseline. Fig. 12b and c show these power image difference plots. Note again that different initial seeds were used for producing the inverse power with a decremented region and the baseline inverse. This produces patches of activity in the image that differ from one computation to another.

The above procedures were employed to detect a crescent shaped region of suppressed activity (Fig. 13a) with the extended MNLS inverse. Under the conditions of this simulation, where the target pattern extends over a wide range in depth (with the top at $z = -2.5$ cm and the bottom at $z = -4.5$ cm) the lower part of the current power image is buried in the noise (Fig. 13b). Of course, where the surrounding activity is more stable over time, it is possible to obtain an image of higher quality. For example, the plot in Fig. 13c is one where the baseline of uniform activity and the distributions containing the target shapes were created by applying the same initial seed to the random number generator. The resulting power image difference plot shows a well-defined crescent, because there is an "exact" cancellation of the background activity. The poorer image of Fig. 13b results from no correlation of baseline and target, while the higher quality image results from perfect correlation. Empirically, the result will probably be intermediate between these two solutions. In particular, the length of time over which recording are made will have a substantial influence on the quality of the subtraction technique.

Conclusions

The main conclusion of this paper is that it is possible to estimate mathematically unique inverse solutions to recover the location, shape and magnitude of a differentially active region of cortex, even when the activity is incoherent. This, together with earlier work, makes it possible to uniquely define both coherent and incoherent activity using maps of the extracranial field and its power together with MRI-based reconstructions of the individual subject's or patient's brain.

Assuming that the differential levels of activity of the different regions of the brain are significantly related to sensory-perceptual and cognitive processes, and all the evidence accumulated thus far suggests that they are, then this makes it possible to envision a new kind of brain mapping. We propose to dub this mapping *dynamic functional imaging* because it will reveal changes in activity in different regions with a temporal resolution measured in fractions of a second. PET blood flow methods also provide functional images, but the time resolution is no better than about 40 s, and data must be averaged over subjects. MRI techniques show promise of better temporal resolution, but this possibility remains to be demonstrated.

While we have restricted our discussion to the brain's magnetic field, it may well become possible to develop similar methods in which electroencephalographic data are used instead. In principle there is no reason why this cannot be accomplished, provided that an accurate picture of the electrical properties, e.g. conductivities, of the individual patient's skull, brain, and other tissues that affect the flow of volume currents are taken into account when computing the solution for the inverse problem.

Finally, although we have emphasized the human cerebral cortex throughout, it should be borne in mind that there is no reason why other subcortical nuclei with electrically active laminar structures cannot be treated in the same manner. Here the only real limitations may be the quality of signal-to-noise, as this will be degraded for very deep source surfaces.

It is obvious that the next step will be to implement the extended MNLS procedures using actual subjects and images of their brains. Also, clinical trials should be attempted where there are confirmed abnormal metabolic levels for comparison with PET procedures, and where there is abnormal field power in some bandwidths associated with epileptoid phenomena.

Reference

- Barnett, S. *Matrices, Methods and Applications*. Clarendon Press, Oxford, 1990.
- Ben-Israel, A., Greville, T.N.E. *Generalized Inverses Theory and Applications*. John Wiley & Sons, New York, 1974.
- Ciarlet, P.G. *Introduction to Numerical Linear Algebra and Optimisation*. Cambridge Univ. Press, Cambridge, 1991.
- Clarke, C.J.S., Ioannides, A.A., and Bolton, J.P.R. Localised and distributed Source Solutions for the Biomagnetic Inverse Problem I. *Advances in Biomagnetism*, S.J. Williamson, M. Hoke, G. Stoinik, and M. Kotani, eds., New York: Plenum, 1989: 587-590.

- Crowley, C.W., Greenblatt, R.E., Khalil, I. Minimum Norm Estimation of Current Distributions in Realistic Geometries. *Advances in Biomagnetism*, S.J. Williamson, M. Hoke, G. Stroink, and M. Kotani, eds., New York, Plenum, 1989: 607-610.
- Cuffin, B.N., and Cohen, D. Magnetic Fields of a Dipole in Special Volume Conductor Shapes. *IEEE Trans. Biomed. Eng.*, 1977, BME-24: 372-381.
- Cycowicz, Y., Kaufman, L., Williamson, S.J., Glanzer, M. Differences in Brain Activity Doing Imaging and Verbal Tasks. 1992: in preparation.
- Dallas, W. J., Fourier Space Solution to the Magnetostatic Imaging Problem. *Applied Optics*, 1985, 24: 4543-4546.
- George, J.S., Lewis, P.S., Ranken, D.M., Kaplan, L. and Wood, C.C. Anatomical Constraints for Neuromagnetic Source Models. 8th Intl. Conf. Biomag. Abs., 1991: 83.
- Graumann, R. The Reconstruction of Current Densities. *Biomagnetic Localization and 3D Modeling*, J. Nenonen, H.-M. Rajala, and T. Katila, eds., Report TKK-F-A689, Helsinki University of Technology, Otaniemi, 1991: 172-178.
- Greenblat, R.E. Spatiotemporal Likelihood Estimator Solutions to the Bioelectromagnetic Inverse Problem. 8th Intl. Conf. Biomag. Abs., 1991: 329.
- Hämäläinen, M.S. and Ilmoniemi, R.J. Interpreting Measured Magnetic Fields of The Brain: Estimates of Current Distributions. Report TKK-F-A559, Helsinki University of Technology, 1984.
- Hämäläinen, M.S. and Ilmoniemi, R.J. Interpreting Magnetic Fields of the Brain: Minimum-Norm Estimates. *IEEE Trans. Biomed. Eng.*, 1992: in press.
- Ioannides, A.A., and Bolton, J.P.R., Hasson, R., Clarke, C.J.S. Localised and distributed Source Solutions for the Biomagnetic Inverse Problem II. *Advances in Biomagnetism*, S.J. Williamson, M. Hoke, G. Stoink, and M. Kotani, eds., New York, Plenum, 1989: 591-594.
- Ioannides, A.A., and Bolton, J.P.R., Clarke, C.J.S. Continuous Probabilistic Solutions to the Biomagnetic Inverse Problem. *Inverse Problems*, 1990, 6: 1-20.
- Kaufman, L., Kaufman, J.H., and Wang, J.-Z. On Cortical Folds and Neuromagnetic Fields. *Electroenceph. clin. Neurophysiol.*, 1991, 79: 211-226.
- Kaufman, L., Curtis, S., Wang, J.-Z., and Williamson, S.J. Changes in Cortical Activity When Subjects Scan Memory for Tones. *Electroenceph. clin. Neurophysiol.*, 1992: in press.
- Kaufman, L., Schwartz, B., Salustri, C., and Williamson, S.J. Modulation of Spontaneous Brain Activity During Mental Imagery. *Cogn. Neurosci.*, 1990, 2: 124-132.
- Kullmann, W.H., Dallas, W.J. Fourier Imageing of Electrical Currents in the Human Brain from

- Their Magnetic Fields. IEEE Trans. Bio. Eng., 1987, 11, BME-34: 837-842.
- Kullmann, W.H., Jandt, K.D., Rehm, K., Schlitt, H.A., Dallas, W.J., Smith, W.E. A Linear Estimation Approach to Biomagnetic Imageing. Advances in Biomagnetism, S.J. Williamson, M. Hoke, G. Stroink, and M. Kotani, eds. New York, Plenum, 1989: 571-574.
- Kullmann, W.H. Can Volume Conductor Modeling Improve Biomagnetic Distributed Source Imaging? Biomagnetic Localization and 3D Modeling. J. Nenonen, H.-M. Rajala, and T. Katila, eds., Report TKK-F-A689, Helsinki Univ. of Technology, Otaniemi, 1991: 137-153.
- Okada, Y.C. and Huang, J.C. Current-Density Imaging as Method of Visualizing Neuronal activities of the Brain, Soc. Neurosci. Abs., 1990, 16: 1241.
- Okada, Y.C., Huang, J.C., Xu, Chibing. A Hierarchical Minimum Norm Estimation Method for Reconstructing Current Densities in the Brain from Remotely Measured Magnetic Fields. 8th Intl. Conf. Biomag. Abs., 1991: 152.
- Penrose, R. A Generalized Inverse for Matrices. Proc. Cambridge Philos. Soc., 1955, 51: 406-413.
- Pfurtscheller, G. and Aranabar, A. Event-related cortical desynchronization detected by power measurements of scalp EEG. Electroencephalogr. Clin. Neurophysiol., 1977, 42: 817-826.
- Pfurtscheller, G. Mapping of event related desynchronization and type of derivation. Electroencephalogr. Clin. Neurophysiol., 70, 1988: 190-193.
- Pfurtscheller, G., Steffan, J., and Maresch, H. ERD-mapping and functional topography - temporal and spatial aspects. Functional Brain Imaging. G. Pfurtscheller and F.H. Lopez da Silva, eds., Hans Huber, Toronto, 1988: 117-130.
- Plonsey, R. Capability and Limitations of Electrocardiography and Magnetocardiography. IEEE Trans. Biomed. Eng., 1972, BME-19: 239.
- Press, W.H., Flannery, B.P., Teukolsky, S.A., Vetterling, W.T. Numerical Recipes, the Art of Scientific Computing. Cambridge Univ. Press, Cambridge, 1986.
- Regan, D.M. Human Brain Electrophysiology: Evoked Potentials and Evoked Magnetic Fields in Science and Medicine. Elsevier Science Publishing Co., Inc., 1989.
- Robinson, E. S. Current Source Image Estimation by Spatially Filtered MEG. 8th Intl. Conf. Biomag. Abs., 1991: 337.
- Roth, B.J., Sepulveda, N.G., and Wikswo, J.P. Jr. Using a Magnetometer to Image a Two-dimensional Current Distribution. J. Appl. Phys., 1989, 65: 361-372.
- Singh, M., Doria, D., Henderson, V.W., Huth, G.C., and Beatty, J. Reconstruction of Images from Neuromagnetic Fields. IEEE Trans. Nuclear Sci., 1984, NS-31: 585-589.

- S. High Speed Scanning in Human Memory, *Science*, 1966, 153: 652-654.
- S. Kuc, R. Application of the SVD to Biomagnetic Imaging, 8th Intl. Conf. Biomag. 1991: 421.
- Tan, S., Roth, B.J., and Wikswo, J.P. Jr. The Magnetic Field of Cortical Current Sources: the Application of a Spatial Filtering Model to the Forward and Inverse Problems. *Electroenceph. clin. Neurophysiol.*, 1990, 76: 73-85.
- Wang, J.-Z., Williamson, S.J. and Kaufman, L. Magnetic Source Images Determined by a Lead-Field Analysis: The Unique Minimum-Norm Least-Squares Estimation. *IEEE Trans. Biomed. Eng.*, 1992: in press.
- Williamson, S.J. and Kaufman, L. Magnetic Fields of the Cerebral Cortex. *Biomagnetism*, S.N. Emé, H.D. Hahlbohm and H. Lübbig, eds., Walter de Gruyter & Co., Berlin New York, 1981: 353-401.
- Williamson, S.J. and Kaufman, L. Analysis of Neuromagnetic Signals. A.S. Gevins and A. Remond, eds., *Handbook of Electroenceph. clin. Neurophysiol.*, Vol.1. Methods of Analysis of Brain Electrical and Magnetic Signals. Elsevier, Amsterdam, 1987: 405-444.

Figure captions

Figure 1: Model configuration in which the component of the magnetic field B_i normal to the *observation plane* is measured by "point sensors" at the nodes of a grid composed of cells of size s . The center of the observation plane lies at $x=+2$ cm. The *source space* is an L-shaped surface formed by two vertical walls. The top edges of the walls are 1 cm below the observation plane, and the corner joining the walls coincides with the z -axis. The *image surface* coincides with the source surface, and inverse computations are carried out to deduce the source density on a grid of size a .

Figure 2: (a) The field pattern given by a single current dipole of strength $Q = 1$ nA·m normal to the xz -plane of the source surface and located at the $(x, z) = (2, -3)$ cm. (b) The inverse solution found on the image surface. Each current dipole represents the deduced contribution of a cell of area a^2 . (c) The same inverse solution is represented by isocurrent contours, i.e., contours of constant current-dipole moment density. The values are indicated in units of $\mu\text{A}/\text{m}$.

Figure 3: (a) An extended crescent-shaped source of uniform current-dipole density on the source surface with upper edge at $z = -2.5$ cm and lower at -4.5 cm. The inverse solution on the image surface is shown on the right as a distribution of current dipoles and as isocontours for current-dipole moment density. The solution has a similar crescent-shaped outline, but is weakened and somewhat spread at greater depths. (b) The same source, but the current density at the bottom is four times that at the top. In this case a field sampling interval of $s = 0.5$ cm was used, and measurements were made across a $14 \text{ cm} \times 14 \text{ cm}$ observation plane.

Figure 4: (a) Average field power across the observation plane from a random array of dipoles with strengths ranging from -1 to $+1$ computed for 100 such independent random samples, one of which is illustrated in (b). (c) Contour plot of the average field power, whose two extensions lie over the walls of the source space.

Figure 5: Simulation for average field power computed in the same manner as for that of Figure 4, except that the underlying source surface was of a more complicated shape. The cross-like shape shown below is the outline of fissures 4 mm wide separating "cortical" walls about 2 cm long and 2 cm wide, and extending about 3 cm into a model "head". (Kaufman et al., 1991a).

Figure 6: (a) The source surface of Fig. 1 is populated with a large number of current dipoles of randomly selected orientations and strengths, but those within a small (0.6-cm radius) region are, on average, 10 times stronger than those in the surrounding. The current power image distribution (b) and isopower density contours (c) are shown on the image surface. The arrow length in (b) is proportional to the average power at each location.

Figure 7: Similar to Fig. 6, except that two 0.6-cm radius regions, one on each wall of the source surface, has current dipole moments incremented by an average factor of 10. The average power distribution is computed for 100 random arrays of dipole moments. The bottom of the figure shows the current power image distribution determined from the average field power pattern and the known shape of the source surface.

Figure 8: (a) Two of the 100 samples used in computing average field power for a crescent-shaped area of incoherent activity. (b) The inverse solution represented as an rms current-dipole distribution and (c) corresponding rms current-dipole moment isodensity plot.

Figure 9: Image rms power distributions when a region 0.6 cm in radius centered at a depth $z = 3$ cm is incoherently active with dipole moments incremented by a factor of (a) 5, (b) 4, and (c) 3 times the level of the surroundings.

Figure 10: Similar to Fig. 9, except that the sources are at a depth $z = 4.5$ cm and dipole moments are incremented by a factor of (a) 7, (b) 6, and (c) 5 times the level of the surroundings.

Figure 11: Image power-difference plots for the sources of Fig. 10, where the image of the background is subtracted from the image of background plus active circular region, for dipole moments in the active region that are incremented by a factor of (a) 5, (b) 4, and (c) 3 times the level of the surroundings.

Figure 12: (a) Sample of a source distribution with a circular region that is decremented. (b,c) Image power-distributions obtained by subtracting the average of 100 such samples from the baseline inverse of 100 different samples of uniform activity, beginning with different seeds.

Figure 13: (a) Crescent shaped source region of suppressed activity. (b) Image power-distribution difference obtained by subtracting the current power image of 100 samples of (a) from the current power image of 100 samples of uniform activity obtained from different initial seeds. (c) Image power-distribution difference obtained as in (b) but starting from the same initial seeds.

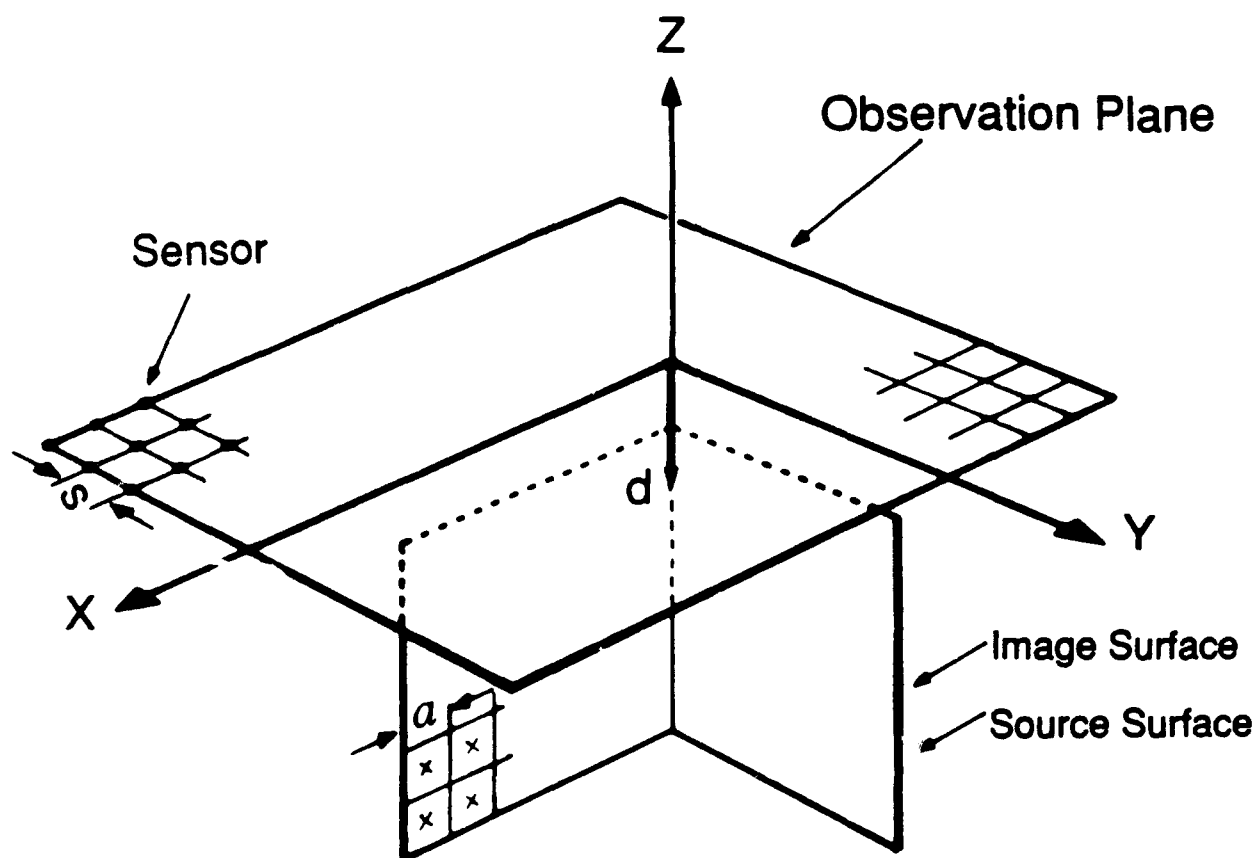


Figure 1

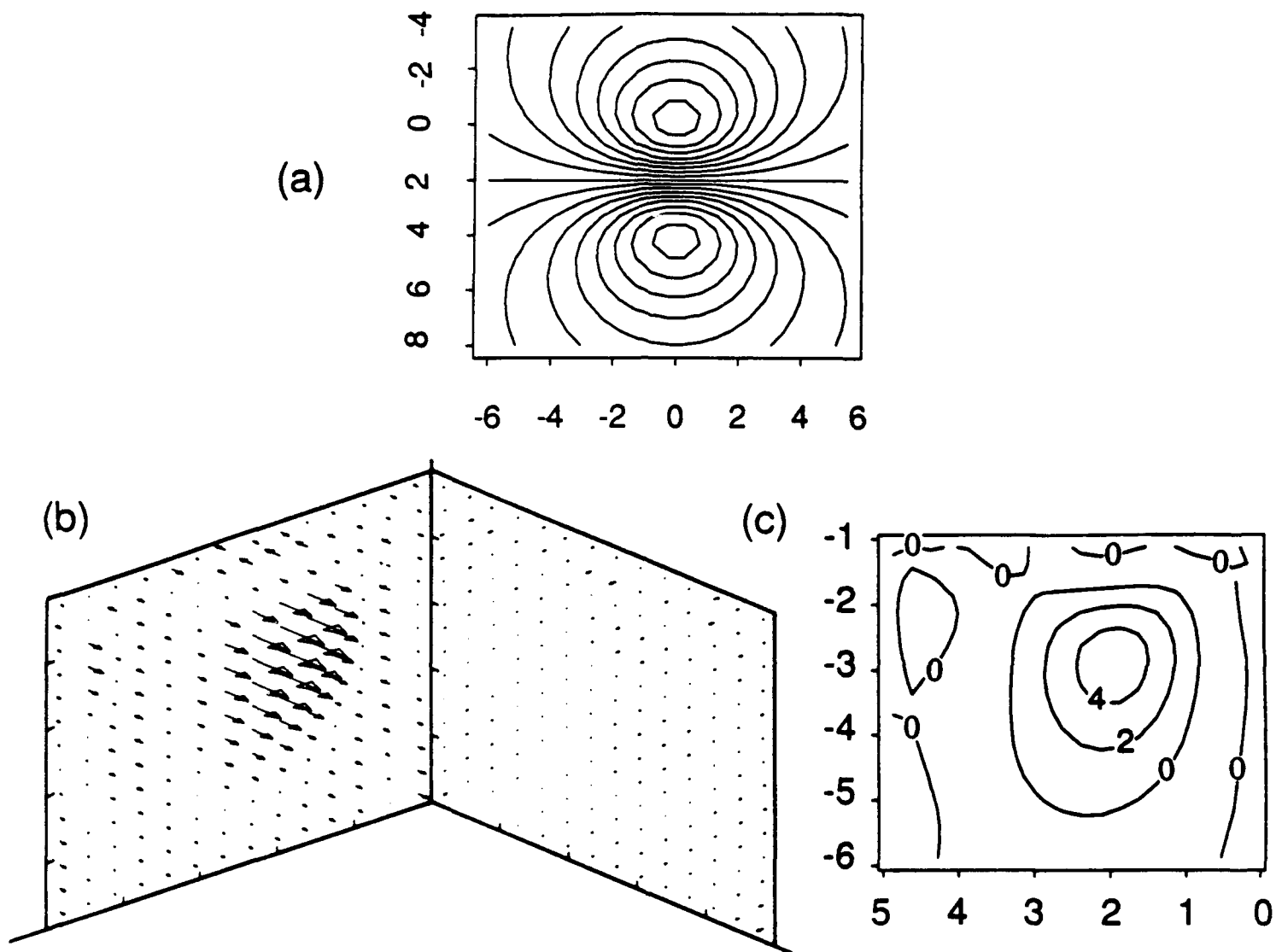


Figure 2

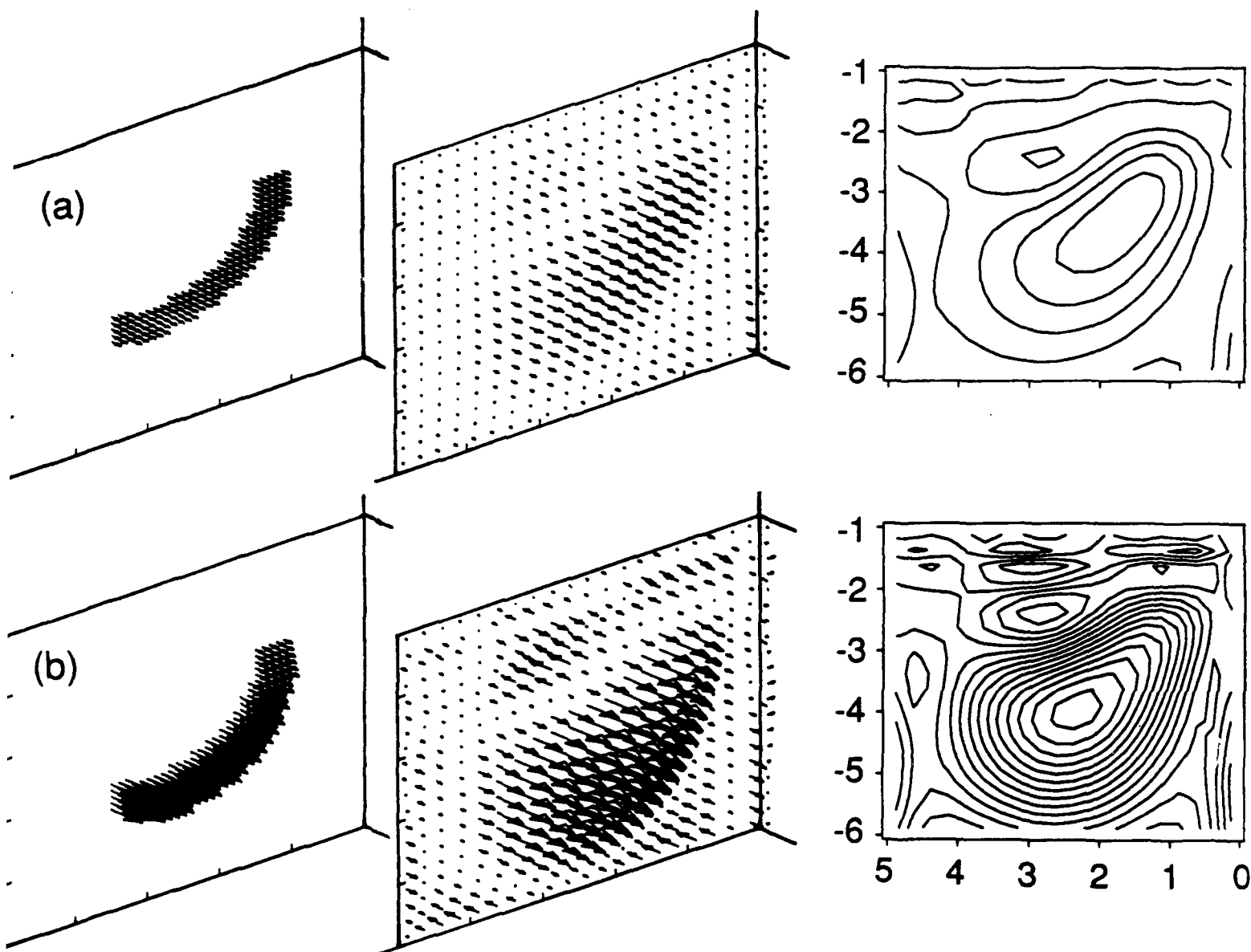
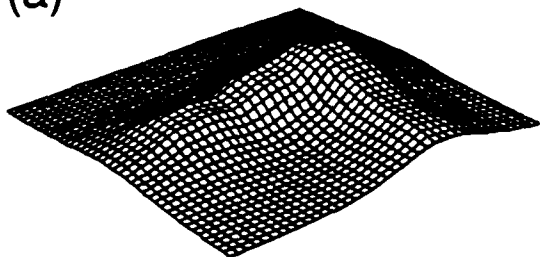
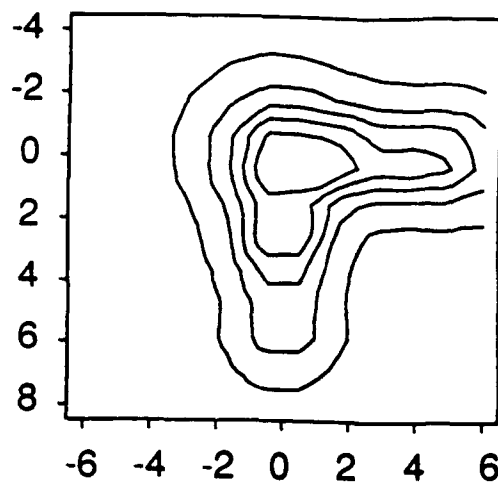


Figure 3

(a)



(b)



(c)

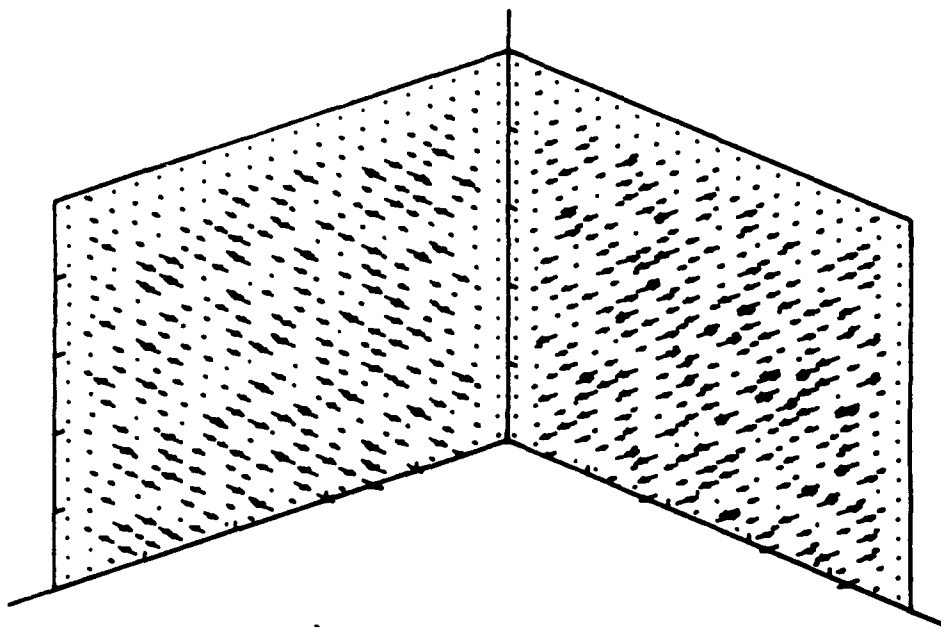


Figure 4

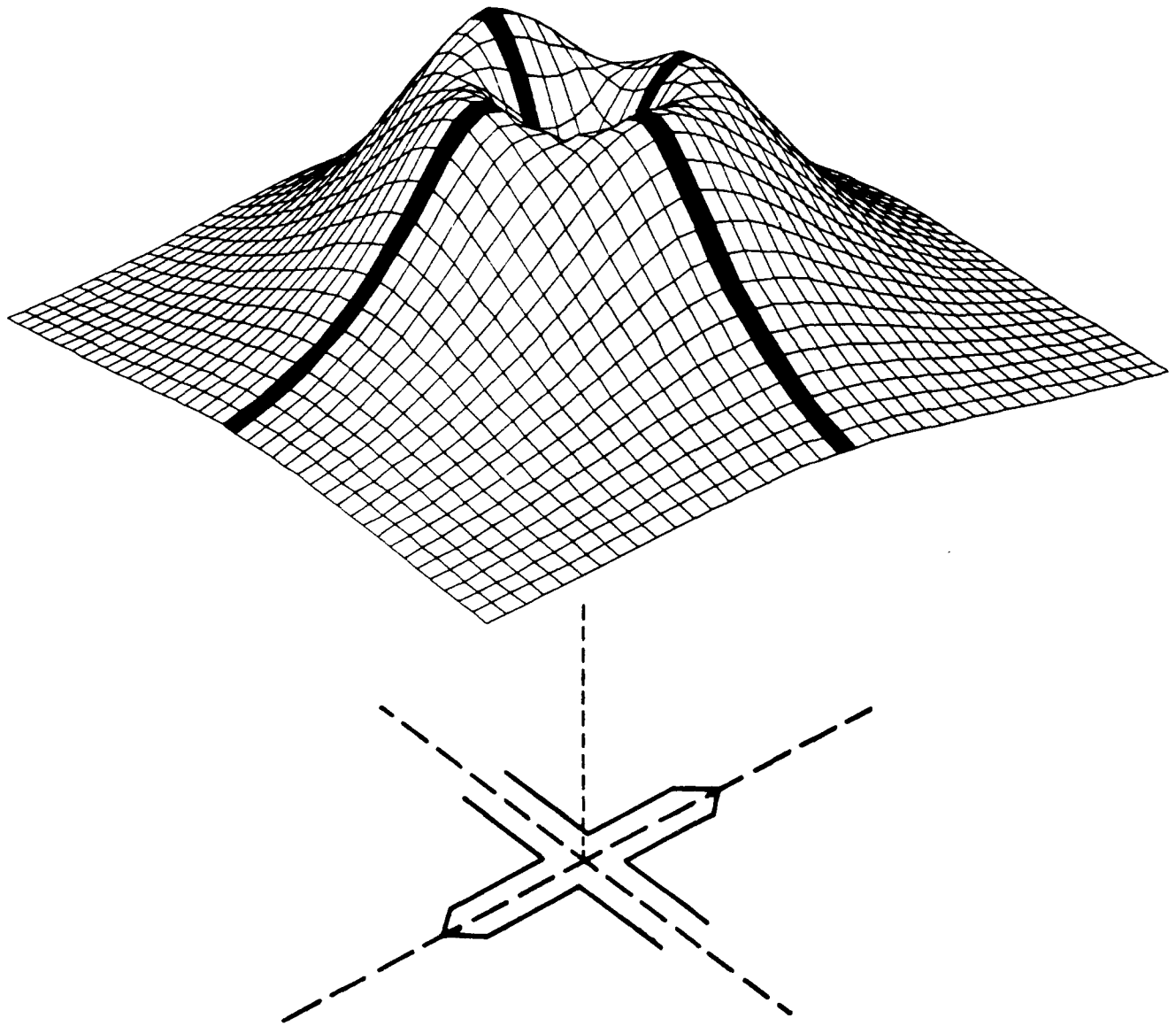


Figure 5

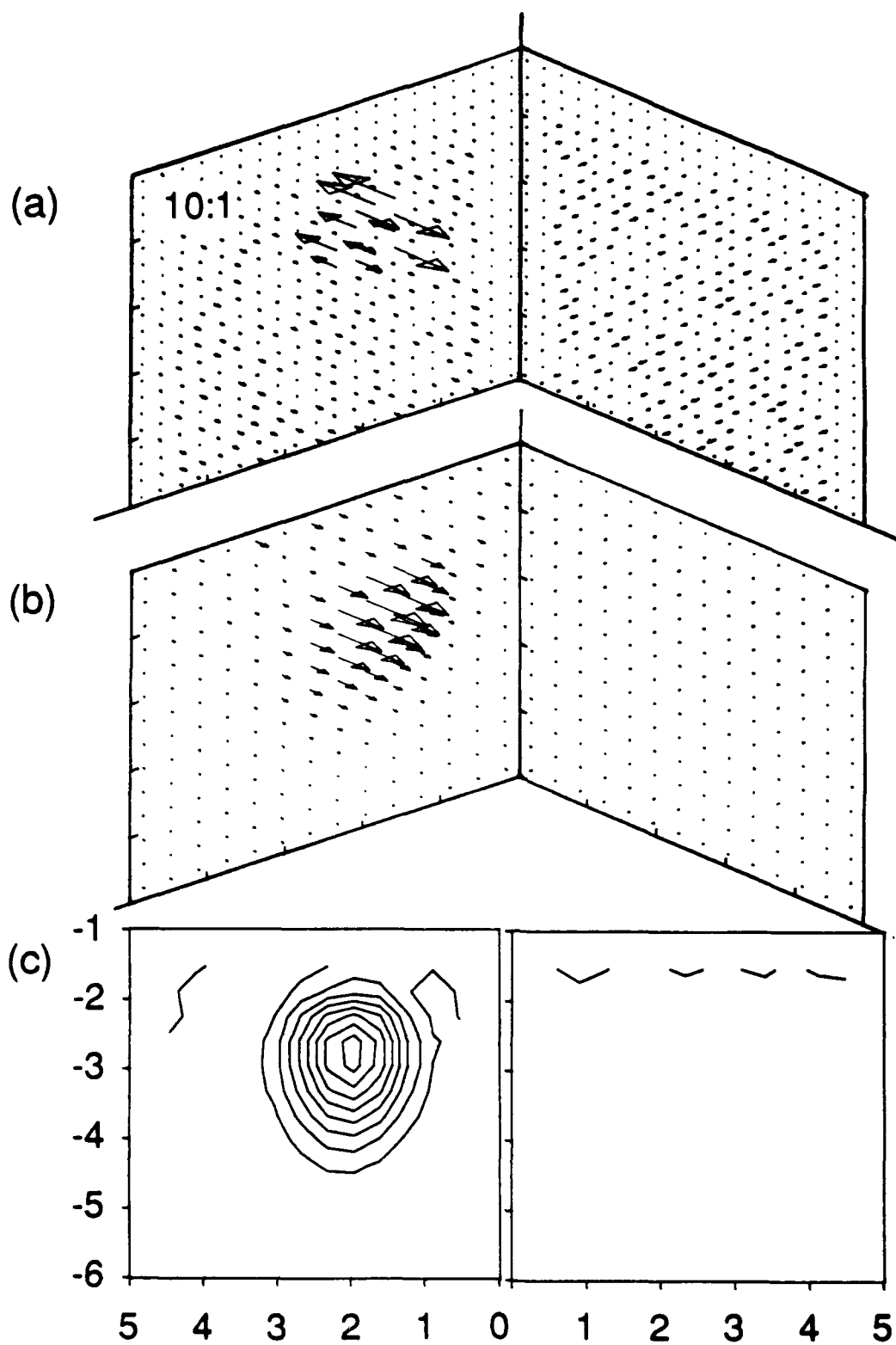
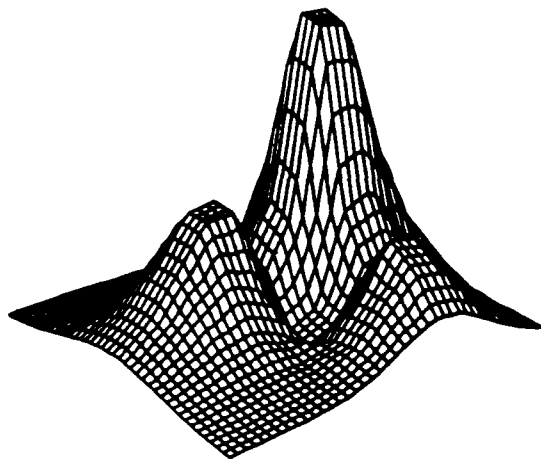
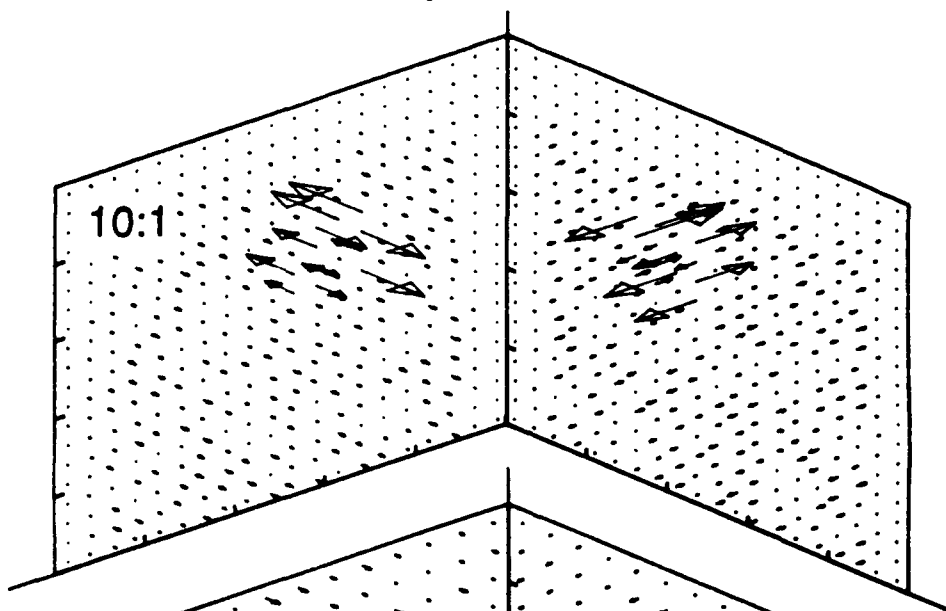


Figure 6

(a)



(b)



(c)

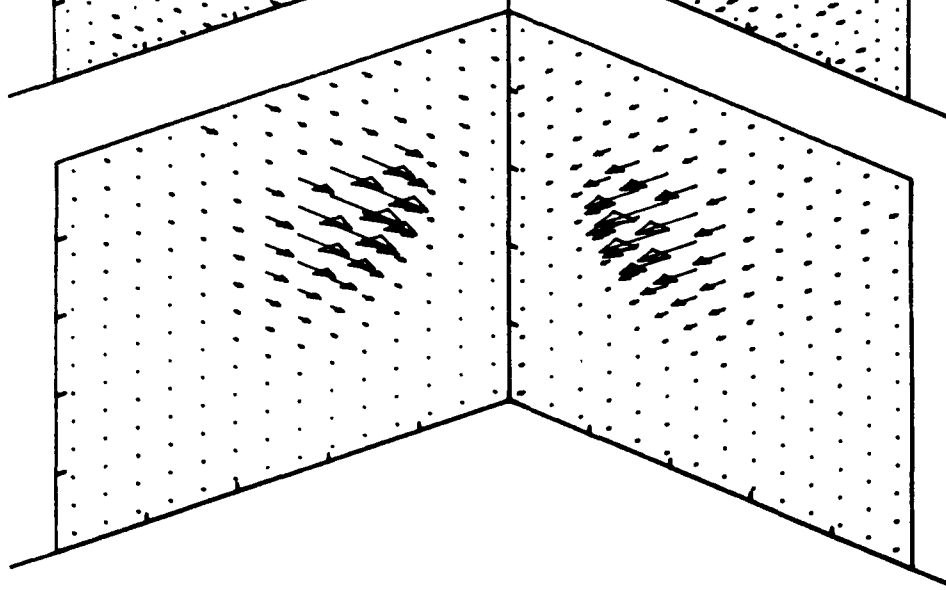


Figure 7

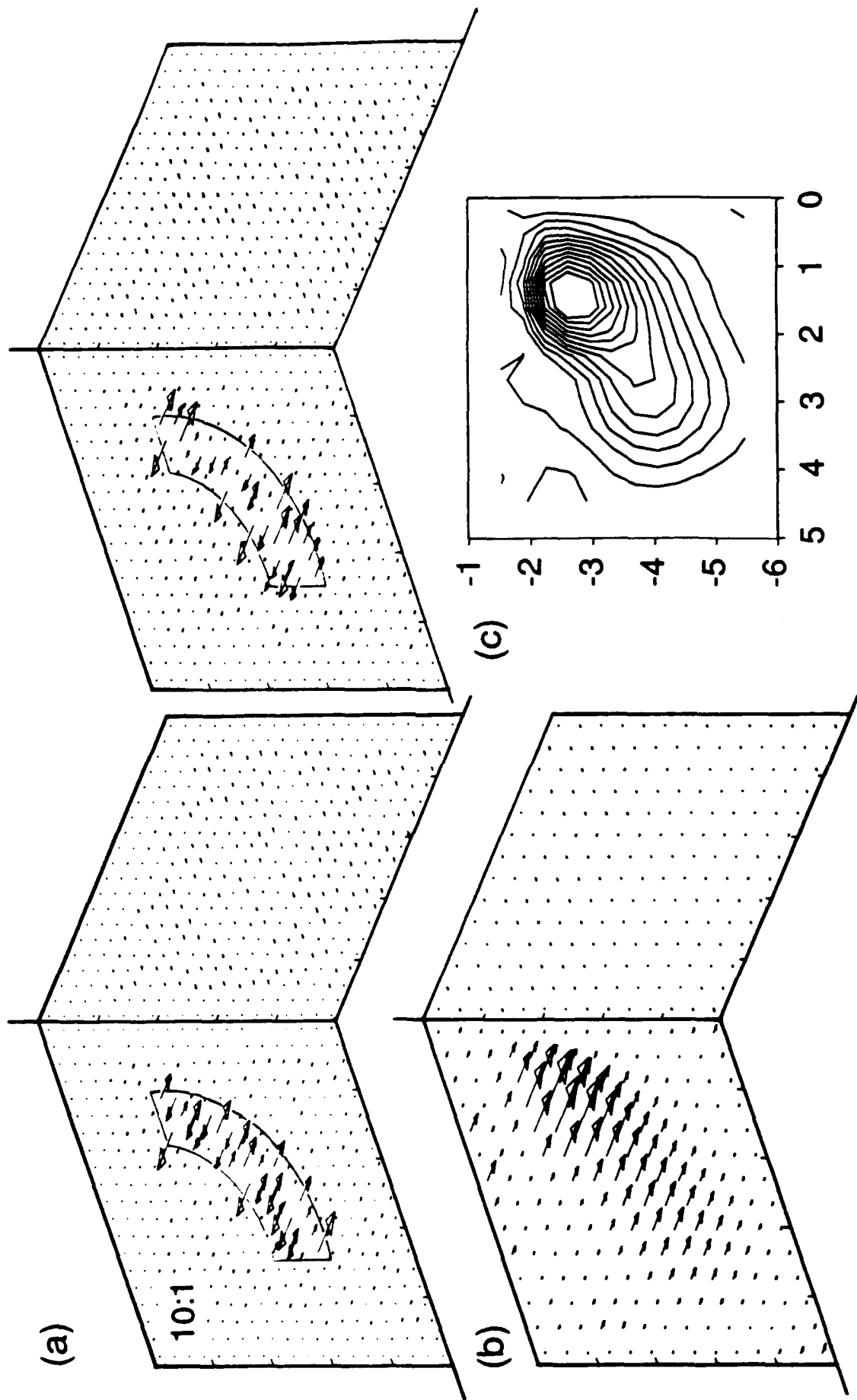


Figure 8

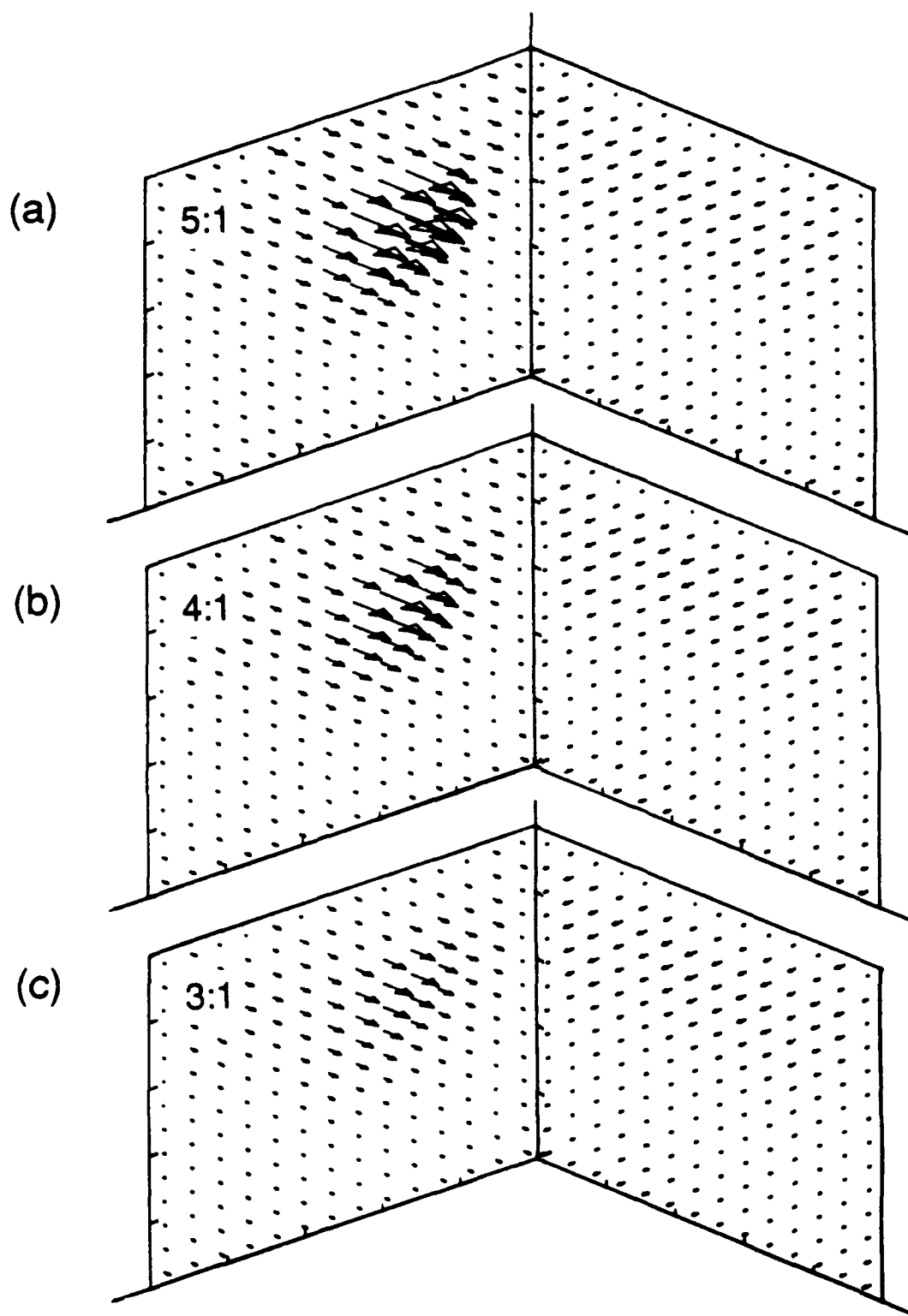


Figure 9

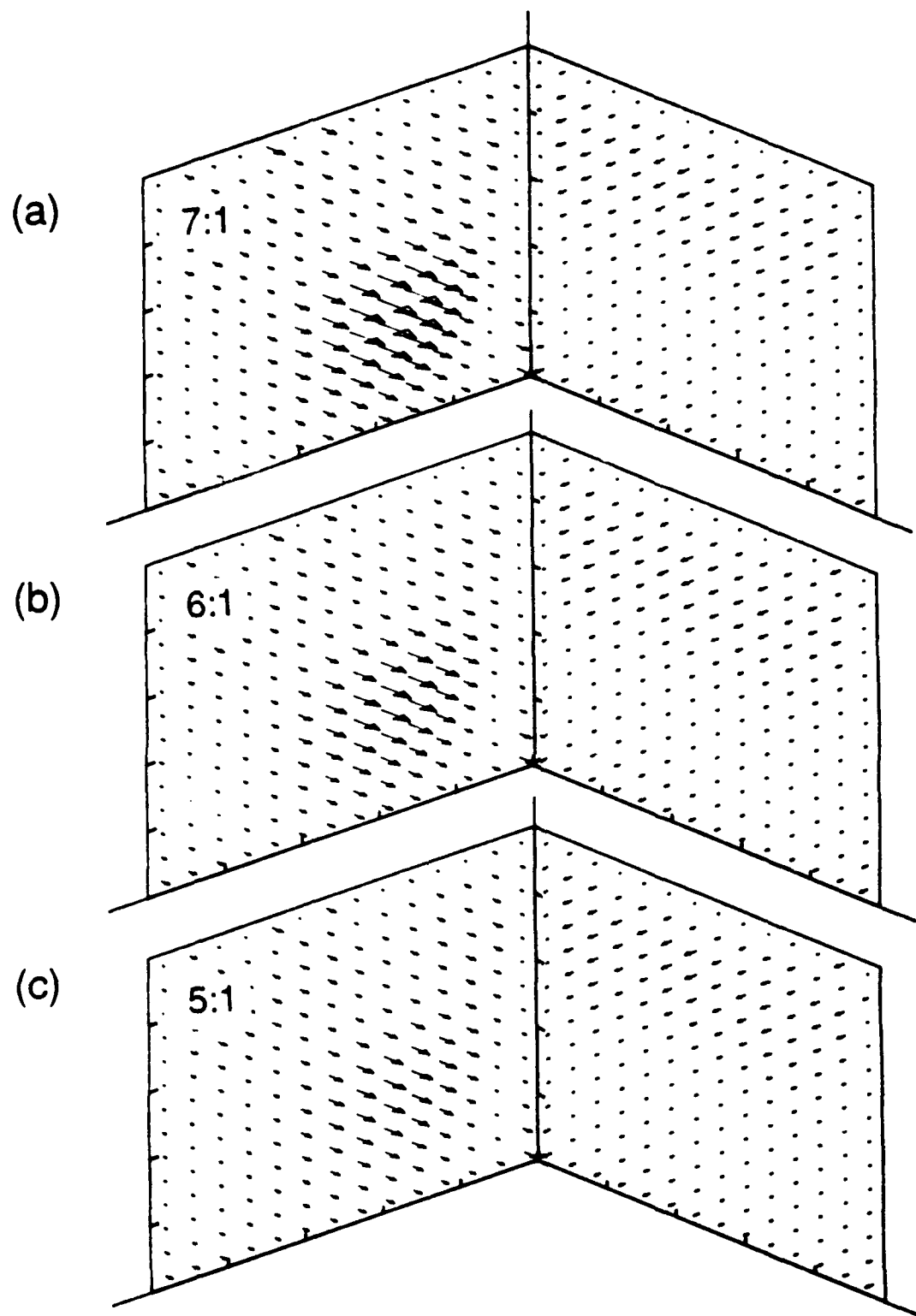


Figure 10

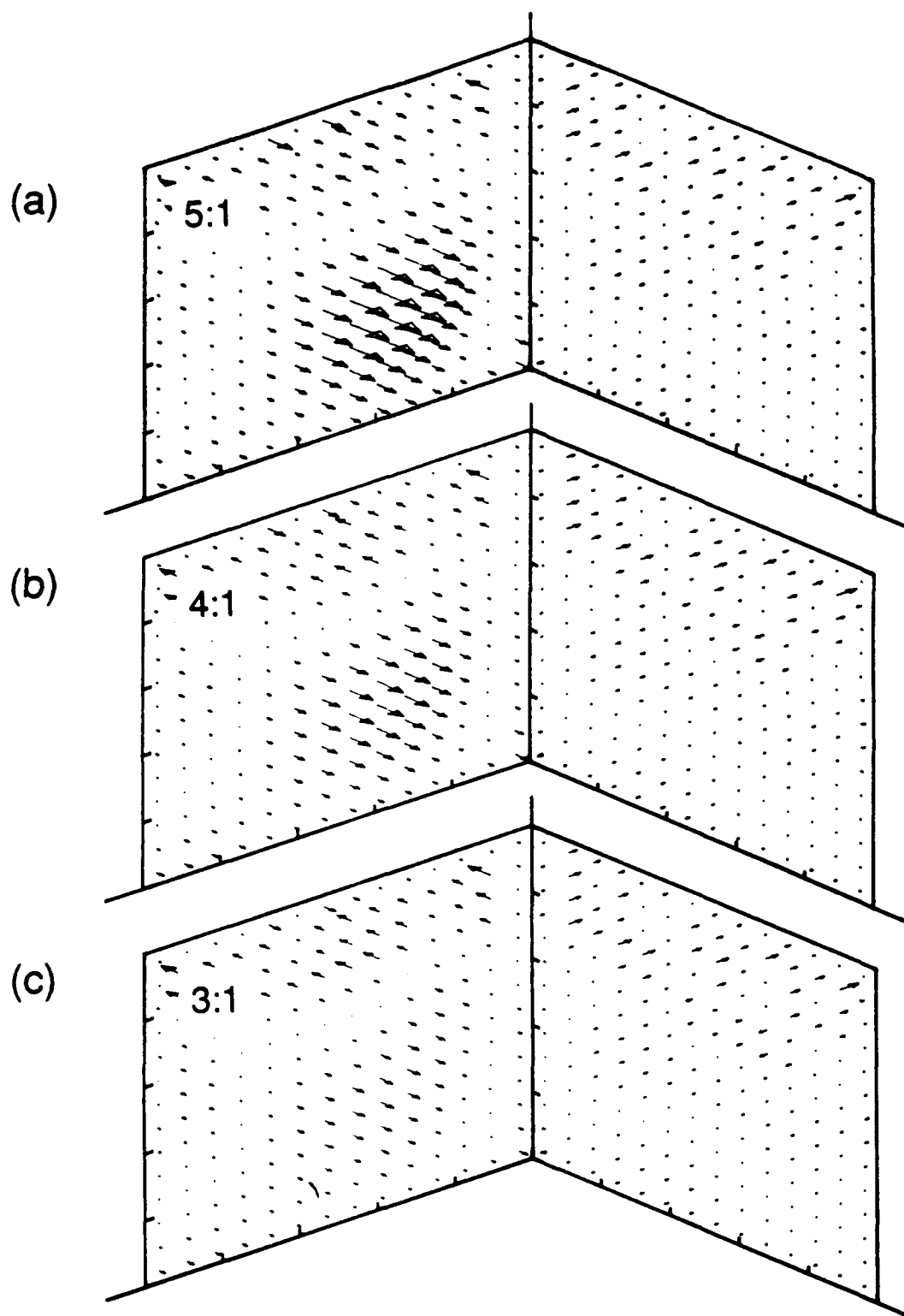


Figure 11

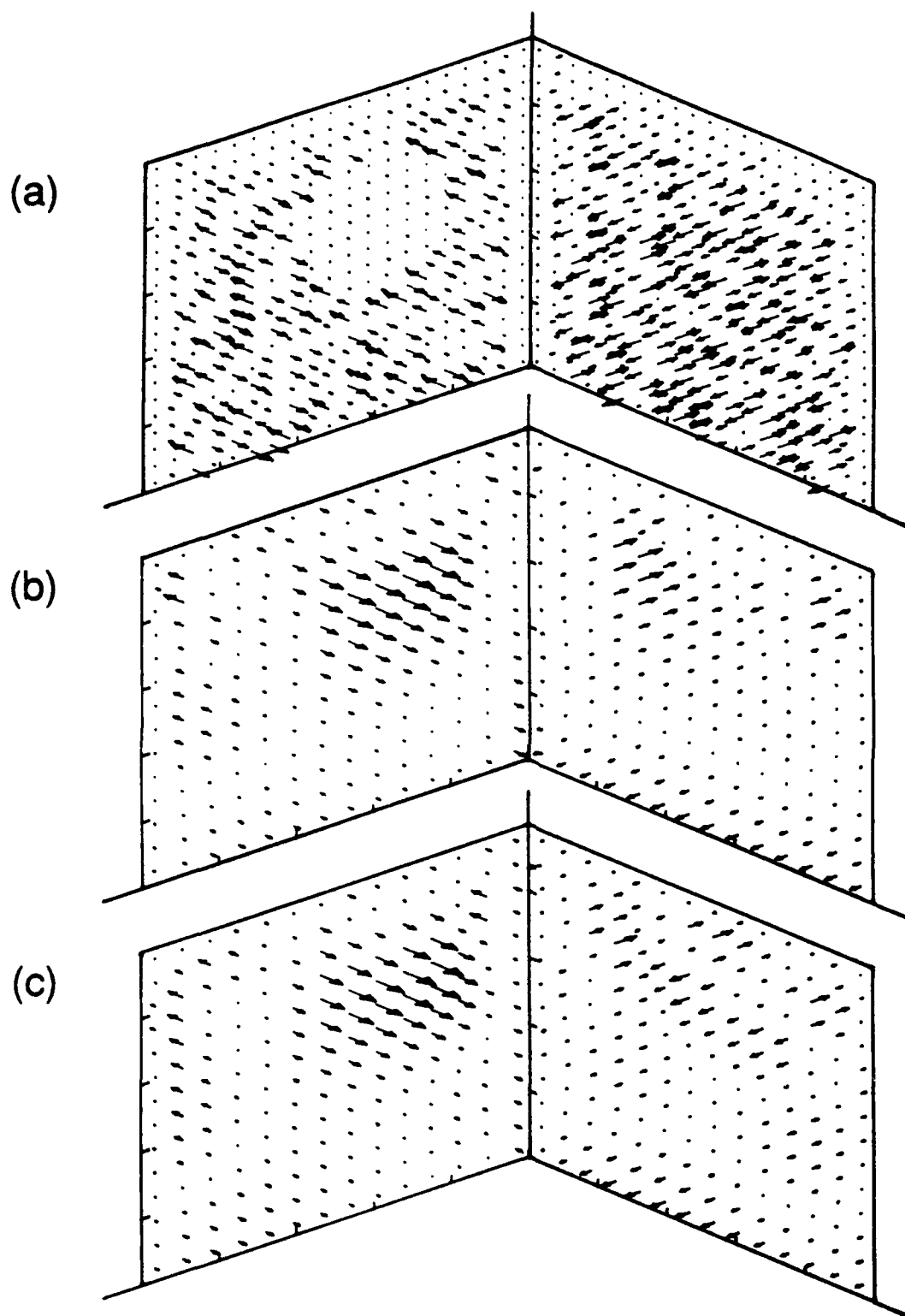


Figure 12

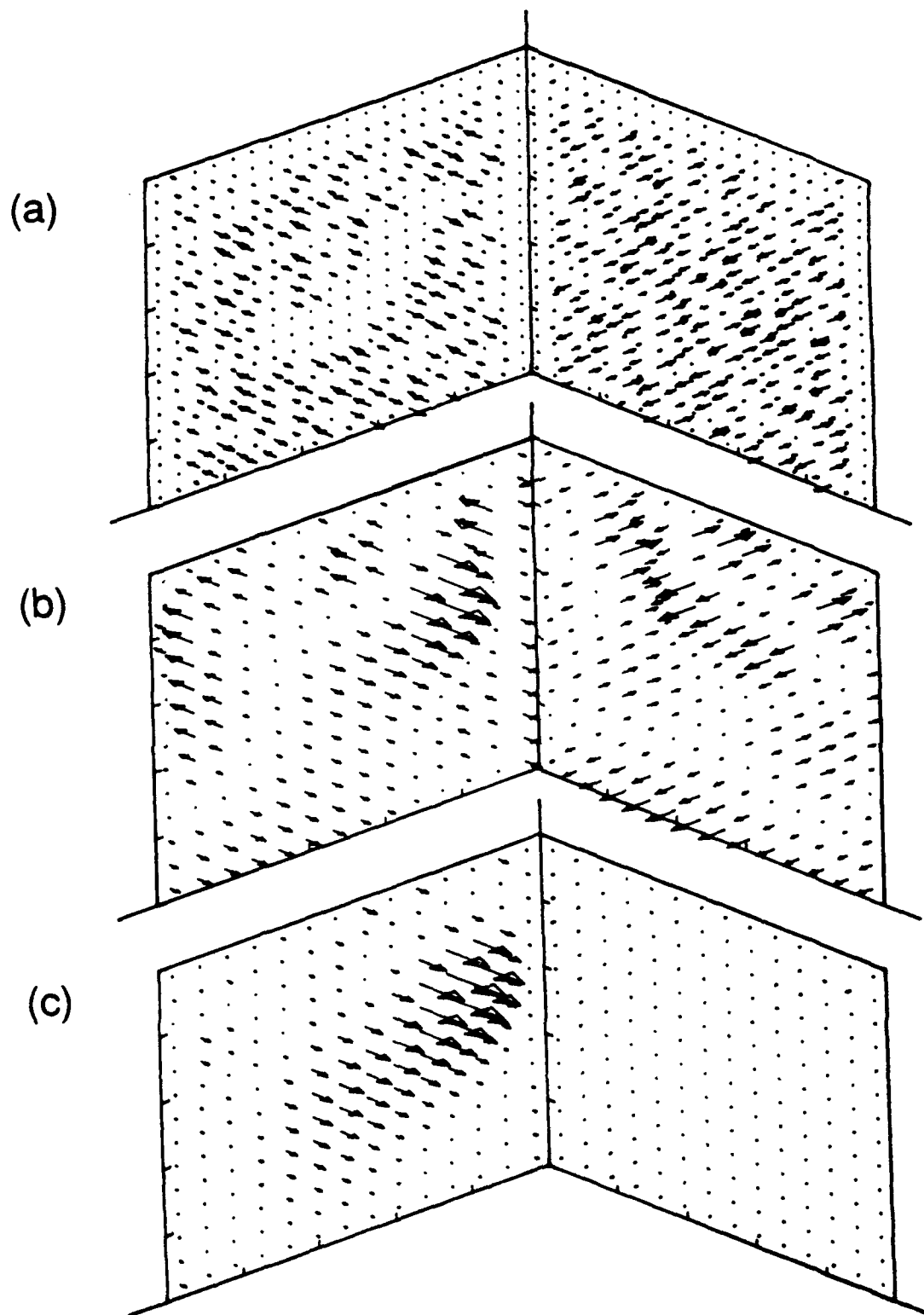


Figure 13